SAND2017-10304R

Advances in Geologic Disposal System Modeling and Shale Reference Cases

Fuel Cycle Research & Development

Prepared for
U.S. Department of Energy
Spent Fuel and Waste Science Technology

P.E. Mariner, E.R. Stein, J.M. Frederick,
S.D. Sevougian, and G.E. Hammond
Sandia National Laboratories

September 22, 2017

SFWD-SFWST-2017-000044

Sandia National Laboratories is a multimission laboratory managed and operated by National Technology and Engineering Solutions of Sandia, LLC., a wholly owned subsidiary of Honeywell International, Inc., for the U.S. Department of Energy's National Nuclear Security Administration under contract DE-NA0003525.

ACKNOWLEDGEMENTS

The authors greatly appreciate the contributions of Sandia technical staff Brad Day, Todd Zeitler, Ramesh Sarathi, Sungtae Kim, Teklu Hadgu, Kris Kuhlman, and Ed Matteo to development and testing of PFLOTRAN and the contributions of Sandia National Laboratories (SNL) staff Carlos Jove Colon, Ed Matteo, Ernie Hardin and Los Alamos National Laboratory (LANL) researcher Frank Perry to development of the shale reference case.

EXECUTIVE SUMMARY

The Spent Fuel and Waste Science and Technology (SFWST) Campaign of the U.S. Department of Energy (DOE) Office of Nuclear Energy (NE), Office of Fuel Cycle Technology (OFCT) is conducting research and development (R&D) on geologic disposal of spent nuclear fuel (SNF) and high level nuclear waste (HLW). Two high priorities for SFWST disposal R&D are design concept development and disposal system modeling (DOE 2011, Table 6). These priorities are directly addressed in the SFWST Generic Disposal Systems Analysis (GDSA) work package, which is charged with developing a disposal system modeling and analysis capability for evaluating disposal system performance for nuclear waste in geologic media (e.g., salt, granite, shale, and deep borehole disposal).

This report describes specific GDSA activities in fiscal year 2017 (FY 2017) toward the development of GDSA Framework, an enhanced disposal system modeling and analysis capability for geologic disposal of nuclear waste. GDSA Framework employs the PFLOTRAN thermal-hydrologic-chemical multi-physics code (Hammond et al. 2011a; Lichtner and Hammond 2012) and the Dakota uncertainty sampling and propagation code (Adams et al. 2012; Adams et al. 2013). Each code is designed for massively-parallel processing in a high-performance computing (HPC) environment. Multi-physics representations in PFLOTRAN are used to simulate various coupled processes including heat flow, fluid flow, waste dissolution, radionuclide release, radionuclide decay and ingrowth, precipitation and dissolution of secondary phases, and radionuclide transport through engineered barriers and natural geologic barriers to the biosphere. Dakota is used to generate sets of representative realizations and to analyze parameter sensitivity.

In FY 2017, major advances in the capabilities and testing of GDSA Framework include:

- Updated analytical derivatives for significantly improved performance of multiphase flow calculations;
- A new reference biosphere dose model for ingestion of well water;
- An improved waste form degradation model for HLW glass;
- The ability to simulate a single waste package using multiple grid cells;
- A new implicit solution for decay and ingrowth of isotopes in both the transport domain and in the waste form;
- Extensive verification testing of flow and transport problems, and documentation of this testing; and
- Development and simulation of two new generic shale repository models.

As these capabilities and advances progressed, integration with other SFWST work continued at a strong pace. The primary focus of direct integration this year was planning the development of a version of GDSA Framework that would be ready for application to a potential site in the year 2020. This planning required careful identification of capabilities to add, prioritization of these capabilities, and consideration of the timeline. The results of that effort are included in this report.

GDSA Framework was exercised in the development of two new shale repository reference cases, one for 12-PWR waste packages emplaced in-drift and one for 4-PWR waste packages emplaced in horizontal boreholes. In each reference case, waste package temperatures reach a maximum at approximately 20 years, with the 12-PWR simulation peaking at 151 °C and the 4-PWR simulation peaking at 104 °C. Despite reference case differences in temperatures and repository layout, concentrations of ^{129}I in the aquifers overlying and underlying the host rock are similar, and none of the realizations result in water

ingestion dose rates exceeding 5×10^{-10} Sv yr^{-1}. Uncertainty in shale porosity has the largest effect on ^{129}I concentrations at observation points in the aquifers directly above and below the repository, but at observation points down gradient in these aquifers, uncertainty in aquifer permeability becomes the largest effect. This situation occurs because low permeability aquifers with low head gradients provide significant natural barriers to ^{129}I transport.

Each year, GDSA Framework and its underlying codes improve as additional modelers and programmers from around the world use, apply, and contribute to it. GDSA Framework is accessible to anyone because the primary codes, PFLOTRAN and Dakota, are open source, available for free download, and have supporting documentation online. This year the GDSA group worked to increase the number of users and participants by

- Launching a collaborative web site (pa.sandia.gov);
- Expanding online documentation of verification testing, generic reference cases, and code features;
- Conducting two PFLOTRAN short courses, one in New Mexico and one in Spain; and
- Presenting multiple papers and posters on GDSA Framework capabilities at international conferences.

Simulation of increasingly complicated problems continues to affirm that HPC-capable codes can be used to simulate important multi-physics couplings directly in a total system performance assessment of a geologic repository. The generic repository applications modeled to date indicate that GDSA Framework can simulate complex coupled processes in a multi-kilometer domain while simultaneously simulating sub-meter-scale coupled behavior in the repository.

Over the past several years GDSA Framework has greatly advanced. Continued development is needed through the next few years to ensure it is ready for application to potential sites that may be selected in the near future. The challenge is to address the remaining needs using available resources. Meeting this challenge will require close integration with technical teams across the SFWST Campaign.

This report fulfills the Generic Disposal System Analysis Work Package Level 3 Milestone – *Advances in Geologic Disposal System Modeling and Shale Reference Cases* (M3SF-17SN010304011).

CONTENTS

FIGURES

Page

TABLES

NOMENCLATURE

1D, 2D, 3D	one-, two-, and three-dimensional
ANL	Argonne National Laboratory
Bq	becquerel
CD	Critical Decision
CFD	computational fluid dynamics
CSNF	commercial SNF
DA	Decision Analysis
DBH	deep borehole
DFN	discrete fracture network
DOE	U.S. Department of Energy
dofs	degrees of freedom
DR	disposal research
DRZ	disturbed rock zone
EBS	engineered barrier system
EDZ	excavation disturbed zone
Eq.	equation
ERB	example reference biosphere
FEP	feature, event, and process
FMDM	Fuel Matrix Degradation Model
FTE	full-time employee
FY	fiscal year
GDSA Framework	Geologic Disposal Safety Assessment Framework
GWd	gigawatt-day
HC	hydride cracking
HDF5	hierarchical data format, version 5
HF	higher fidelity
HLW	high-level radioactive waste
HPC	high-performance computing
IAEA	International Atomic Energy Agency
LANL	Los Alamos National Laboratory
LBNL	Lawrence Berkeley National Laboratory
LF	lower fidelity
LHS	latin hypercube sampling
LOE	level of effort
MTHM	metric tons heavy metal
MTIHM	metric tons initial heavy metal
MUA	multi-attribute utility analysis
MWd	megawatt-day
My	million years

NOMENCLATURE (CONT.)

NA	not applicable
NBS	natural barrier system
NE	Office of Nuclear Energy
OFCT	Office of Fuel Cycle Technology
OoR	(age) out-of-reactor
ORNL	Oak Ridge National Laboratory
OWL	Online Waste Library
PA	performance assessment
PDE	partial differential equation
PETSc	Portable Extensible Toolkit for Scientific Computation
PNNL	Pacific Northwest National Laboratory
PWR	pressurized water reactor
QA	quality assurance
R&D	research and development
RB1	reference biosphere 1
RBSN	Rigid-Body-Spring-Network
SA	safety assessment
SFWST	Spent Fuel and Waste Science and Technology
SIAM	Society for Industrial and Applied Mathematics
SNF	spent nuclear fuel
SNL	Sandia National Laboratories
Sv	sievert
TBD	to be determined
TH	thermal-hydrologic
THC	thermal-hydrologic-chemical
THM	thermal-hydrologic-mechanical
THMC	thermal-hydrologic-mechanical-chemical
UFD	Used Fuel Disposition
UFDC	Used Fuel Disposition Campaign
V&V	verification and validation
WF	waste form
WFPM	Waste Form Process Model
WIPP	Waste Isolation Pilot Plant
WP	waste package

1. INTRODUCTION

The Spent Fuel and Waste Science and Technology (SFWST) Campaign of the U.S. Department of Energy (DOE) Office of Nuclear Energy (NE), Office of Fuel Cycle Technology (OFCT) is conducting research and development (R&D) on geologic disposal of spent nuclear fuel (SNF) and high level nuclear waste (HLW). Two of the highest priorities for SFWST disposal R&D are design concept development and disposal system modeling (DOE 2011, Table 6). These priorities are directly addressed in the SFWST Generic Disposal Systems Analysis (GDSA) work package, which is charged with developing a disposal system modeling and analysis capability for evaluating disposal system performance for nuclear waste in geologic media. Disposal options for SNF and HLW include mined repository concepts in salt, shale, and crystalline rock and deep borehole disposal in crystalline rock (Arnold et al. 2011; Hardin et al. 2012).

In 2013, GDSA transitioned to a framework based on PFLOTRAN and Dakota, a framework that GDSA continues to develop today. PFLOTRAN is a multiphase flow and reactive transport model for describing surface and subsurface processes (Hammond et al. 2011a; Lichtner and Hammond 2012), and Dakota is an uncertainty quantification and sensitivity analysis code (Adams et al. 2012; Adams et al. 2013). These codes were chosen to provide the primary GDSA framework because they are open source, massively parallel, and together have the potential to simulate a total integrated geologic repository system and its surroundings probabilistically and in three dimensions. The developing modeling capability is called GDSA Framework, which stands for Geologic Disposal Safety Assessment Framework.

This report describes GDSA accomplishments for fiscal year 2017 (FY 2017). Prior development and accomplishments are documented in Mariner et al. (2015); Mariner et al. (2016); Sevougian et al. (2013); Sevougian et al. (2014); Freeze et al. (2013b); Clayton et al. (2011); Freeze and Vaughn (2012); and Vaughn et al. (2013).

The overall objective of the GDSA work package is to develop a disposal system modeling and analysis capability that supports the prioritization of Disposal Research (DR) R&D and the evaluation of disposal system performance, including uncertainty, for a range of disposal options (e.g., salt, shale, crystalline, deep borehole). The purpose is to develop a GDSA capability that:

- integrates updated conceptual models of subsystem processes and couplings developed under this and other DR work packages;
- is used to evaluate DR R&D priorities;
- leverages existing computational capabilities (e.g., meshing, visualization, high-performance computing (HPC)) where appropriate; and
- is developed and distributed in an open-source environment.

Five major tasks were identified for FY 2017:

- Identify additional capabilities needed to advance GDSA Framework to a robust performance assessment (PA) model ready for application to a candidate site (e.g., multiphase processes, temperature dependencies, colloids, control variate method, code efficiency, convergence, grid refinement). The GDSA group will work closely with other work packages as applicable in identifying these needs, determining what is required to sufficiently address them, and working to fulfill them by 2020.
- Integrate subsystem models developed under other DR work packages into the GDSA Framework architecture (e.g., colloid transport, discrete fracture model, waste package degradation).

- Develop, perform, and document verification and validation analyses of relevant GDSA model processes and expand regression testing to demonstrate and assure continued quality.
- Develop and perform simulations of selected reference case demonstration problems and conduct sensitivity and uncertainty analyses to inform R&D planning.
- Demonstrate the freely-available GDSA Framework modeling capability at national and international forums and conduct an international workshop to promote accelerated use of the capability worldwide. Expanding the user base is expected to provide additional testing of the code and opportunities for additional development by outside contributors.

This report fulfills the GDSA Work Package Level 3 Milestone – *Advances in Geologic Disposal System Modeling and Shale Reference Cases* (M3SF-17SN010304011). It incorporates information from the following supporting milestones: M2FT-14SN0806051 (Jové Colón et al. 2014); M2FT-15SN0807071 (Wang et al. 2015); M2FT-14SN0807051 (Wang et al. 2014); M3FT-16SN080304011 (Mariner et al. 2016); M2FT-15SN0808011 (Mariner et al. 2015); M3FT-14SN0808032 (Sevougian et al. 2014); and M3FT-13SN0808062 (Freeze et al. 2013a).

Section 2 discusses the GDSA PA vision and summarizes the conceptual model framework and the PFLOTRAN-based computational framework of GDSA Framework. Section 3 reports progress on process model development and specific integration activities that facilitated process model development. Section 4 applies the GDSA Framework to a generic commercial repository in shale. Conclusions are summarized in Section 5.

2. GDSA PERFORMANCE ASSESSMENT

A performance assessment (PA) for underground disposal of nuclear waste requires a comprehensive analysis of features, events, and processes (FEPs) potentially affecting the release and transport of radionuclides to the biosphere. The foundation of a PA is the computational framework. Section 2.1 discusses the GDSA long-term vision for GDSA Framework. The present computational framework and conceptual model framework are summarized in Section 2.2.

2.1 PA Vision

A 2013 DOE timeline, which assumed supportive action by Congress, projected selection of multiple new candidate sites by 2022, selection of a single site by 2026, and submittal of a license application by 2037 (DOE 2013). With continued advances in general computational capabilities over time, a computational framework will need to keep up. The long-term vision for the GDSA effort is therefore to ensure that GDSA Framework can adapt to, and take advantage of, future advances in computational software and hardware and future advances in process modeling. In line with this vision, the near term mission is to develop a robust suite of fully functional generic repository reference case applications (1) for application to candidate sites by the time they are selected and (2) for evaluation of the effects of FEPs and input parameters on repository performance to inform R&D planning.

In consideration of the long-term vision, two open-source, HPC codes will serve as the core of GDSA Framework: PFLOTRAN and Dakota. PFLOTRAN is a massively-parallel thermal-hydrologic-chemical (THC) flow and transport code, and Dakota is a versatile probabilistic code (Section 2.2.2). The PFLOTRAN code will be developed over time by the GDSA group to accommodate new geologic disposal process models and capabilities through additional code development or coupling with external process models. The HPC capabilities of PFLOTRAN and Dakota will allow for ever higher fidelity in GDSA Framework total system performance assessments as more powerful HPC resources become available.

As GDSA Framework evolves, the GDSA group will continue to generate and refine three-dimensional models of disposal repository concepts complete with surrounding geospheres and connected biospheres. Sensitivity analyses will be performed on these models to distinguish the importance of features, processes, and parameters on model results. These analyses will help to prioritize future disposal R&D.

2.2 PA Framework

A PA model is an important component of a comprehensive PA for a nuclear waste repository. In a comprehensive PA all plausible scenarios and processes that may affect repository performance are addressed. FEPs and scenarios are evaluated and screened. Potentially pertinent FEPs are identified for simulation in the PA model. Probabilistic simulations are performed, and results are evaluated against performance metrics. Uncertainty and sensitivity analyses may also be performed to inform prioritization of additional research and model development.

The PA framework consists of a conceptual model framework (Section 2.2.1) and a computational framework (Section 2.2.2). An overview of PA methodology and terminology is presented in Sevougian et al. (2014, Section 2.2) and Meacham et al. (2011, Section 1).

2.2.1 Conceptual Model Framework

A conceptual model framework requires a coherent representation of pertinent FEPs. Figure 2-1 schematically illustrates the conceptual model framework for a repository system. To calculate a dose to a receptor in the biosphere, radionuclides released from the waste form must pass through the repository engineered barrier system (EBS) and the surrounding natural barrier system (NBS).

A FEPs database like the one developed and described in Freeze et al. (2011) can be used to help identify a full set of potentially important FEPs for a specific conceptual repository model. Many of the FEPs in a FEPs database may be directly simulated in the PA model. In a comprehensive PA, excluded FEPs (i.e., FEPs not simulated in the PA model) must be addressed in separate analyses and arguments.

Important processes and events in the conceptual model are those that could significantly affect the movement of radionuclides in the EBS and NBS. Such processes and events include waste package corrosion, waste form dissolution, radionuclide release, radioactive decay, heat transfer, aqueous transport, advection, diffusion, sorption, aqueous chemical reactions, precipitation, buffer chemical reactions, gas generation, colloidal transport, earthquakes, and inadvertent human intrusion of the repository.

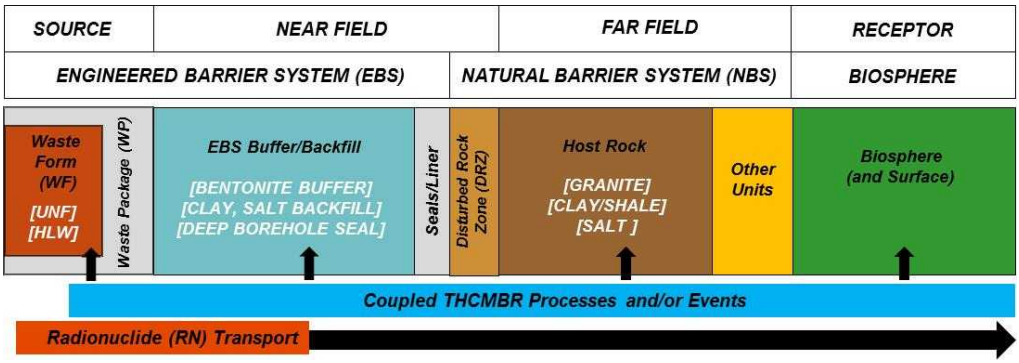

Figure 2-1. Schematic diagram of the conceptual model framework of a generic geologic disposal system.

2.2.2 Computational Framework

PA model simulations require a large number of realizations. For this reason, GDSA Framework is designed for massively-parallel processing in a HPC environment. GDSA Framework consists of the following components:

- Input parameter database
- Software for sampling, sensitivity analysis, and uncertainty quantification (Dakota)
- Petascale multiphase flow and reactive transport code (PFLOTRAN), working in concert with coupled process model codes (e.g., Fuel Matrix Degration Model (FMDM))
- Computational support software and scripts for meshing, processing, and visualizing results (e.g., CUBIT, Python, ParaView, VisIt).

The flow of data and calculations through these components is illustrated in Figure 2-2. In a probabilistic simulation, Dakota generates stochastic input for each PA realization based on parameter uncertainty distributions defined in the input set. The sampled inputs are used by PFLOTRAN and its coupled process models to simulate source term release, EBS evolution, flow and transport through the EBS and NBS, and uptake in the biosphere. After the simulation, various software may be used to reduce and illustrate the output calculations of parameters and performance metrics. Dakota may also be used to evaluate the effects of parameter uncertainty on specific outputs.

Dakota and PFLOTRAN are the core simulation codes of GDSA Framework, the computational framework. These components are described in more detail in Sections 2.2.2.1 and 2.2.2.2.

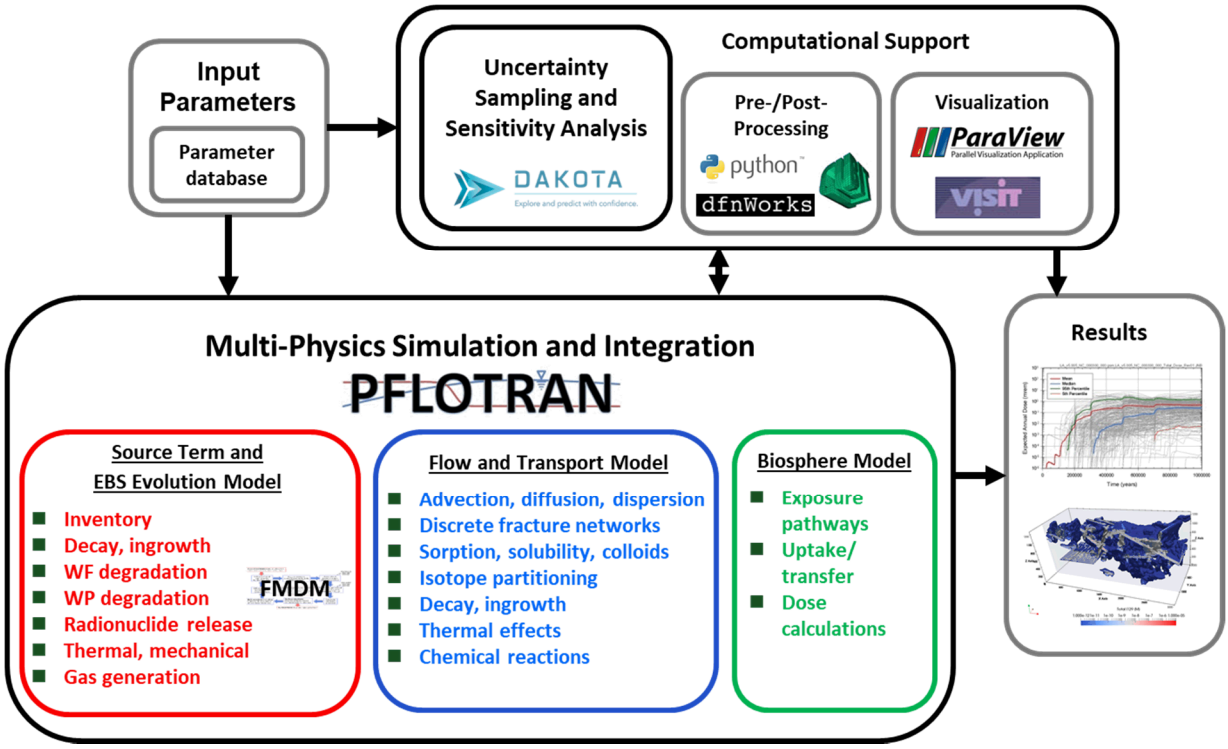

Figure 2-2. GDSA Framework structure.

2.2.2.1 Dakota

The Dakota software toolkit is open source software developed and supported at Sandia National Laboratories (Adams et al. 2012; Adams et al. 2013). GDSA modeling uses Dakota as the interface between input parameters and PFLOTRAN. Dakota is also used to analyze the effects of uncertainty in GDSA parameter values on repository performance.

Dakota can be used to manage uncertainty quantification, sensitivity analyses, optimization, and calibration. Specific Dakota capabilities important to GDSA include (Figure 2-3):

- Generic interface to simulations
- Mixed deterministic/probabilistic analysis
- Uncertainty quantification with sampling methods
- Scalable parallel computation on clusters.

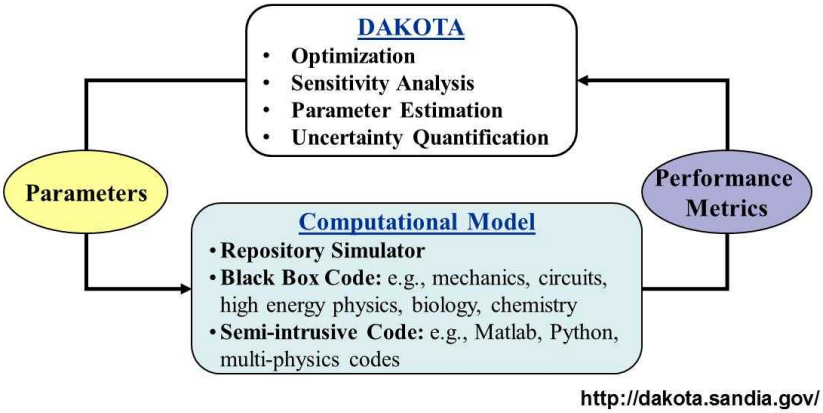

Figure 2-3. Dakota software workflow and capabilities.

2.2.2.2 PFLOTRAN

PFLOTRAN (Hammond et al. 2011a; Lichtner and Hammond 2012) is an open source, reactive multi-phase flow and transport simulator designed to leverage massively-parallel high-performance computing to simulate subsurface earth system processes. PFLOTRAN has been employed on petascale leadership-class DOE computing resources (e.g., Jaguar [at Oak Ridge National Laboratory (ORNL)] and Franklin/Hopper [at Lawrence Berkeley National Laboratory (LBNL)]) to simulate THC processes at the Nevada Test Site (Mills et al. 2007), multi-phase CO_2-H_2O for carbon sequestration (Lu and Lichtner 2007), CO_2 leakage within shallow aquifers (Navarre-Sitchler et al. 2013), and uranium fate and transport at the Hanford 300 Area (Hammond et al. 2007; Hammond et al. 2008; Hammond and Lichtner 2010; Hammond et al. 2011b; Chen et al. 2012; Chen et al. 2013). PFLOTRAN is also under development for use in PA at the Waste Isolation Pilot Plant (WIPP).

PFLOTRAN solves the non-linear partial differential equations describing non-isothermal multi-phase flow, reactive transport, and geomechanics in porous media. Parallelization is achieved through domain decomposition using the Portable Extensible Toolkit for Scientific Computation (PETSc) (Balay et al. 2013). PETSc provides a flexible interface to data structures and solvers that facilitate the use of parallel computing. PFLOTRAN is written in Fortran 2003/2008 and leverages state of the art Fortran programming (i.e. Fortran classes, pointers to procedures, etc.) to support its object-oriented design. The code provides "factories" within which the developer can integrate a custom set of process models and time integrators for simulating surface and subsurface multi-physics processes. PFLOTRAN employs a single, unified framework for simulating multi-physics processes on both structured and unstructured grid discretizations (i.e. there is no duplication of the code that calculates multi-physics process model functions in support of structured and unstructured discretizations). The code requires a small, select set of third-party libraries (e.g., MPI, PETSc, BLAS/LAPACK, HDF5, Metis/Parmetis). Both the unified structured/unstructured framework and the limited number of third-party libraries greatly facilitate usability for the end user.

Specific PFLOTRAN capabilities for the simulation of generic disposal systems include:

- Multi-physics
  - Multi-phase flow
  - Multi-component transport
  - Biogeochemical processes
  - Thermal and heat transfer processes

- High-Performance Computing (HPC)
    - Built on PETSc – parallel solver library
    - Massively parallel
    - Structured and unstructured grids
    - Scalable from laptop to supercomputer
- Modular design based on object-oriented Fortran 2003/2008 for easy integration of new capabilities

3. GDSA Process Model Development

Incorporating process models into the GDSA framework greatly facilitates evaluation of the importance of FEPs in PA applications. The approach of using detailed models directly in a PA is a continuation of the successful modeling approach adopted for the Waste Isolation Pilot Plant (WIPP) PAs (Rechard 1995; Rechard 2002; Rechard and Tierney 2005) and differs from the modeling approach adopted for past PAs for disposal of SNF and HLW in volcanic tuff (Rechard and Stockman 2014). Section 3.1 describes the integration activities GDSA performed this year to incorporate process models developed by other SFWST work packages into GDSA Framework. Section 3.2 discusses additional process models that were added or advanced this year. Section 3.2.6.3 addresses the outreach work performed this year to promote wider use of GDSA Framework and to help establish GDSA Framework as a prominent tool in the repository PA community.

3.1 Process Model Integration

During the development of a repository project, the Safety Assessment (SA), or Performance Assessment (PA), is the main component of the post-closure Safety Case (see IAEA 2012, Section 4.4), along with the underlying Technical Bases (engineering and scientific knowledge). It is also a key tool for prioritizing project R&D activities, i.e., for prioritizing future scientific and engineering endeavors that will bring the safety case to its next documentation stage according to the project schedule. Figure 3-1 is an illustration of the main components of a safety (or licensing) case, indicating the emphasis on R&D activities related to the post-closure technical bases (FEPs) and the generic safety assessment during the current generic stage of the U.S. program (DOE 2012).

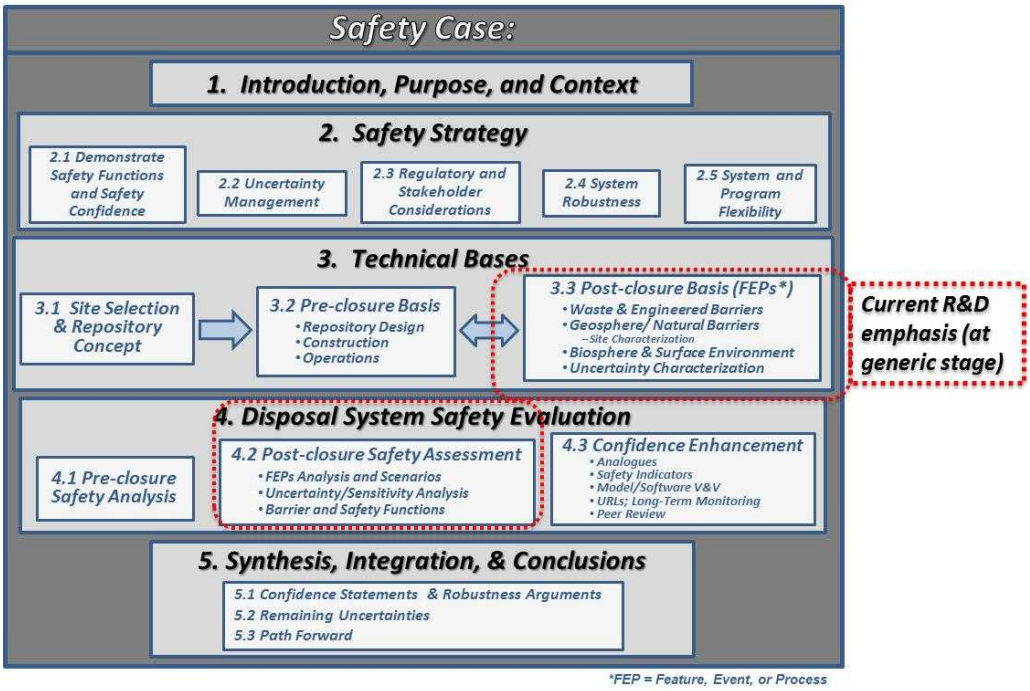

Figure 3-1. Typical components of a deep geologic repository safety case.

Figure 3-2 is a schematic illustration of the progression of these main components of a safety case (the PA and the technical bases) from a generic evaluation phase to a site-specific phase during the typical stages of a geologic disposal project. The maturation of the safety case through these various stages is driven by R&D decisions made at key decision points (e.g., Critical Decision (CD) points, as described in (DOE

2010), via a formal decision making process involving major project stakeholders. Superimposed on Figure 3-2 are some specific years (2020 and 2024) that were used as guidelines for process model integration with the GDSA Framework, as described in more detail below (DOE 2015).[1]

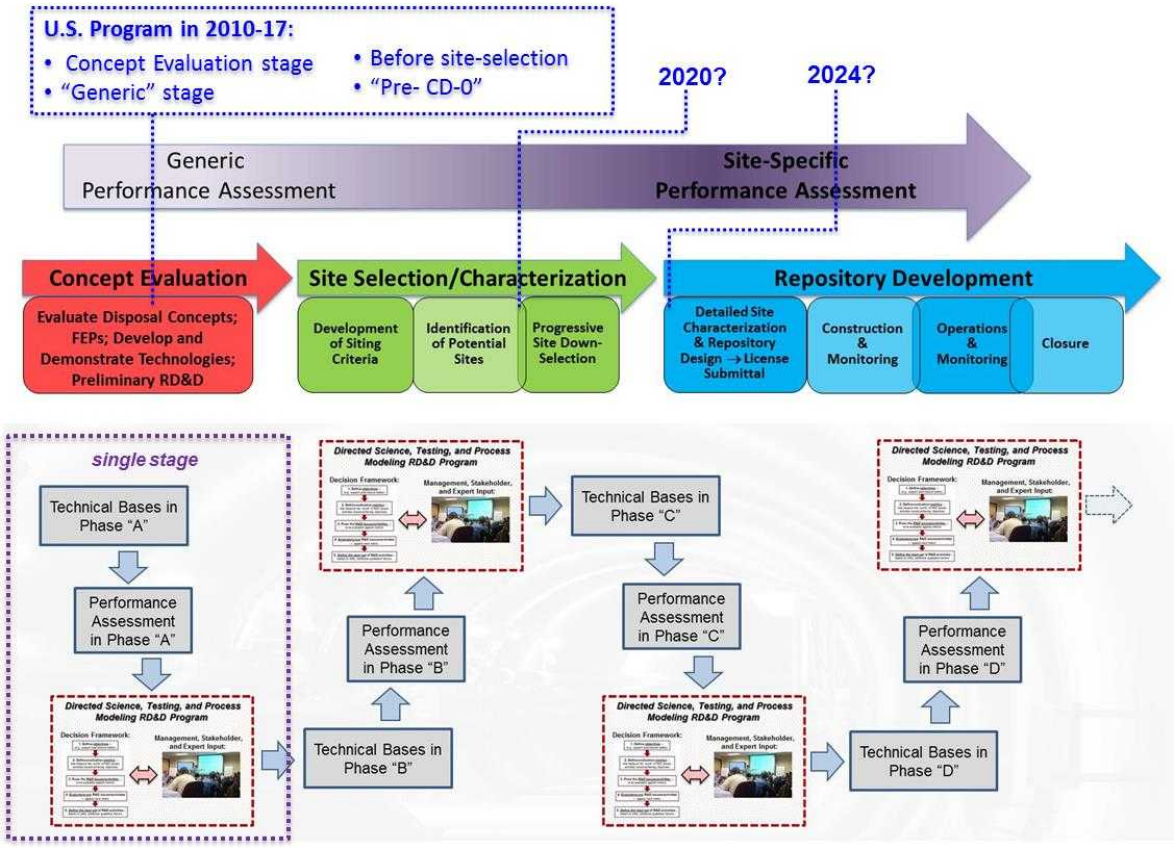

Figure 3-2. Evolution and iteration of the technical bases and performance assessment via R&D through multiple stages of repository development.

Figure 3-3 shows the information flow during a single stage of a repository program and how the GDSA Framework (performance assessment model) is intended to fill a key role in guiding the directed R&D program. This use of GDSA Framework was one of the key drivers for some of the FY 2017 integration activities described here. For example, early in FY 2017 (Nov. 30) an integration meeting was held between project managers and work package managers to organize and coordinate SFWST modeling activities to achieve specific performance assessment ("GDSA Framework") *capabilities* at defined *times* (e.g., at the 2020 point in Figure 3-2, the hypothetical beginning of progressive site down-selection) (NWTRB 2015).[2] Additional goals of the integration meeting were to answer the questions:

[1] It should be understood in Figure 3-2 and throughout this discussion that the dates are merely illustrative for planning purposes, and are clearly subject to political and funding constraints. They are more aggressive than the dates mentioned in Section 2.1, primarily because the assumption was made that a separate repository for defense waste (DOE 2015) could be ready prior to a repository for commercial spent fuel.

[2] It has been argued (NWTRB 2015) that a safety assessment model cannot be used for site down-selection at the earliest stages because it is "technically complex" and "the data needed to employ sensibly such an approach simply are not available at the earliest stages of any siting effort." This report does not prejudge the amount of data available at different project stages but merely assumes a safety assessment model, as well as underlying process models, are as good as the data and assumptions they

- Do current modeling/testing activities support R&D priorities in the Used Fuel Disposition (UFD) R&D Roadmap (DOE 2012)? If not, how to adjust them?
- Are there gaps in our process modeling, PA modeling, and/or testing activities based on UFD Roadmap priorities?

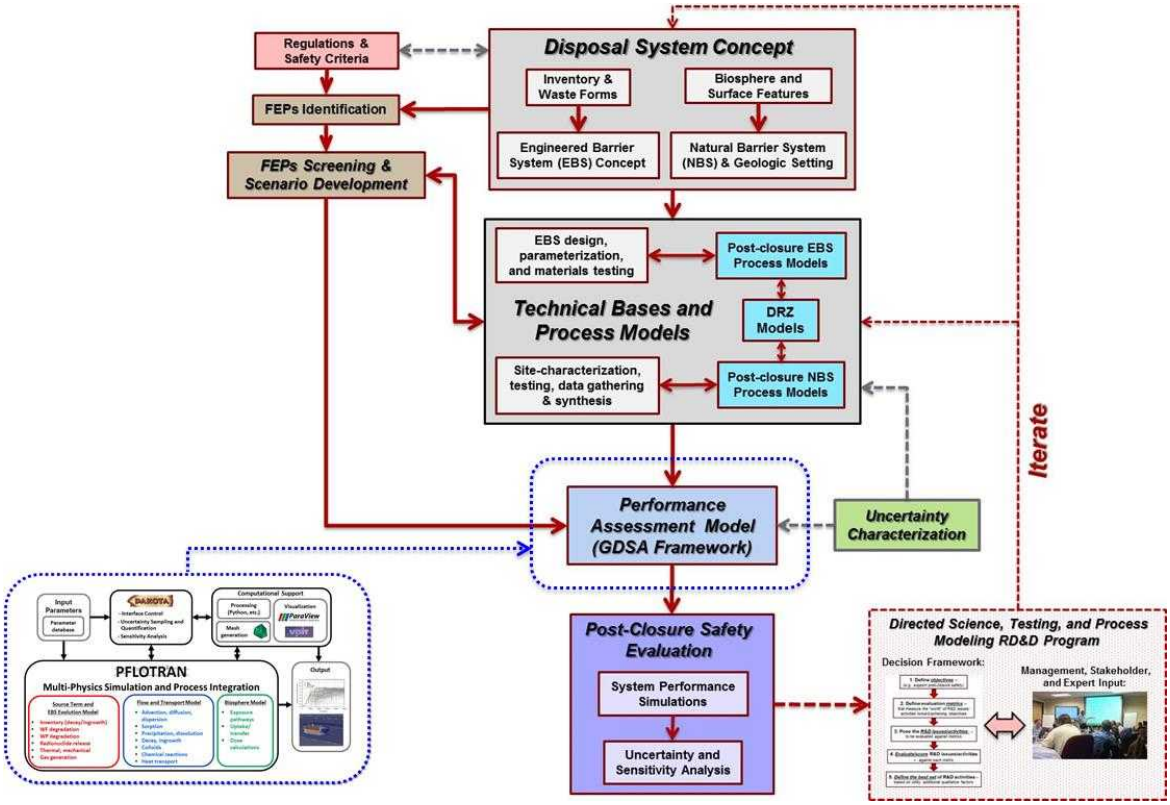

Figure 3-3. Information flow and the role of performance assessment for R&D prioritization during a single stage of repository development.

The tool developed to achieve these goals and answer these questions was an Excel spreadsheet containing three linked tables:

(1) the *R&D Activities* table (Table 3-1), which is an updated version of the Table 3-1 in Mariner et al. (2016);

(2) the *GDSA Tasks* table (Table 3-2), which is a list of the primary items from the *R&D Activities* table that were considered for integration into GDSA Framework during the timeframe from 2017 to 2020 and from 2020 to 2024; and

are based upon, as well as the verification and validation testing they have undergone. Modern and complex computer programs are relied upon to assure safety and reliability of nuclear weapons, to predict weather patterns and climate change, and to safely operate modern transportation systems. It is quite likely that a safety assessment model of some appropriate level of complexity will be employed during all stages of site selection and repository development, subject to the judgment of major stakeholders involved.

(3) the *GDSA Timeline* table (Table 3-3), which is a year-by-year model activity list for 2017, 2018, 2019, and 2020 specifying which items (process models and other activities) from the *GDSA Tasks* table will potentially be integrated into GDSA Framework between 2017 and 2020.

As mentioned above, one of the key drivers for this year's integration planning was to assure that the project R&D prioritization guidance, contained in the UFD R&D Roadmap, is being used to develop a complete PA model (i.e., a complete GDSA Framework) by the year 2020. This is not to say that the GDSA Framework will include *detailed* process models (and/or PA submodels) for every FEP by the year 2020 but, rather, that it will include some version of each important FEP by 2020. As mentioned above in Section 3, one of the key goals of the GDSA Framework is to achieve a higher fidelity representation of the total system behavior by the use of fewer abstractions and by less decoupling of inherently coupled physical-chemical processes. This will result in a simpler defense and validation of the total system model and will produce more confidence in the results. However, because of (1) the complexity of repository performance, (2) the need to make GDSA Framework applicable to at least three different host-rock media (shale, crystalline, salt),[3] and (3) limited funding, some compromises (reduced order models) are necessary in the 2020 timeframe. Nevertheless, the principle of directly solving the entire system model in three dimensions with the least possible process decoupling is still being adhered to.

Two "capability points" were defined, as illustrated in Table 3-2: (1) a near-term (2020) "complete" capability such that process models and their implementation in *GDSA Framework* will have a certain "fidelity" sufficient enough to be used for site down-selection, and (2) a farther-term (2024) "more complete" capability such that process models and their implementation in *GDSA Framework* will have a certain higher fidelity sufficient enough for developing a site-specific safety case (but still requiring additional model development during the course of assembling a license-application safety case).

[3] An important caveat regarding Tables 3-2 and 3-3 is the current requirement to develop the capability to model any of the three primary host-rock geologies: shale, crystalline, and salt. If a decision is made to focus on only one type of geology, the activities, prioritizations, and timeline will need to be revisited; and may result in the elimination of some items in these tables.

UFD FEP ID No., Title, and Media	Overall Priority Score
2.2.01.01 - Evolution of EDZ - Clay/Shale	8.00
2.2.08.01 - Flow Through the Host Rock - Salt	7.73
2.2.08.02 - Flow Through the Other Geologic Units - Confining units - Aquifers - Salt	7.73
2.2.08.06 - Flow Through EDZ - Salt	7.73
2.2.08.04 - Effects of Repository Excavation on Flow Through the Host Rock - Salt	7.10
2.2.08.07 - Mineralogic Dehydration - Salt	6.49
2.2.01.01 - Evolution of EDZ - Deep Boreholes	6.13
2.2.09.01 - Chemical Characteristics of Groundwater in Host Rock - Deep Boreholes	5.86
2.2.09.02 - Chemical Characteristics of Groundwater in Other Geologic Units (Non-Host-Rock) - Confining units - Aquifers - Deep Boreholes	5.86
2.2.09.05 - Radionuclide Speciation and Solubility in Host Rock - Deep Boreholes	5.86
2.2.09.06 - Radionuclide Speciation and Solubility in Other Geologic Units (Non-Host-Rock) - Deep Boreholes	5.86
2.2.09.03 - Chemical Interactions and Evolution of Groundwater in Host Rock - Deep Boreholes	5.40
2.2.09.04 - Chemical Interactions and Evolution of Groundwater in Other Geologic Units (Non-Host-Rock) - Confining units - Aquifers - Deep Boreholes	5.40
1.2.03.01 - Seismic Activity Impacts EBS and/or EBS Components -	4.94
2.1.09.13 - Radionuclide Speciation and Solubility in EBS - In Waste Form - In Waste Package - In Backfill - In Tunnel -	4.86
2.1.03.02 - General Corrosion of Waste Packages -	4.34
2.1.03.03 - Stress Corrosion Cracking (SCC) of Waste Packages -	4.34
2.1.03.04 - Localized Corrosion of Waste Packages -	4.34
2.1.03.05 - Hydride Cracking of Waste Packages -	4.34
2.1.02.01 - SNF (Commercial, DOE) Degradation - Alteration / Phase Separation - Dissolution / Leaching - Radionuclide Release -	4.01
2.2.07.01 - Mechanical Effects on Host Rock - Salt	3.83

Figure 3-4. Highest priority issues and associated priority scores from the UFD R&D Roadmap (DOE 2012, Appendix B).

The itemized integration schedule in Table 3-3 is based on known capability needs as defined by GDSA modelers and process modelers (in the Nov. 30 integration meeting and at the May 23-25 SFWST Working Group meeting) but was compared to the UFD R&D roadmap to ensure completeness and priorities. Figure 3-4 illustrates some of the priority rankings from the UFD R&D Roadmap (DOE 2012), while Figure 3-5 illustrates the general steps in a multi-attribute utility analysis (MUA) or decision analysis (DA) that can generate numerical rankings such as those in Figure 3-4. While the MUA in DOE (2012) was a bit more detailed than that shown in Figure 3-5, the general criteria in Figure 3-5 must be considered when generating a quantitative R&D prioritization. In DOE (2012), expert opinion, based in large part on previous performance assessment models and analyses, was used to decide the FEP (issue) rankings in Figure 3-4.

- **Major steps in a Multi-attribute Utility Analysis (MUA):**
  1. Identify a set of objectives and associated metrics, e.g.,
     - *Importance* to components of the safety case: safety assessment, technical bases, confidence-building
     - Potential to reduce key *uncertainties*
     - Other factors, e.g., *cost*, maturity (TRL) of activity, redundancies, synergies
  2. Evaluate each RD&D activity ("value of the information" obtained) against the metrics
  3. Define a "utility function" to combine the metric scores
  4. Compare utilities ("rankings") of the activities

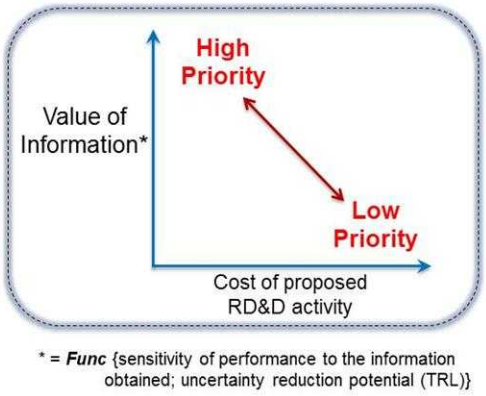

Figure 3-5. Major steps in an MUA or decision analysis.

Going forward with a generic repository program, GDSA Framework simulations and analyses can provide the input for future R&D prioritization MUAs or, in the context of this document, the input for prioritizing process model and submodel integration/development for achieving a given GDSA Framework capability in 2020 or 2024 (or whichever dates are chosen in the future). In establishing the integration timeline (Table 3-3), the following points were considered:

- How does current process modeling work support the necessary *GDSA Framework* capability?
- What type of process model coupling and integration with *GDSA Framework* is appropriate at key times (i.e., at the "capability points")? [The type of coupling is generally one of three types: (1) direct integration/solution of the process model with PFLOTRAN, (2) integration of a reduced order representation with PFLOTRAN, or (3) a separate, but detailed, analysis with the process model to show that a particular FEP may be excluded from the system PA simulations.]
- Are work package R&D priorities based on most important FEPs to performance assessment, i.e., to post-closure system performance?
- How do current R&D activities address UFD R&D Roadmap Issues?

If the U.S. repository program changes direction in FY 2018 from its current generic stage to the former site-specific stage (Yucca Mountain), the integration efforts described herein can be continued for the GDSA Framework, with one of the goals being a state-of-the-art, advanced PA capability ready to employ for future stages of repository development and licensing, such as the "receive and possess" stage that follows repository construction (10 CFR 63.41). It takes years of preparation to develop a state-of-the-art modeling and simulation tool that is capable of utilizing ever-evolving computational and numerical solver capabilities. GDSA Framework is intended to be exactly such a living and evolving state-of-the-art tool for current and future performance assessment modeling of geologic disposal systems.

Table 3-1. SFWST R&D activities considered for potential integration into GDSA Framework.

Task #	Task Name/ (and Work Package #, if needed or helpful for more specificity)	Brief Task Description including Relevance (and/or input) to PA/GDSA (nPA = not direct input to PA)	Personnel	Type of Activity L = Literature review M = Modeling T = Testing or Experimental	Code (if applicable)	Relevance to Safety Case and/or Process Models (only necessary if activity is not directly part of PA—see third column of this table)	Related UFD Roadmap Issue(s)/FEP(s), and associated priority scores*	Other notes/comments	CURRENT STATUS Level of Readiness/ Technical Maturity for Integration with PA, Process Models, or Other Safety Case activities How soon could we start integrating?	GDSA LEVEL OF EFFORT (LOE) required for Integration with PA, Process Models, or Other Safety Case activities C = Complete L = 1 month M = 6 months H = 1 year or more (# FTEs/yr, if known) How long once we start?	INTEGRATION TIME FRAME ("Priority Order/ and Urgency") N = Near term (FY17) M = Medium term (FY17 – FY19) F = Far term (FY19+) How soon should we start?
Crystalline/Argillite/Salt Activities (WBS#1.08.01.03.01, 1.08.01.03.02, 1.08.01.03.03)											
1	CSNF repository argillite reference case	• Revise properties, EBS/repositorydesign, conceptual models, etc., as necessary • Include multiphase flow (e.g., buffer resaturation) • Assess need for M and THM coupled processes in PA • Assess need for C and THC coupled processes in PA (e.g., for buffer and DRZ)	SNL et al.	**L, M, T (mainly L, M)**	GDSA	•	• FEP not explicitly scored, but "disposal system modeling" rated as "high" priority as a "cross-cutting" issue.	•	**Ongoing**	**Funding dependent**	**N**
2	CSNF repository crystalline reference case	• Develop a modeling capability to capture main stages of repository evolution. • Revise properties, EBS/repositorydesign, conceptual models, etc., as necessary • Refine spatial heterogeneity by including deformation zone and more realistic fracture sets (and associated connectivity • Include multiphase flow (e.g., buffer resaturation) • Dual/multi-continuum for transport in granite	SNL et al.	**L, M, T (mainly L, M)**	GDSA	•	• FEP not explicitly scored, but "disposal system modeling" rated as "high" priority as a "cross-cutting" issue.	•	**Ongoing**	**Funding dependent**	**N**
3	CSNF repository bedded salt reference case	• Revise properties, EBS/repositorydesign, conceptual models, etc., as necessary • Include multiphase flow, if needed (e.g., heat pipes) • Assess need for M and THM coupled processes in PA • Assess need for Pitzer model for C	SNL et al.	**L, M, T (mainly L, M)**	GDSA	•	• FEP not explicitly scored, but "disposal system modeling" rated as "high" priority as a "cross-cutting" issue.	•	**Ongoing**	**Funding dependent**	**N**
4	SNF Degradation	• Mixed potentia lmodel of spent fuel matrix degradation (including possible effect of Fe corrosion) • Radiolysis	Frederick, Hammond SNL Jerden, ANL	**M**	PFLOTRAN/FMDM	•	• Primary FEP is 2.1.02.01; score = 4.01 • Other related FEPs have lower scores	• Direct implementation in PFLOTRAN already complete and now at the testing stage. • Additional development and more efficient coding suggested	**Ongoing**	**M**	**N**
5	(Pseudo) Colloid-Facilitated Transport Model	• Formation, stability, and transport of pseudocolloids in the near field and far field	Hammond SNL Reimus LANL Zavarin LLNL	**M**	PFLOTRAN	•	• FEP 2.2.09.59 and 2.2.09.60; scores = 3.29	• Direct implementation in PFLOTRAN suggested, with perhaps some simplification of the conceptual model.	**Now**	**M**	**N**
6	Intrinsic Colloids	• Intrinsic Pu colloid formation,stability, and transport in the near and the far fields, as a function of T	Hammond SNL Reimus LANL Zavarin LLNL	**M**	PFLOTRAN	•	• FEP 2.2.09.59 and 2.2.09.60; scores = 3.29	• Direct implementation in PFLOTRAN, with perhaps some simplification of the conceptual model.	**TBD**	**M**	**M**
7	Discrete Fracture Network (DFN) Model	• Generation and representation of realistic fracture networks • Fluid flow& transport in fracture networks • Mapping tools (dfnWorks to PFLOTRAN) • Dual continuum; matrix diffusion	Stein, Hammond SNL Hyman, Makedonska LANL	**M**	DFNWorks, PFLOTRAN, mapDFN.py	•	• Primary FEP is 2.2.09.51 (crystalline); score = 3.74 • Other related FEPs also have relatively high scores: 2.2.08.01,2.2.02.01,2.2.05.01, 2.2.08.02	• potential FY17 enhancements: heat transport; fracture intersects borehole • Dual continuum/matrix diffusion ready now	**Ongoing**	**M - H**	**N**
8	HLW WF degradation (process model)	• Glass waste degradation • Radiolysis • Transition state theory	Rieke, PNNL Ebert, ANL	**M**	PFLOTRAN et al.	•	• Primary FEP is 2.1.02.02; score = 0.00 (because not considered part of UFD)	• Needed for Defense Waste Repository • Integration with Waste Form Campaign	**Now**	**H**	**N - M**

Table 3-1 (cont.). SFWST R&D activities considered for potential integration into GDSA Framework.

9	Waste Package Degradation Model (mechanistic)	• Degradation of waste packages and canisters • Carbon steel; stainless steel; copper waste packages • Include various degradation processes (SCC, GC, LC, MIC, early failure)	Jove Colon SNL	**M**	PFLOTRAN et al.	•	• FEPs 2.1.03.02, 2.1.03.03, 2.1.03.04, 2.1.03.05; scores = 4.34	• Direct implementation in PFLOTRAN suggested (1D model), similar to SNF degradation • Currently evaluating development of thermodynamic relations for high T 316 SS corrosion phase assemblage (e.g., chromite, magnetite)	**1 to 3 years?**	**H**	**M**
10	Salt Coupled THM processes	• Coupled thermal-hydrological-mechanical processes in salt EBS and EDZ	Rutqvist. Martin LBNL	**M**	TOUGH-FLAC	•	• Primary FEP is 2.2.08.06 (salt); score = 7.73 • Other related FEPs include2.1.08.03 and 2.2.01.01	• Response surface suggested (permeability and porosity fields/surfaces for DRZ and emplacement drifts)	**Now for 2-D** **Several years for 3-D**	**H**	**N - M**
11	Coupled THC processes in Salt	• Coupled thermal-hydrologic-chemical processes in a salt repository	Stauffer LANL Hammond SNL	**M**	PFLOTRAN	•	• Primary FEP is 2.2.08.06 (salt); score = 7.73 • Another high-score FEP is 2.2.08.04; score = 7.10	• Hammond indicates that chemical components can be added to gas phase in PFLOTRAN formulation. • Important constitutive relationships still needed in PFLOTRAN include (Kuhlman): - Crushed salt thermal conductivity dependence on porosity and temperature, - Salt solubility in brine as a function of temperature, - Changes in salt porosity including precipitation and dissolution of salt, - Water vapor diffusion coefficient as a function of pressure, temperature, and porosity, - Power-law permeability-porosity relationship, - Water vapor pressure as a function of brine strength and temperature, and - Temperature-dependent clay dehydration source term.	**Now**	**M**	**N - M**
12	Two-Part Hooke's Model (saturated)	• Clay deformation	Rutqvist, Zheng LBNL	**M**	TPHM-FLAC3D	•	• Primary FEP is 2.2.01.01 (granite); score = 2.58	• Used to calculate the permeability/porosity evolution of EBS in clay formation using a continuum approach • Abstraction suggested (permeability, porosity, stress).	**1 year**	**L**	**M - F**
13	Simplified Representation of THMC processes in EBS (clay illitization)	• THMC (includes clay illitization)	Rutqvist, Zheng LBNL	**M**	TOUGH REACT/FLAC3D	•	• Primary FEP is 2.1.04.01; score = 3.50	• Response surface suggested (permeability, porosity, cation exchange capacity, swelling stress). • Chemical processes still under development	**M, C indicated to need "work"**	**H**	**M - F**
14	Simplified Representation of THM (BBM) model of buffer materials (unsaturated)	• Coupled thermal-hydrological-mechanical processes in compacted clays	Rutqvist LBNL	**M**	BBM+TOUGHREACT+FLAC	•	• Primary FEP is 2.1.04.01; score = 3.50	• Response surface suggested (permeability and porosity fields)	**Now for 2-D** **Several years for 3-D**	**H**	**M - F**
15	Simplified Representation of Rigid-Body-Spring-Network (RBSN)	• Discrete Fracture Network (DFN) with THM (argillite/clay)	Kim, Rutqvist LBNL	**M**	TOUGH2-RBSN	•	• Primary FEP is 2.2.01.01 (clay/shale); score = 8.00	• Abstraction suggested (fracture property response surface). A coupled version of RBSN requires dynamic input (T, p,s).	**??**	**M - H**	**M - F**
16	Diffusion of actinides through bentonite (including speciation)	• Speciation, sorption, diffusion input data	C. Joseph, M. Zavarin LLNL	**T**	N/A	•	• Primary FEP is 2.1.09.13; score = 4.86	• Direct implementation in PFLOTRAN suggested (but not clear if this is a model or just a data-gathering experiment for Fick's Law). Data gathering time frame up to 6 years. (Need to review Joseph et al. 2016 for implementation suggestions.)	**TBD**	**L – M?**	**F**
17	Thermodynamic and sorption database(s)	• Probably nPA • Thermodynamic, surface complexation/ion-exchange databases	M. Zavarin, C. Joseph, C. Duffin, T. Wolery LLNL	**T, M**	N/A	• Thermodynamic, surface complexation/ion-exchange databases, used as input to process models • Surface complexation unlikely to be represented in PA	• Primary FEP is probably 2.2.09.01 (deep borehole); score = 5.86 • FEP 2.1.09.13 is related; score = 4.86	•	**TBD**	**TBD**	**F**
18	Borehole-based Field Testing in Salt	• Horizontal borehole test(s) in salt to verify: geochemical, geohydraulic, and geomechanical phenomena	Kuhlman SNL Stauffer LANL Rutqvist LBNL	**T**	PFLOTRAN, FEHM, TOUGH-FLAC	•	•	• Modeling before and after field experiments. Test plans to be developed in FY17, execution in FY18 based on available funding	**Now**	**H**	**N**

Table 3-1 (cont.). SFWST R&D activities considered for potential integration into GDSA Framework.

19	Possibly simplified representation of drift resaturation process	• Use TH(M) to simulate development of "initial conditions" used in long-term GDSA PA model. Especially with respect to the re-saturation of the DRZ. All media (except DBH) have some amount of increased porosity and decreased saturation in the DRZ surrounding the drift. In salt and clay, the re-hydration process is likely to be coupled with mechanical drift deformation and swelling/healing. The thermal conductivity and heat capacity of the buffer/backfill are very sensitive to the distribution of moisture. If the backfill or DRZ are dry, they will be more thermally insulating.	Kuhlman(?) SNL	**M**	PFLOTRAN	• Development of saturation and pressure initial conditions (or possibly start time, when a fully saturated domain is justified).	•	• The TH (no mechanical) assessment of resaturation could be carried out with PFLOTRAN. This would be a first step to explore the dependence of the resaturation on the vadose zone parameters (i.e., van Genuchten parameters), and the sensitivity of the resaturation to these parameters, and related back to the uncertainty of these parameters. Even though these processes may never be included in the GDSA PA model, they should be explored at an appropriate scale and dimension (e.g., a 2D cross-section through a drift).	Now (if just in PFLOTRAN, without M)	M	M
20	Possibly simplified representation of drift resaturation process with chemistry	• Use TH(M)C to simulate development of "initial conditions" used in long-term GDSA PA model. Especially with respect to the re-saturation of the DRZ. In salt and clay, the re-hydration process is likely to be coupled with mechanical drift deformation and swelling/healing. All media (except DBH) have some amount of increased porosity and decreased saturation in the DRZ surrounding the drift. In salt and clay, the re-hydration process is likely to be coupled with mechanical drift deformation and swelling/healing.	Kuhlman(?) SNL Jove-Colon(?) SNL	**M**	PFLOTRAN	• Development of saturation and pressure initial conditions (or possibly start time, when a fully saturated domain is justified), including the effects of chemistry and two-phase flow and transport.	•	• The THC (no mechanical, with reactive chemistry) assessment of resaturation could be carried out with PFLOTRAN. This would be a first step to explore the dependence of the full chemistry on the resaturation on the . Performing a full chemistry simulation at the drift scale (rather than the GDSA PA scale of several km), will illustrate how resaturation slows down some chemical processes and may speed up others. Dry early-time conditions in the DRZ and backfill may slow down canister corrosion.	Now (just in PFLOTRAN). May require some additional fidelity to represent relevant processes (e.g., vapor pressure lowering, pitzer)	M	M
		•				•	•	•			
Deep Borehole Activities (WBS#1.08.01.03.06)											
25	Deep borehole reference case	• Modification of any models or code capabilities to model a deep borehole concept	SNL	**M**	GDSA	•	•	•	**Ongoing**	**Funding dependent**	**N**
26	Salinity gradient / Density stratification	• Salinity-dependent density	SNL	**M**	PFLOTRAN	•	• 2.2.09.01; score = 5.86 • 2.2.09.03; score = 5.40	•	**Ongoing**	**L**	**N**
27	Flow and transport in Borehole Annulus	• Might require CFD	SNL	**M**	PFLOTRAN?	•	• 2.2.09.03; score = 5.40 • 2.2.08.06(EDZ); score=3.65 • 2.2.11.01; score = 3.10 • 2.2.11.02; score = 3.10	•	**Now**	**M**	**M**
28	High-Temperature Behavior	• Ability to apply PA model at temperatures up to 200C.	SNL	**M**	PFLOTRAN	•	• 2.2.01.01(EDZ); score=6.13 • 2.2.08.01(H); score=3.65	•	**Now**	**M**	**N**
29	Cement plug degradation	• Physical and chemical effects	SNL	**M**	PFLOTRAN	•	• 2.2.08.06(EDZ); score=3.65 • 2.2.09.03; score = 5.40	•	**TBD**	**Funding dependent**	**F**
International Activities (WBS#1.08.01.03.07)											
35	Radionuclide transport as pseudocolloids, Grimsel	• Rates of radionuclide desorption from mineral colloids; input to PA, depending on type of model used in PA NOT SURE IF THIS IS CURRENT	J. Begg, P. Zhao, C. Joseph, M. Zavarin (LLNL)	**T, M**	N/A	•	• Primary FEP is probably 2.2.09.64 (crystalline or clay/shale); score = 3.55	• Basic model has been developed in the last couple of years and will be improved upon (redox effect) in the next 3 years.	**2 years?**	**M**	**M**
36	Long term in situ test at Grimsel (part of Full scale engineering barriers Experiment (FEBEX))	• Thermal, hydrological, mechanical and chemical alteration of bentonite backfilled EBS • Validation of coupled THMC model and PA model • Supply GDSA with the porosity, permeability, swelling pressure evolution and clay mineral alteration over the course hydration	L. Zheng H. Xu J. Rutqvist	**T, M**	TOUGHREACT-FLAC3D	•	• Primary FEP is 2.1.04.01; score = 3.50	• The THMC model was developed and tested against THM data, model validation with chemical data is ongoing	**2 years**	**M**	**M**

Table 3-1 (cont.). SFWST R&D activities considered for potential integration into GDSA Framework.

37	Experiment of bentonite EBS under high temperature, HotBENT	• Thermal limit of crystalline and argillite repository with bentonite EBS. • Hydrological, mechanical and chemical alteration of bentonite backfilled EBS under high temperature (200 °C) • Validation of coupled THMC model and PA model • Supply GDSA with the porosity, permeability, swelling pressure, vapor pressure evolution and clay mineral alteration under high temperature	L. Zheng H. Xu J. Rutqvist	**T, M**	TOUGHREACT-FLAC3D	•	• Primary FEP is 2.1.04.01; score = 3.50	• The test was proposed in FY15, is planned to start in FY17 and will last for 5 years.	**TBD**	**M**	**F**
38	Mont Terri FE (Full-scale Emplacement) Experiment	• Thermally driven THM evolution in both the EBS components and the host-rock behavior in argillaceous formations • Resaturation and swelling of the protective buffer around the waste package • Validation of coupled THM model of bentonite and clay host rocks • Supply GDSA with flow properties (e.g. porosity and permeability) evolution in the buffer, excavation disturbed zone and host rock • Inform GDSA related to local flow created by coupled THM processes.	J. Rutqvist, H. Xu	**T,M**	TOUGH-FLAC	•	• Primary FEP is 2.1.04.01; score = 3.50 • Other related FEP is 2.2.01.01: Score = 8.0,	• The Mont Terri FE Experiment will be one of the largest and longest running heater tests worldwide. Heating started in 2015 and will go on for at least 15 years	**Now**	**M**	**M**
39	DECOVALEX-2019 Task E: Upscaling of modeling results from small scale to one-to-one scale based in heater test data in Callovo-Oxfordian claystone (COx) at MHM underground research laboratory in France.	• Thermally driven THM evolution in both the EBS components and the host-rock behavior in argillaceous formations • Resaturation and swelling of the protective buffer around the waste package • Validation of coupled THM model of bentonite and clay host rocks • Supply GDSA with flow properties (e.g. porosity and permeability) evolution in the buffer, excavation disturbed zone and host rock • Inform GDSA related to local flow created by coupled THM processes.	J. Rutqvist, H. Xu	**T,M**	TOUGH-FLAC	•	• Primary FEP is 2.1.04.01; score = 3.50 • Other related FEP is 2.2.01.01: Score = 8.0,	• The Mont Terri FE Experiment will be one of the largest and longest running heater tests worldwide. Heating started in 2015 and will go on for at least 15 years	**2 years**	**M**	**M**
40	DECOVALEX-2019 Task A: Advective gas flow in bentonite and clay stone	• Pressure buildup and gas migration in bentonite and clay stone	J. Rutqvist K. Kim	**T, M**	TOUGH-FLAC TOUGH-RBSN	•	• Primary FEP is 2.2.08.06 ; Score 3.65	• The DECOVALEX-2019 project will provide extensive experimental and field test results on the behavior of gas generation and pressurization in bentonite and clay stone, including dilation and fracture formation.	**2 years**	**M**	**M**
41	DECOVALEX-2019 Task C: GREET (Groundwater REcovery Experiment in Tunnel) at Mizunami URL, Japan	• Geochemistry: Evaluate groundwater chemistry in a crystalline repository and the effect of repository construction • Utilize fracture data for validation of fracture models in crystalline rock	Y. Wang Jove-Colon T. Hadgu	**T, M**	PFLOTRAN, EQ3/6, DFN, FCM	•	• Primary FEP is 2.2.05.01 (crystalline) score = 3.74; applicable FEP 2.2.09.51 (crystalline); 2.2.08.04 (crystalline) score = 3.23; 2.2.09.02 (crystalline) score = 5.86;	• The DECOVALEX-2019 project Task C will provide comprehensive geochemical and fracture characterization of host-rock at various locations and times. Experimental and field test results (groundwater recovery, monitoring) will provide key information about groundwater chemical evolution.	**2 years**	**M**	**M, H**
42	FEBEX-DP: Dismantling phase of the long-term FEBEX heater test	• Evaluate post-test state of FEBEX barrier clay and interactions at EBS interfaces • Effects of dryout and mineral dehydration on backfill/buffer	C. Jove-Colon L. Zheng	**T**	N/A	•	• Primary FEPs 2.1.04.01, 2.1.05.01 score = 3.5; 2.2.08.07 score = 2.82; 2.1.07.09 score = 2.56	• Analysis of FEBEX-DP samples will provide insights on clay buffer degradation and interactions at EBS interfaces to inform modeling approaches.	**2 years**	**M**	**M, H**
		•				•	•	•			
Collaborative process model implementation – not currently scoped/funded in UFD DR:											
50	Biosphere pathways	• Detailed biosphere pathways, processes, and FEPs	Mariner, et al SNL Others?	**M**	GDSA	•	• Biosphere FEPs score low (<1), but this is needed eventually to satisfy regulations	• This should probably wait until there are actual candidate sites • Needs to consider the various biosphere FEPs in the UFDC list (3.3.XX.YY)	**3 years?**	**H**	**F**
51	Cladding Degradation	• Cladding degradation processes (e.g., HC)	?	**M, T (mainly M)**	PFLOTRAN?	•	• FEP 2.1.02.06; score = 3.62	•	**1 year**	**H**	**F**
52	In-Package Flow	• Modeling of flow and transport inside waste packages/canisters • Evolution of corrosion products	GDSA team?	**M, T (mainly M)**	PFLOTRAN	•	• Primary FEP is probably 2.1.09.51; score = 3.06	• Requires development of a tractable conceptual model	**2 years**	**H**	**F**
53	In-Package Chemistry	• Fully coupled in-package chemistry model, as it impacts degradation, mobilization, and transport inside the WP • Effect of corrosion product degradation	Mariner? Jove Colon?	**M**	PFLOTRAN	•	• Primary FEP is probably 2.2.09.13; score = 4.86	•	**2 to 3 years**	**H**	**F**

Table 3-1 (cont.). SFWST R&D activities considered for potential integration into GDSA Framework.

GDSA and DWR Safety Analysis Activities (WBS#1.08.01.03.04 and 1.08.01.05.04)											
60	Commercial waste repository reference cases SF-17SN01030401	• Modification of any models or code capabilities to accommodate a repository for commercial HLW/SNF	SNL	**L, M**	GDSA	•	• FEP not explicitly scored, but "disposal system modeling" rated as "high" priority as a "cross-cutting" issue.	•	**Ongoing**	**Funding dependent**	**N**
61	Defense waste repositories reference cases SF-17SN01050401	• Modification of any models or code capabilities to accommodate a repository for DOE-managed HLW/SNF	SNL	**L, M**	GDSA	•	• FEP not explicitly scored, but "disposal system modeling" rated as "high" priority as a "cross-cutting" issue.	•	**Ongoing**	**Funding dependent**	**N**
62	QA, V&V (documentation and tests)	• V&V, benchmarking, and documentation of codes, including pre- and post-processors	Frederick, Stein, Mariner, etc. SNL	**L, M**	GDSA	•	• FEP not explicitly scored, but "disposal system modeling" rated as "high" priority as a "cross-cutting" issue.	• PFLOTRAN wiki already has significant regression testing, but documentation could be improved.	**Now**	**Ongoing**	**N**
63	Basic biosphere model	• Aquifer; overlying sediments; infiltration; withdrawal well(s); IAEA ERB-1A dose calculation (GDSA)	Mariner SNL	**L, M**	GDSA	•	• Biosphere FEPs score low (<1), but this is needed to portray a dose metric	• Instead use drinking water standards from YMP, i.e., a concentration metric instead of a dose metric?	**Now**	**L**	**N (but see notes)**
64	Grid refinement	• Octree-grid adaptive mesh refinement using p4est • Block grid refinement	Hammond, SNL	**M**	PFLOTRAN; p4est	•	• FEP not explicitly scored, but "disposal system modeling" rated as "high" priority as a "cross-cutting" issue.	• Octree capability is still being developed by the originators	**1 year**	**H**	**M**
65	Nested EBS, near-field, far-field models	• Nesting of domains with process models of varying sophistication	G. Hammond, P. Mariner, E. Stein, J. Frederick SNL	**M**	PFLOTRAN	•	• FEP not explicitly scored, but "disposal system modeling" rated as "high" priority as a "cross-cutting" issue.	• e.g., embedding 3D domains with increasing numbers of processes, unknowns, complexity	**1 to 2 years?**	**H**	**M**
66	Operator splitting for reactive transport	• Add operator-splitting numerical method for reactive transport	Hammond SNL	**M**	PFLOTRAN	•	• FEP not explicitly scored, but "disposal system modeling" rated as "high" priority as a "cross-cutting" issue.	• Enables larger simulations as the system of equations is smaller	**Now**	**L - M**	**N**
67	Numerical solution methods (analytical derivatives)	• Improve GENERAL multiphase convergence (analytical derivatives)	Hammond SNL	**M**	PFLOTRAN	•	• FEP not explicitly scored, but "disposal system modeling" rated as "high" priority as a "cross-cutting" issue.	•	**Now**	**M**	**N**
68	Simplified Representation of Mechanical processes in PA	• ROMs for creep closure • General representationof "M" in PFLOTRAN? • Simplest representation in PA is a set of initial conditions from a process model	Hammond SNL Kara LANL	**M**	PFLOTRAN	•	• Highest scoring mechanical FEP is 2.2.07.01; score = 3.83 • But FEP 2.2.01.01 (clay/shale) could be argued to apply; score = 8.0	• Important for salt at early times, but how important for directly including this process in a long-term PA?	**1 to 2 years?**	**H**	**M**
69	Full Representation of Chemical processes in PA	• Effect of chemistry on near-field degradation and transport • Possibly a separate, "nested" model	Hammond, Jove-Colon, Mariner et al. SNL	**M**	PFLOTRAN	•	• Highest scoring chemical FEP is 2.2.09.03 (deep borehole); score = 5.40 • But FEP 2.2.01.01 could be argued to apply (clay/shale); score = 8.0	•A separate nested model from Task #83 •Different equations in different domains •~~Hee~~Ho dissertation? •Loose coupling using different processes in different domains •Compare loose coupling with tight coupling	**Now**	**H**	**M**
70	Pitzer model	• Implement Pitzer activity coefficients (Wolery version)	Hammond, Jove-Colon SNL	**M**	PFLOTRAN	•	• Highest scoring speciation FEP is 2.2.09.05 (deep borehole); score = 5.86 • FEP 2.1.09.13 is also relevant (EBS); score = 4.86	• We prefer the Wolery, rather than the Felmy, implementation • Important for repositories in salt and for deep borehole	**Now**	**M - H**	**M**
71	Performance metrics SF-17SN01050405 SF-17SN01050408	• Develop a "standardized" set of performance metrics for each reference case (e.g., a grid of wells for granite)	Sevougian, Stein, Mariner SNL	**L, M**	GDSA	•	• FEP not explicitly scored, but "disposal system modeling" rated as "high" priority as a "cross-cutting" issue.	• This issue arose for the granite repository where the granite and fractures were effectively outcropping	**Now**	**M**	**N**
72	Surface processes and features	• Develop model parameters for infiltration & surface discharge	Mariner, et al SNL	**L, M**	GDSA	•	• Surface FEPs score low (<2)	• Consider processes such as precipitation, evapotranspiration, surface runoff, streams, lakes, etc	**1 year**	**M**	**M**

Table 3-1 (cont.). SFWST R&D activities considered for potential integration into GDSA Framework.

73	Other missing FEPs (processes) SF-17SN01030401 SF-17SN01050402	• Gas generation and movement • Ongoing climatic effects • Neutron activation	Mariner, et al. SNL	**M**	GDSA	•	• Highest scoring gas FEP is 2.2.12.02 (salt); score = 3.23 • Highest scoring climate FEP is 1.3.01.01; score = 1.85	• Gas generation/ movement might be important with regard to corrosion processes and buffer stability	**1 year**	**H**	**M - F**
74	Implicit solution for decay and ingrowth	• Use global implicit solution instead of operator splitting for PFLOTRAN "sandbox" capability	Hammond SNL	**M**	PFLOTRAN	•	•	•	**Now**	**M**	**M**
75	Implicit solution for decay and ingrowth	• Use implicit solution instead of operator splitting for PFLOTRAN reactive transport equations	Hammond SNL	**M**	PFLOTRAN	•	•	•	**Now**	**H**	**M**
76	Solution density	• Liquid density dependence onsalinity	Hammond SNL	**M**	PFLOTRAN	•	•	• Need to implement salinity dependence in PFLOTRAN TH mode	**Now**	**L**	**N**
77	UA/SA	• Standardized set of UA/SA, including rank regression • Stability of mean, including control variates	Stein, MacKinnon, Kuhlman SNL	**L, M**	Dakota, etc.	•	•	• We already have the Dakota capability (e.g., PRCCs) • Not clear that we have a stepwise linear regression capability	**Now**	**M**	**N**
78	PFLOTRAN improvements	• Checkpoint/restart capability for new process models • Gridded dataset support for initial solute concentrations	Hammond SNL	**M**	PFLOTRAN	•	•	•	**Now**	**L**	**N**
79	Disruptive events SF-17SN01030401 SF-17SN01050402	• PA processes initiated ordependentupon external events, such as human intrusion, glaciation, and seismicity. Also, include early WP failures.	Mariner, Sevougian, Hammond, et al. SNL et al.	**L, M**	GDSA	•	• Highest scoring disruptive event FEP is 1.2.03.01 (seismic); score = 4.94	• Requires stylized scenarios and regulations for generic repositories and for site-screening activities • Should remain on hold until there are candidate sites	**TBD**	**H+**	**F**
80	Species and element properties	• Solute-specific diffusivities • Temperature-dependent solubilities	Hammond, Mariner SNL	**M**	PFLOTRAN	•	•	• Probably only a second order effect.	**6 months**	**L**	**M**
81	Solid solution model	• Precipitationand dissolution of solid solutions	Lichtner, Hammond SNL	**M**	PFLOTRAN	•	•	• A simpler version (ignoring molar volumes) may be implemented sooner	**2 years**	**H**	**F**
82	Isotope partitioning in presence of colloids	• The isotope partitioning and solubility model will need to account for isotopes in colloid phase when colloid model is added	Mariner, Hammond SNL	**M**	PFLOTRAN	•	• FEP 2.1.09.13, 2.2.09.05, and 2.2.09.06 are related; highest score = 5.86	• Implementation of LANL/LLNL/SNL colloid model takes precedence; adjustment to isotope partitioning model depends on colloid model implementation	**Now**	**L**	**N**
83	Waste Form-Canister-Buffer Discretization (1D -> 3D)	• 1-D transport WF-WP-Buffer transport model connected into 3-D grid	Hammond, Stein SNL	**M**	PFLOTRAN	•	• FEP not explicitly scored, but "disposal system modeling" rated as "high" priority as a "cross-cutting" issue.	•	**Now**	**M**	**N**
84	HLW WF degradation (simplified)	• Glass waste degradation	Frederick, Mariner SNL	**M**	PFLOTRAN	•	• Primary FEP is 2.1.02.02; score = 0.00	•	**Complete**	**C**	**Complete**
85	WP Degradation Model Framework	• Degradation of WP outer barrier over time	Mariner, Frederick SNL	**M**	PFLOTRAN	•	• FEPs 2.1.03.02, 2.1.03.03, 2.1.03.04, 2.1.03.05; scores = 4.34	•	**Complete**	**C**	**Complete**
86	Multi-Component Gas Transport	• Ability to model chemical species in the gas and liquid phases.	SNL et al.	**M**	PFLOTRAN	•	• Primary FEP 2.2.09.64; score = 3.55	• We assume equilibrium between the gas and liquid phases; so the number of reactive transport degrees of freedom does not increase	**Now**	**L – M**	**M**
Other DWR Activities (WBS#1.08.01.05.01, 1.08.01.05.02, 1.08.01.05.03)											
90	DWR Disposal Overpack and Waste Package Options SF-17SN01050203	• Evaluate options for waste package design for each of the considered host rocks for DWR. • Crosscut with Jové-Colón's mechanistic waste package degradation model	Matteo, Hardin, SNL	**L, M**	NA; PFLOTRAN, Mathcad	•	• FEPs 2.1.03.02, 2.1.03.03, 2.1.03.04, 2.1.03.05; scores = 4.34	• Thermal analyses may be necessary (with PFLOTRAN or Mathcad)	**Ongoing**	**M**	**N**

Table 3-1 (cont.). SFWST R&D activities considered for potential integration into GDSA Framework.

91	EBS Concepts and Thermal Analysis SF-17SN01050201	• Crosscuts with crystalline, argillite, and saltDRfor EBS concepts, plus: (see next bullet) • Cementitious materials -drift and shaft seals -buffer and waste package constituents (e.g. Belgian supercontainer) -structural elements, cement/ bentonite and cement/host media interfaces (certain disposal concepts and/or host media may necessitate (or benefit) from use of cementitious EB elements – this task, in addition from integrating with GDSA, integrates with crystalline, argillite, and salt DR)	Matteo, Hardin, Jove-Colon SNL	**L, M, T**		•	• Primary FEP 2.1.09.02; score = 2.8	• There are large uncertainties in the long-term performance of cementitious materials in repository environments. However, certain concepts will require their usage. • This FEP seems to cover only chemical effects, but there could be significant implications for mechanical and hydrologic EBS performance.	**FY18 or 19**	**M, H**	**N, M, F**
92	Repository Layout and Waste Package Emplacement SF-17SN01050205	• Design input for DWR repository argillite reference case • Designinput for DWR repository crystalline reference case • Designinput for DWR repository salt reference case (design input is distributed amongst all 3 WPs, but placed in this bin since ultimate impact and integration with GDSA lies in the layout and emplacement concepts)	Matteo, Hardin SNL	**L, M**		•	• FEP not explicitly scored, but "disposal system modeling" rated as "high" priority as a "cross-cutting" issue.	•	**Ongoing**	**M**	**N**
93	Complete and Populate Online Waste Library (OWL) SF-17SN01050101	• Develop/update a listing and inventory of DOE-managed HLW and SNF radioactive wastes which were assessed in the disposal options evaluation work and identify any additional wastes and/or waste forms to be added/updated • The On-Line Waste Library will be constructed for information on DOE-managed HLW, SNF, and other wastes that are potential candidates for deep geologic disposal, with links to supporting documents	Sassani, Price, Rogers, Walkow, et al., SNL Carter, SRNL	**L, M**	Web Develop	• Inventory for source term	• FEP2.1.01.01; score = 2.05	•	**Preliminary developed, Ongoing**	**M**	**N**
94	Characterize Alternative Wasteforms Long-Term Performance – SNL SF-17SN01050102	• Characterize long-term performance of alternative waste forms. • Organize and coordinate information on both the performance of waste forms to be disposed, and conditions for various repository concepts for disposal, to inform safety assessments.	Sassani, Rigali, Mariner et al., SNL Buck, PNNL	**L, M**		• Degradation models for waste forms for GDSA	• Highest FEP is2.1.02.01; score = 4.01	•	**Preliminary developed, Ongoing**	**M**	**N**
		•				•	•	•			
		•				•	•	•			

*FEP scores are from the UFD R&D Roadmap (DOE 2012). Higher scores indicate higher importance. Scale = 0 to 8 (see App. B. of UFD Roadmap).

Table 3-2. *GDSA Tasks*: items from the *R&D Activities* table considered for integration into GDSA Framework in the timeframes 2017 to 2020 and 2020 to 2024.

	This sheet is linked to the R&D Activities sheet...	C = complete; LF = lower fidelity (or what can be done by 2020); HF = higher fidelity (see R&D Activities spreadsheet); ? = uncertain													
		By 2020 (e.g., *candidate sites* selected for evaluation)							By 2024 (e.g., *final site* selected)						
Priority	Task #	Process Model	Argillite	Crystalline	Salt	DBH (Cs/Sr)	2020 GDSA LOE	Notes	Status	Argillite	Crystalline	Salt	DBH (Cs/Sr)	2024 GDSA LOE	Notes	Status
N/A	A	Hydrology (H)	HF	HF	HF	HF			done	HF	HF	HF	HF			done
N/A	B	Thermal (T)	HF	HF	HF	HF			done	HF	HF	HF	HF			done
1	C	Radionuclide Transport & Chemistry	LF -> HF?	LF -> HF?	LF -> HF?	LF -> HF?		LF = Kds	done	HF	HF	HF	HF	H	HF = full reactive transport	available
2	83	Waste Form-Canister-Buffer Discretization (1D -> 3D)	LF	LF	LF	LF	M			HF?	HF?	HF?	HF?	H	see Task #65	
3	63	Basic biosphere model	LF	LF	LF	LF	L									
4	4	SNF Degradation	LF -> HF?	LF -> HF?	LF -> HF?		M	LF = Arrhenius law		HF	HF	HF			HF = FMDM	
N/A	84	HLW WF degradation (simplified)	LF	LF	LF		C		done	HF	HF	HF				
5	8	HLW WF degradation (process model)								HF	HF	HF		H		
6	68	Simplified Representation of Mechanical processes in PA			LF (IC)	?	M	Initial condition at closure				HF	?	H		
7	5	(Pseudo) Colloid-Facilitated Transport Model	HF	HF		HF	M			HF	HF		HF		Assume complete by 2020	
8	6	Intrinsic Colloids	HF	HF	?	HF	M			HF	HF	HF	HF		Assume complete by 2020	
9	13	Simplified Representation of THMC processes in EBS (clay illitization)	LF	LF	LF	?	M	LF = response surface by 2020		LF	LF	LF	?	H	Probably not complete at HF level even in 2024	
9	14	Simplified Representation of THM (BBM) model of buffer materials (unsaturated)	LF	LF	LF	?	M	LF = response surface by 2020		LF	LF	LF	?	H	Probably not complete at HF level even in 2024	
9	15	Simplified Representation of Rigid-Body-Spring-Network (RBSN)	LF	LF	LF	?	M	LF = response surface by 2020		LF	LF	LF	?	M - H	Probably not complete at HF level even in 2024	
10	7	Discrete Fracture Network (DFN) Model		LF		LF	M - H				HF		HF	H		
N/A	85	WP Degradation Model Framework	?	LF	?	LF	C									
11	9	Waste Package Degradation Model (mechanistic)	?	LF	?	LF	L - M	Some additional effort to include all mechanisms		?	HF	?	HF	H		
12	69	Full Representation of Chemical processes in PA	LF -> HF?	LF -> HF?	LF -> HF?	LF -> HF?	M	part of Task #83		HF	HF	HF	HF	H		
13	70	Pitzer model			HF	HF	M - H			HF	HF	HF	HF	M - H		
14	52	In-Package Flow	LF	LF	LF		M			LF	LF	LF		H	Probably not implemented even for 2024 (so maybe only M)	
14	53	In-Package Chemistry	LF	LF	LF	LF	M	Assume some LF version of Task 53		HF	HF	HF	HF	H		
15	51	Cladding Degradation	LF	LF	LF		M	Assume some LF version of Task 51		HF	HF	HF		H		
16	86	Multi-Component Gas Transport	HF	HF	HF	HF	L – M			HF	HF	HF	HF		Assume complete by 2020	
17	26	Salinity gradient / Density stratification	HF	HF	HF	HF	L			HF	HF	HF	HF		Assume complete by 2020	
18	10	Salt Coupled THM processes	LF	LF	LF		H	LF = response surface by 2020		LF	LF	LF		H	Probably not complete at HF level even in 2024	
19	72	Surface processes and features	LF	LF	LF	LF	M			HF	HF	HF	HF	M - H		

Table 3-2 (cont.). *GDSA Tasks*: items from the *R&D Activities* table considered for integration into GDSA Framework in the timeframes 2017 to 2020 and 2020 to 2024.

	This sheet is linked to the R&D Activities sheet…	C = complete; LF = lower fidelity (or what can be done by 2020); HF = higher fidelity (see R&D Activities spreadsheet); ? = uncertain													
		By 2020 (e.g., *candidate sites* selected for evaluation)							By 2024 (e.g., *final site* selected)						
Priority	Task #	Process Model	Argillite	Crystalline	Salt	DBH (Cs/Sr)	2020 GDSA LOE	Notes	Status	Argillite	Crystalline	Salt	DBH (Cs/Sr)	2024 GDSA LOE	Notes	Status
		Conceptual Model														
TBD	73	Other missing FEPs (processes) SF-17SN01030401 SF-17SN01050402	X	X	X	X	M - H			X	X	X	X	H	Unclear how much effort required	
TBD	79	Disruptive events SF-17SN01030401 SF-17SN01050402	LF	LF	LF	LF	H+			HF	HF	HF	HF	H+	Significant conceptual model and implementation effort	
TBD	50	Biosphere pathways								HF	HF	HF	HF	H	Only needed after site selection	
		Numerical Implementation														
1	67	Numerical solution methods (analytical derivatives)	X	X	X	X	M								Assume complete by 2020	
2	62	QA, V&V (documentation and tests)	LF	LF	LF	LF	H			LF	LF	LF	LF	H	Effort depends on rigor desired	
3	78	PFLOTRAN improvements	X	X	X	X	L								Assume complete by 2020	
4	74	Implicit solution for decay and ingrowth	LF	LF	LF	LF	M	Note sure if this is the same as Task #75		HF	HF	HF	HF	H		
5	66	Operator splitting for reactive transport	X	X	X	X	L - M								Assume complete by 2020	
6	80	Species and element properties	X	X	X	X	L	Temperature-dependent solubilities							Assume complete by 2020	
7	80	Species and element properties	LF (no Z balance)	LF	LF	LF	L	Species-specific diffusivities		HF (Z balance)	HF	HF	HF	H		
8	65	Nested EBS, near-field, far-field models								HF	HF	HF	HF	H		
8	64	Grid refinement	LF	LF	LF	LF	M	Block grid		HF	HF	HF	HF	H	Octree AMR	
10	81	Solid solution model								HF	HF	HF	HF	H	Need to formulate the conceptual model	
		Parameters (from Testing)														
TBD	16	Diffusion of actinides through bentonite (including speciation)	LF	LF	LF	LF	L – M?			HF	HF	HF	HF	L – M?		
TBD	17	Thermodynamic and sorption database(s)	?	?	?	?	TBD			?	?	?	?	TBD	Unlikely that surface complexation is ever used directly in PA	

Table 3-3. *GDSA Timeline*: year-by-year model activity list for 2017, 2018, 2019, and 2020 specifying which items from the *GDSA Tasks* (Table 3-2) will be integrated into GDSA Framework between 2017 and 2020.

	This sheet is linked to the GDSA Tasks sheet...	GDSA LOE	Fraction of task	Status/ Notes
2017				
4	SNF Degradation	M		LF = Arrhenius; no FMDM till optimized
83	Waste Form-Canister-Buffer Discretization (1D -> 3D)	M	/2	ongoing; integrate with Carlos
63	Basic biosphere model	L		mostly done
67	Numerical solution methods (analytical derivatives)	M		mostly done
62	QA, V&V (documentation and tests)	H		ongoing, partly funded by WIPP

		GDSA LOE	Fraction of task	GDSA Priority	Status/ Notes
2018					
5	(Pseudo) Colloid-Facilitated Transport Model	M	/2	H	start this year
13	Simplified Representation of THMC processes in EBS (clay illitization)	M	/2	H	use GDSA reference case; LF = response surf
14	Simplified Representation of THM (BBM) model of buffer materials (unsaturated)	M	/2	H	use GDSA reference case; LF = response surf
10	Salt Coupled THM processes	H	/2	H	use GDSA reference case; LF = response surf
7	Discrete Fracture Network (DFN) Model	M - H	/3	H	real DFN w/ matrix diffusion & heat
68	Simplified Representation of Mechanical processes in PA	M		H	from Reedlunn? From WIPP, too? LF = response surf
83	Waste Form-Canister-Buffer Discretization (1D -> 3D)	M	/2	M	ongoing; integrate with Carlos
78	PFLOTRAN improvements	L		M	Checkpoint/restart capability for new process models
80	Species and element properties	L		M	temp-dependent solubilities
80	Species and element properties	L		M	Species-specific diffusivities
9	Waste Package Degradation Model (mechanistic)	L - M	/2	M	Start in 2018 for LC (include breach area)
70	Pitzer model	M - H	/2	L	Wolery version - do we have enough staff to do?
74	Implicit solution for decay and ingrowth	M		L	lower priority for 2018
62	QA, V&V (documentation and tests)	H		H	ongoing, partly funded by WIPP

		GDSA LOE	Fraction of task	GDSA Priority	Status/ Notes
2019					
6	Intrinsic Colloids	M			combine with pseudo-colloids
5	(Pseudo) Colloid-Facilitated Transport Model	M	/2	H	finish this year
13	Simplified Representation of THMC processes in EBS (clay illitization)	M	/2	H	use GDSA reference case; LF = response surf
14	Simplified Representation of THM (BBM) model of buffer materials (unsaturated)	M	/2	H	use GDSA reference case; LF = response surf
10	Salt Coupled THM processes	H	/2	H	use GDSA reference case; LF = response surf
15	Simplified Representation of Rigid-Body-Spring-Network (RBSN)	M			DRZ fractures (not needed in Pierre shale?) LF = response surf
7	Discrete Fracture Network (DFN) Model	M - H	/3	H	real DFN w/ matrix diffusion & heat
53	In-Package Chemistry	M	/2		Jerden's work?
69	Full Representation of Chemical processes in PA	M	/2		Carlos' model? Also, HeeHo
70	Pitzer model	M - H	/2	L	Wolery version - do we have enough staff to do?
9	Waste Package Degradation Model (mechanistic)	L - M	/2	M	Start in 2018 for LC (include breach area)
73	Other missing FEPs (processes) SF-17SN01030401 SF-17SN01050402	M - H	/2		Funding dependent
79	Disruptive events SF-17SN01030401 SF-17SN01050402	H+	/2		Funding dependent
66	Operator splitting for reactive transport	L - M		L	low priority
86	Multi-Component Gas Transport	L – M		L	low priority
64	Grid refinement	M	/2	L	low priority
62	QA, V&V (documentation and tests)	H		H	ongoing, partly funded by WIPP

		GDSA LOE	Fraction of task	GDSA Priority	Status/ Notes
2020					
7	Discrete Fracture Network (DFN) Model	M - H	/3	H	real DFN w/ matrix diffusion & thermal
53	In-Package Chemistry	M	/2		Jerden's work?
52	In-Package Flow	M			
69	Full Representation of Chemical processes in PA	M	/2		Carlos' model? Also, HeeHo
51	Cladding Degradation	M			
73	Other missing FEPs (processes) SF-17SN01030401 SF-17SN01050402	M - H	/2		Funding dependent
79	Disruptive events SF-17SN01030401 SF-17SN01050402	H+	/2		Funding dependent
72	Surface processes and features	M			
64	Grid refinement	M	/2	L	
62	QA, V&V (documentation and tests)	H			ongoing, partly funded by WIPP

3.2 Code and Process Model Development

In addition to planning future GDSA Framework development (Section 3.1), the GDSA group implemented several code improvements in FY 2017. They include:

- Section 3.2.1 – Analytical derivatives for improved convergence of flow and transport solutions (added)
- Section 3.2.2 – Numerous flow and transport validation tests, executed and documented (added)
- Section 3.2.3 – Biosphere model for ingestion of well water (added)
- Section 3.2.4 – Updated waste form process models (improved)
- Section 3.2.5 – Implicit solution for decay and ingrowth for the waste form (added)
- Section 3.2.6 – Other initiatives in progress

Progress made on the code and process models in FY 2017 is described in the subsections indicated.

3.2.1 Analytical Derivatives

To simulate multiphase flow, PFLOTRAN solves the nonlinear equations governing energy and mass conservation (Eqs. 3.2.1.1-3.2.1.9) over the entire problem domain using Newton's method.

$$\frac{\partial \phi \left(s_l \rho_l \chi_w^l + s_g \rho_g \chi_w^g \right)}{\partial t} = -\nabla \cdot \left(\rho_l \chi_w^l \boldsymbol{q}_l + \rho_g \chi_w^g \boldsymbol{q}_g + \boldsymbol{J}_w^l + \boldsymbol{J}_w^g \right) + q_w \quad \text{Eq. 3.2.1.1}$$

$$\frac{\partial \phi \left(s_l \rho_l \chi_a^l + s_g \rho_g \chi_a^g \right)}{\partial t} = -\nabla \cdot \left(\rho_l \chi_a^l \boldsymbol{q}_l + \rho_g \chi_a^g \boldsymbol{q}_g + \boldsymbol{J}_a^l + \boldsymbol{J}_a^g \right) + q_a \quad \text{Eq. 3.2.1.2}$$

$$\frac{\partial \phi \left(s_l \rho_l U_l + s_g \rho_g U_g \right) + (1-\phi) C_p^{rock} \rho_{rock} T}{\partial t} = -\nabla \cdot \left(\rho_l H_l \boldsymbol{q}_l + \rho_g H_g \boldsymbol{q}_g - k_{eff} \nabla \mathrm{T} \right) + q_e \quad \text{Eq. 3.2.1.3}$$

$$\boldsymbol{q}_l = -\frac{k k_{rl}}{\mu_l} \nabla (p_l - \gamma_l g z) \quad \text{Eq. 3.2.1.4}$$

$$\boldsymbol{q}_g = -\frac{k k_{rg}}{\mu_g} \nabla \left(p_g - \gamma_g g z \right) \quad \text{Eq. 3.2.1.5}$$

$$\boldsymbol{J}_a^l = -\tau \phi s_l D_l \rho_l \nabla \chi_a^l \quad \text{Eq. 3.2.1.6}$$

$$\boldsymbol{J}_a^g = -\tau \phi s_g D_g^0 \left(\frac{T}{T_K} \right)^{\theta} \frac{p_0}{p_g} \rho_g \nabla \chi_a^g \quad \text{Eq. 3.2.1.7}$$

$$\boldsymbol{J}_w^l = 1 - \boldsymbol{J}_a^l \quad \text{Eq. 3.2.1.8}$$

$$\boldsymbol{J}_w^g = 1 - \boldsymbol{J}_a^g$$

Eq. 3.2.1.9

where

C_p^{rock} = rock heat capacity [MJ/kg rock-K]
D_l = liquid diffusivity [m^2/sec]
D_g^0 = gas diffusivity at reference temperature T_K and pressure p_0 [m^2/sec]
g = gravity [m/sec^2]
H_l = liquid phase enthalpy [MJ/kmol]
H_g = gas phase enthalpy [MJ/kmol]
$\boldsymbol{J}_w^l$ = water diffusive flux in liquid phase [kmol/m^2-sec]
$\boldsymbol{J}_w^g$ = water diffusive flux in gas phase [kmol/m^2-sec]
$\boldsymbol{J}_a^l$ = air diffusive flux in liquid phase [kmol/m^2-sec]
$\boldsymbol{J}_a^g$ = air diffusive flux in gas phase [kmol/m^2-sec]
k_{eff} = effective thermal conductivity [W/K-m]
k = intrinsic permeability [m^2]
k_{rl} = relative permeability for liquid phase [-]
k_{rg} = relative permeability for gas phase [-]
q_l = water source/sink [kmol/sec]
q_g = gas source/sink [kmol/sec]
q_e = energy source/sink [MJ/sec]
$\boldsymbol{q}_l$ = liquid phase Darcy flux [m/sec]
$\boldsymbol{q}_g$ = gas phase Darcy flux [m/sec]
s_l = liquid phase saturation [-]
s_g = gas phase saturation [-]
U_l = liquid phase internal energy [MJ/kmol]
U_g = gas phase internal energy [MJ/kmol]
z = elevation [m]
γ_l = liquid phase density [kg/m^3]
γ_g = gas phase saturation [kg/m^3]
θ = exponential term in gas diffusive flux [-]
μ_l = liquid viscosity [Pa-sec]
μ_g = gas viscosity [Pa-sec]
ρ_l = liquid phase density [kmol/m^3]
ρ_g = gas phase density [kmol/m^3]
ρ_{rock} = rock particle density [kg/m^3 rock]
τ = tortuosity [-]
ϕ = effective porosity [-]
χ_w^l = mole fraction of water in liquid phase [-]

χ_w^g = mole fraction of water in gas phase [-]
χ_a^l = mole fraction of air in liquid phase [-]
χ_a^g = mole fraction of air in gas phase [-]

Eqs. 3.2.1.1 and 3.2.1.2 are mass conservation equations for the water and air components in the system summed over the liquid and gas phases. Eq. 3.2.1.3 is the energy conservation for the liquid, gas, and rock phases in the system. Eqs. 3.2.1.4 and 3.2.1.5 define the Darcy flux for the liquid and gas phases while Eqs. 3.2.1.6-3.2.1.9 define the diffusive fluxes of the water and air components in each phase.

Within PFLOTRAN, these nonlinear equations are discretized using the finite volume method with backward Euler time discretization. The three primary dependent variables (also referred to as unknowns or degrees of freedom [dofs]) are chosen based on the state of the system in each grid cell, as outlined in Table 3-4. For instance, when both the liquid and gas fluid phases exist in a grid cell (two phase state), the cell's primary dependent variables are gas pressure, gas saturation and temperature.

Table 3-4. Primary dependent variables as a function of the state of the system.

Single Phase Liquid State	Single Phase Gas State	Two Phase State (Liquid and Gas)
Liquid Pressure (p_l)	Gas Pressure (p_g)	Gas Pressure (p_g)
Air mole fraction in liquid phase (χ_a^l)	Air Partial Pressure (p_a)	Gas Saturation (s_g)
Temperature (T)	Temperature (T)	Temperature (T)

To illustrate the steps of Newton's method, suppose there is a nonlinear polynomial $f(x)$ that is a function of primary dependent variable x, as show in Eq. 3.2.1.10.

$$f(x) = 1 + x + x^2 + x^3 + \cdots + x^n = 0 \qquad \text{Eq. 3.2.1.10}$$

and illustrated as the red line in Figure 3-6.

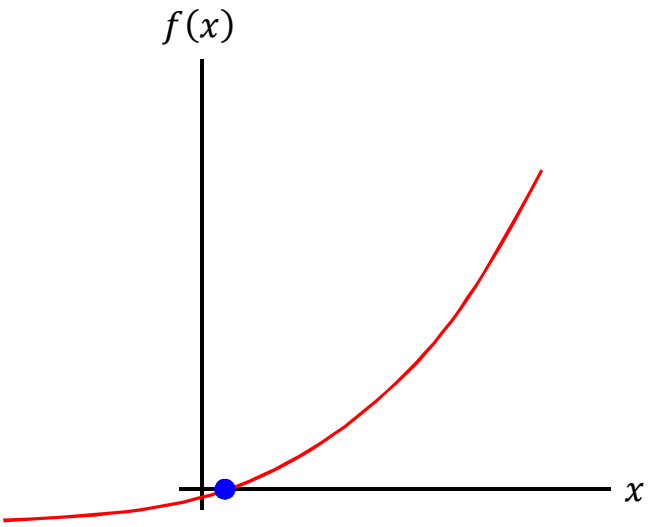

Figure 3-6. A nonlinear polynomial $f(x)$ with a solution ($f(x) = 0$) at the blue dot.

The goal of Newton's method is to find the value for x at which $f(x) = 0$, depicted by the blue dot in Figure 3-6. This is achieved by repeatedly calculating derivatives along the curve and updating the estimated value for x. The derivative of $f(x_1)$ for a given value x_1, represented by $f'(x_1)$, is equal to the tangent to the curve at x_1, and an updated value x_2 can be calculated by dividing $f(x_1)$ by its derivative as shown in Figure 3-7. These steps constitute a single Newton iteration.

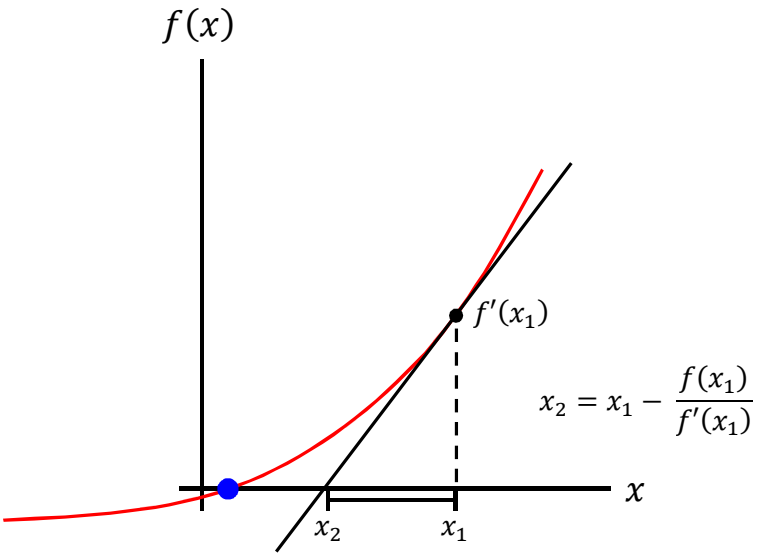

Figure 3-7. A single Newton iteration updated to x_1 as a function of it derivative $f'(x_1)$.

In general terms, the update of x for the i^{th} iteration of Newton's method is calculated as

$$x_{i+1} = x_i - \frac{f(x_i)}{f'(x_i)}.$$

Eq. 3.2.1.11

Newton iteration (updates to x_i) continues until the magnitude of $f(x_i)$ is below a prescribed threshold or tolerance as shown in Figure 3-8, at which point it "converges". Therefore, in order to employ Newton's method in the nonlinear solution of an equation, the derivatives of the nonlinear function must be available at any point along x. Newton derivatives can be calculated analytically or numerically as shown below.

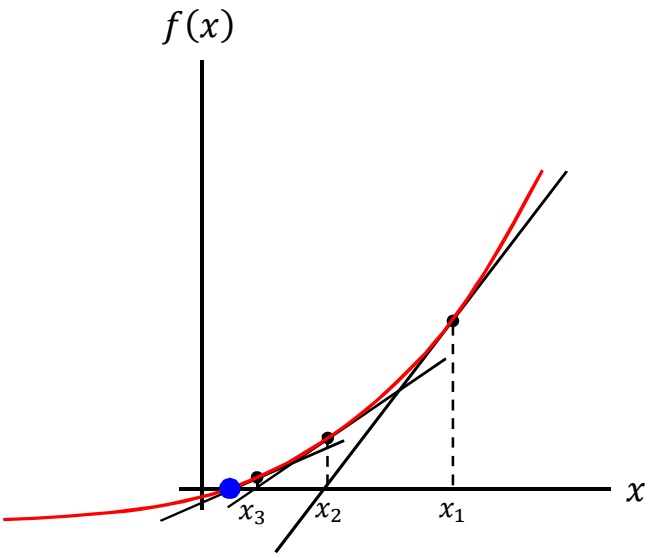

Figure 3-8. Multiple successive Newton updates for x.

To illustrates the calculation of derivatives, consider the functional relationship

$$f(x) = x^2$$

Eq. 3.2.1.12

Using basic calculus, the analytical derivative is calculated as

$$f'(x)_{analytical} = 2x$$

Eq. 3.2.1.13

To calculate the same derivative numerically, one may use perturbation theory, which for this simple equation simplifies to the fundament theorem for calculus,

$$f'(x)_{numerical} = \frac{f(x + \Delta x) - f(x)}{\Delta x}$$

Eq. 3.2.1.14

Given the function in Eq. 3.2.1.12,

$$f'(x)_{numerical} = \frac{(x + \Delta x)^2 - x^2}{\Delta x}$$

Eq. 3.2.1.15

The accuracy of a numerical derivative is highly dependent upon the size of Δx. If Δx is too large or too small, the derivative may lose accuracy. Take for instance $x = 0.5$ and $\Delta x = 0.25$, the resulting numerical derivative of 1.25

$$f'(x)_{numerical} = \frac{f(x + \Delta x) - f(x)}{\Delta x} = \frac{(x + \Delta x)^2 - x^2}{\Delta x} = \frac{(0.5 + 0.25)^2 - 0.5^2}{0.25} = 1.25$$

Eq. 3.2.1.16

is much larger than the analytical derivative of 1.0

$$f'(x)_{analytical} = 2(0.5) = 1.0.$$

Eq. 3.2.1.17

Table 3-5 illustrates the improved accuracy of the numerical derivative as the perturbation decreases in size where a perturbation of 1.e-6 provides superior accuracy relative to the 0.25 (above). It should be noted that if the perturbation becomes too small, the calculation of the derivative can become numerically unstable due to cancellation, overflow and/or underflow. Therefore, care must be taken in choosing an appropriate perturbation size.

Table 3-5. Comparison of the accuracy of analytical and numerical derivatives as a function of perturbation size (Δx).

x	$f(x)$	$f'(x)_{analytical}$	Δx	$f(x+\Delta x)$	$f'(x)_{numerical}$
0.5	0.25	1	10^{-1}	0.36	1.1
0.5	0.25	1	10^{-3}	0.251001	1.001
0.5	0.25	1	10^{-6}	0.250001000001	1.000001

The calculation of analytical derivatives can also be problematic. For functions with discontinuities as shown in Figure 3-9, the derivative is undefined at the discontinuity, and without smoothing (e.g. a polynomial fit through the discontinuity with matching derivatives on either side) the nonlinear solver can oscillate around the discontinuity should the solution be close it. Examples of functions with discontinuities include constitutive relations such as the Brooks-Corey capillary pressure function where the capillary pressure is nonzero at a liquid saturation of 1, or inhibited biogeochemical reaction rates where the effective rate is zeroed below limiting threshold concentrations.

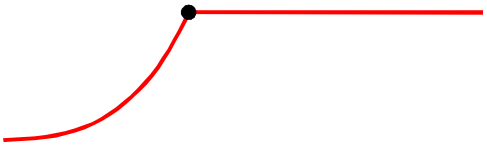

Figure 3-9. Schematic of a function with a discontinuity.

Analytical derivatives are also more challenging to implement within the simulation code. With numerical derivatives, only the function $f(x)$ needs to be encoded as the same function is evaluated with a perturbed input for the derivative calculation, while all variants of the analytical derivative must be implemented. For complex nonlinear equations, where many variables within the equation are nonlinear functions of the primary variables and/or variables are inter-coupled, accounting for all variants of the derivatives can be challenging.

For multiphase flow, where PFLOTRAN is solving the partial differential equations (PDEs) for energy and mass conservation for N grid cells in the problem domain, there are $3 \times N$ equations and unknowns in the problem. Three discretized residual equations $\boldsymbol{f}(\boldsymbol{x})$ are formed at each grid cell and the resulting system of PDEs that must be solved as a nonlinear system PDE. Linear updates are calculated by solving the linear system

$$\boldsymbol{J}\boldsymbol{\delta x} = -\boldsymbol{f}(\boldsymbol{x})$$

Eq. 3.2.1.18

where $\boldsymbol{J}$ is a Jacobian, the derivative of the discrete residual vector $\boldsymbol{f}(\boldsymbol{x})$ with respect to all unknowns in the system, and $\boldsymbol{\delta x}$ is the update to the unknowns in the system. Note that $\boldsymbol{\delta x}$ and $\boldsymbol{f}(\boldsymbol{x})$ are vectors while $\boldsymbol{J}$ is a sparse matrix with block diagonal fill corresponding to cell-to-cell coupling in the problem domain.

To illustrate the complexity in calculating the derivatives for the multiphase problem, consider the discrete form of the water mass conservation equation (Eq. 3.2.1.1) for a two-phase state where the primary dependent variables are gas pressure (p_g), gas saturation (s_g) and temperature(T).

$$\frac{V}{\Delta T}\left[\left(\phi\left(s_l\rho_l\chi_w^l + s_g\rho_g\chi_w^g\right)\right)^{k+1} - \left(\phi\left(s_l\rho_l\chi_w^l + s_g\rho_g\chi_w^g\right)\right)^{k}\right]$$
$$- \sum A\rho_l\chi_w^l\frac{kk_{rl}}{\mu_l}\left(\frac{p_l^{i+1} - p_l^i}{\Delta x} - \gamma_l gz\right) - \sum A\rho_g\chi_w^g\frac{kk_{rg}}{\mu_g}\left(\frac{p_g^{i+1} - p_g^i}{\Delta x} - \gamma_g gz\right)$$
$$- \sum A\tau\phi s_l D_l\rho_l\left(\frac{{\chi_w^l}^{i+1} - {\chi_w^l}^{i}}{\Delta x}\right) - \sum A\tau\phi s_g D_g^0\left(\frac{T}{T_K}\right)^{\theta}\frac{p_0}{p_g}\rho_g\left(\frac{{\chi_w^g}^{i+1} - {\chi_w^g}^{i}}{\Delta x}\right) - q_w = 0$$

Eq. 3.2.1.19

The variables shown in red are dependent upon gas pressure. The blue box encompasses water component mass transfer due to Darcy fluxes in the liquid and gas phases. The derivative equation for the Darcy fluxes (e.g., $F_{w,i}^{Darcy}$) with respect to the gas pressure in the upwind cell $(p_{g,up})$ is composed of eight partial derivatives (one each for the density, water component mole fraction, viscosity and pressure gradient in the liquid and gas phases) as shown in red below.

$$\frac{\partial F_{w,i}^{Darcy}}{\partial p_{g,up}} = -A\left(\rho_{l_{p_{g,up}}}\chi_w^l\frac{kk_{rl}}{\mu_l}\left(\frac{p_{l_{dn}} - p_{l_{up}} - \gamma_l gz}{\Delta x}\right) + \rho_l\chi_{w_{p_{g,up}}}^l\frac{kk_{rl}}{\mu_l}\left(\frac{p_{l_{dn}} - p_{l_{up}} - \gamma_l gz}{\Delta x}\right)\right.$$
$$+ \rho_l\chi_w^l\left(-\frac{kk_{rl}}{{\mu_l}^2}\mu_{l_{p_{g,up}}}\right)\left(\frac{p_{l_{dn}} - p_{l_{up}} - \gamma_l gz}{\Delta x}\right) + \rho_l\chi_w^l\frac{kk_{rl}}{\mu_l}\left(\frac{-p_{l_{dn}p_{g,up}} - \gamma_{l_{p_{g,up}}}gz}{\Delta x}\right)$$
$$+ \rho_{g_{p_{g,up}}}\chi_w^g\frac{kk_{rg}}{\mu_g}\left(\frac{p_{g_{dn}} - p_{g_{up}} - \gamma_g gz}{\Delta x}\right) + \rho_g\chi_{w_{p_{g,up}}}^g\frac{kk_{rg}}{\mu_g}\left(\frac{p_{g_{dn}} - p_{g_{up}} - \gamma_g gz}{\Delta x}\right)$$
$$\left.+ \rho_g\chi_w^g\left(-\frac{kk_{rg}}{{\mu_g}^2}\mu_{g_{p_{g,up}}}\right)\left(\frac{p_{g_{dn}} - p_{g_{up}} - \gamma_g gz}{\Delta x}\right) + \rho_g\chi_w^g\frac{kk_{rg}}{\mu_g}\left(\frac{-1 - \gamma_{g_{p_{g,up}}}gz}{\Delta x}\right)\right)$$

Eq. 3.2.1.20

The implementation of these derivatives within the PFLOTRAN Fortran source code (with minor modifications for clarity) is as follows:

```
case(TWO_PHASE_STATE)
  ! derivative water equation wrt gas pressure
  ! pl = pg - pc and dpl_dpg = 1.  Therefore, we can use all the
  !   liquid pressure derivatives.
  ! derivative total mole flux for liquid phase wrt gas pressure
  J(1,1) = xmol(water_component_id,liquid_phase) * &
    ! ave. liquid density
    (q * ddensity_ave_dden_up * gen_auxvar_up%d%denl_pl + &
    ! liquid mobility
      up_scale * tot_mole_flux / mobility * gen_auxvar_up%d%mobilityl_pl + &
    ! liquid pressure gradient
      tot_mole_flux_ddel_pressure * ddelta_pressure_dpup) + &
    ! water mole fraction in liquid_phase
    up_scale * tot_mole_flux * &
      gen_auxvar_up%d%xmol_p(water_component_id,liquid_phase) +
    xmol(water_component_id,gas_phase) * &
    ! ave. gas density
    (q * ddensity_ave_dden_up * gen_auxvar_up%d%deng_pg + &
    ! gas mobility
      up_scale * tot_mole_flux / mobility * gen_auxvar_up%d%mobilityg_pg + &
    ! gas pressure gradient
      tot_mole_flux_ddel_pressure * ddelta_pressure_dpup) + &
    ! water mole fraction in gas phase
    up_scale * tot_mole_flux * gen_auxvar_up%d%xmol_p(water_component_id,gas_phase)
```

This code covers 2/5th of the derivatives in Eq. 3.2.1.19. Considering that there are three primary dependent variables, three equations, three states, and the opposite side of the flux $(p_{g,dn})$, there are approximately 135 times as many derivatives yet to calculate:

$$\sim \frac{5}{2} \times 3 \times 3 \times 3 \times 2 = 135 \, .$$

The table in Figure 3-10, extracted from the PFLOTRAN design documentation, further illustrates the complexity of dependent variable coupling. The table lists the primary dependent variables for each state, and through X marks the dependence of secondary variables listed in the left column. The two-phase state is shown on the right-hand-side where most secondary variables are shown to be dependent upon gas pressure and temperature, whereas only capillary pressure (p_c), liquid saturation and the relative permeabilities are dependent upon gas saturation. Overall, the LaTeX formatted PFLOTRAN design document for multiphase analytical derivatives contains over 38 pages of derivatives.

To demonstrate the influence of analytical versus numerical derivatives on multiphase simulation performance, the gas injection regression tests within the PFLOTRAN repository (PFLOTRAN_DIR/regression_tests/general/gas_injection*.in) were run with increasingly tight solver tolerances on the two-norm of the residual. Figure 3-11 is a schematic of the problem where a gas injection well is centerline in the lower portion of a liquid saturated 9×10 m^2 domain. A zone of lower permeability is shown immediately above the injection point forcing the buoyant gas to flow around in its upward migration. The one-year simulation runs quickly and is effective in demonstrating solver performance with the two approaches to calculating derivatives.

The purpose of demonstrating performance with decreasing (tighter) solver tolerances is to demonstrate that increasingly accurate derivatives are needed to converge to a solution quickly. The results presented

in Table 3-6 and Figure 3-12 demonstrate that for the default tolerance of 1.e-8, the analytical simulation ran in 1.36 seconds, slightly faster than the numerical's 1.99 seconds. As solver tolerances are tightened to 1.e-9, the simulations take slightly more time, but the analytical simulation significantly outperforms the numerical by a factor of three, and the numerical simulation fails at tighter tolerances.

A comparison in Table 3-7 for a defense waste version of the large scale repository documented in Section 4.5.1 of this report demonstrates that for a large nuclear waste repository composed of thousands of (nuclear) waste packages, 10.8 million grid cells (32.7 million unknowns altogether) and executed on 1024 processes, PFLOTRAN's analytical derivative implementation outperforms the numerical again by a factor of three, taking 1.37 hours to the numerical's 4.05. PFLOTRAN's analytical implementation of derivatives clearly outperforms the numerical variant.

	State								
	Liquid			Gas			Two Phase		
Variable	p_l	X_a^l	T	p_g	p_a	T	p_g	s_g	T
p_l	—						X	X	
p_g				—			—		
p_a					—		X		X
p_c								X	
p_v				X	X				X
p_s						X			X
s_l								X	
s_g								—	
K_H						X			X
ρ_l	X		X				X		X
ρ_g				X	X	X	X		X
T			—			—			—
H_l	X		X				X		X
H_g				X	X	X	X		X
H_v				X	X	X			X
H_a					X	X	X		X
U_l	X		X				X		X
U_g				X	X	X	X		X
U_v				X	X	X			X
U_a					X	X	X		X
ρ_v				X	X	X			X
ρ_a					X	X	X		X
X_w^l		X					X		X
X_a^l		—					X		X
X_w^g				X	X		X		X
X_a^g				X	X		X		X
μ_l	X		X				X		X
μ_g				X	X	X	X		X
k_{rl}								X	
k_{rg}								X	
ϕ	X		X	X		X	X		X

Figure 3-10. A table extracted from the PFLOTRAN design documentation listing the coupling (X) of each primary variable for each state to the secondary variables in the problem. The dash (–) indicates that the primary and secondary variable are identical.

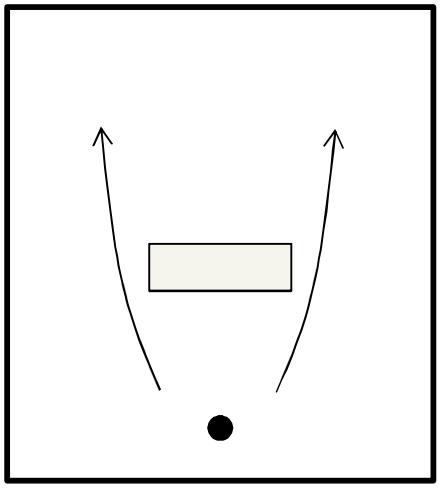

Figure 3-11. Schematic of gas injection scenario.

Table 3-6. Comparison of performance for the gas injection scenario using analytical and numerical derivatives, where analytical derivatives out-perform numerical by a factor of three at tight tolerances.

L^2-norm	Analytical Derivatives				Numerical Derivatives			
Tolerance	# Time Steps	# Newton Iterations	# Time Step Cuts	Time [s]	# Time Steps	# Newton Iterations	# Time Step Cuts	Time [s]
1e-8	185	576	7	1.36	185	577	7	1.99
5e-9	185	593	7	1.35	185	595	7	1.97
2e-9	179	581	5	1.42	179	583	5	1.97
1.5e-9	211	818	14	1.78	206	770	13	2.46
1e-9	206	770	13	1.86	425	1877	51	5.65
5e-10	211	837	14	1.82	Did not finish			

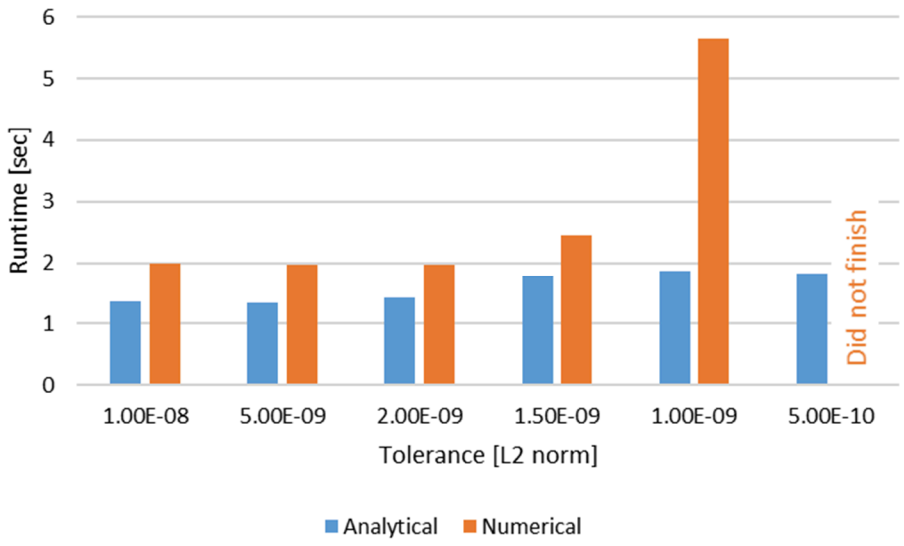

Figure 3-12. Comparison of the gas injection scenario runtimes for analytical and numerical derivatives as a function of the nonlinear solver tolerance [L^2 norm].

Table 3-7. Comparison of analytical and numerical derivative performance for a large hypothetical defense waste repository composed of 10.8M grid cells and 32.7M unknowns (total) and run on 1024 processes. Simulations run with analytical derivatives are three times faster.

	# Time Steps	# Newton Iterations	# Linear Iterations	# Time Step Cuts	Time [h]
Analytical	684	2790	544,632	61	1.37
Numerical	1617	6003	1,692,396	85	4.05

To assess any differences between the solution generated with analytical and numerical derivatives, the temperature at an observation point downgradient from the repository was monitored over time. Figure 3-13 shows that there is little difference between the two solutions. The results are essentially identical.

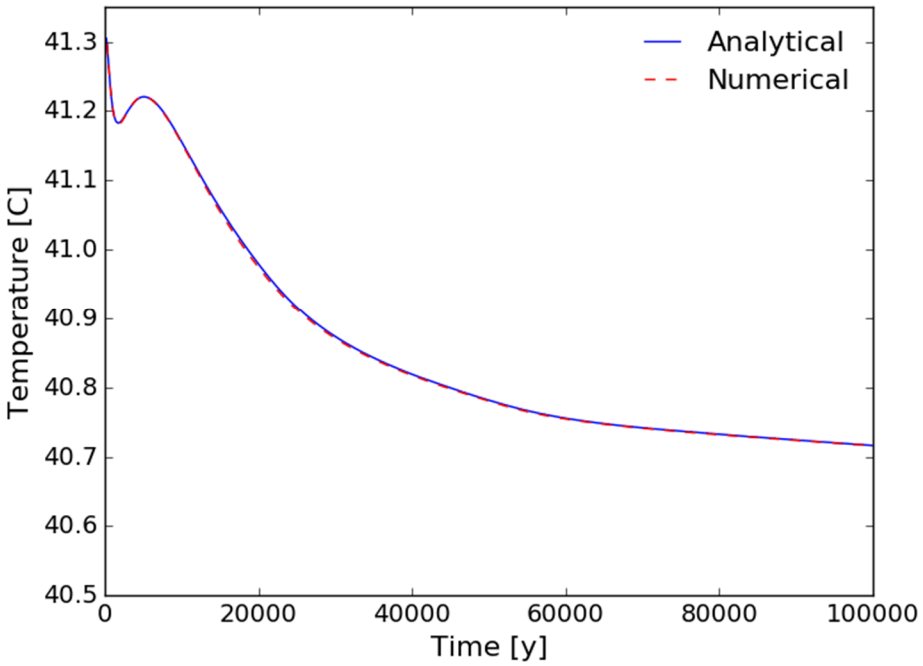

Figure 3-13. Temperature at a well downgradient from a hypothetical nuclear waste repository simulated separately with analytical and numerical derivatives for multiphase flow. The comparison illustrates that there is little difference in solution for both scenarios.

3.2.2 Verification Testing for Flow and Transport in PFLOTRAN

In scientific computing, code verification ensures the reliability and numerical accuracy of a model simulation by comparing the simulation results to experimental data or known analytical solutions. The model is typically defined by a set of partial differential equations with initial and boundary conditions, and verification ensures whether the mathematical model is solved correctly by the software. Code verification is especially important if the software is used to model high-consequence systems which cannot be physically tested in a fully representative environment (Oberkampf and Trucano 2007), which is directly relevant to the GDSA's objective. Justified confidence in a particular computational tool requires clarity in the exercised physics and transparency in its verification process with proper documentation.

This FY, a new quality assurance (QA) testing suite has been developed that performs code verification for several basic processes in PFLOTRAN. The goal is to test each basic process, such as fluid flow, gas flow, heat transfer, mass transfer, radionuclide decay, density driven convection, etc., by developing the test suite to compare the numerical solution of benchmark problems against the known, closed-form, analytical solution for each process. An additional requirement is the documentation of the tests or benchmark problems, with emphasis on documenting how error is evaluated.

3.2.2.1 Challenges and Limitations

The verification strategy taken so far comes with some limitations. By using analytical solutions to benchmark problems as a comparison metric, the benchmark problems must remain simple. Complex problems with coupled physical processes often do not have analytical solutions. More complicated verification methods do exist, such as the Method of Manufactured Solutions (Roache 2002), for

benchmarks without analytical solutions, but these methods are beyond the scope of the testing suite developed so far.

Not all errors arise because the software is incorrectly solving the mathematical model. Another challenge in test suite development relates to the discretization process. When solving a problem numerically, the domain is discretized into finite pieces (e.g., the grid or mesh), and properties of the material such as the permeability, porosity, etc., which are naturally continuous, are described as discrete values typically at the center of each grid cell. The averaging scheme used to interpolate the material property value between discrete points (e.g. arithmetic vs. harmonic schemes) can contribute to differences between an analytical solution and the numerical simulation results. Moreover, when a grid cell contains several materials or components, the mixture model used to describe the effective mixture property values can also contribute to error. Similarly, time discretization can lead to error for unsteady problems if boundary conditions or source/sink terms are described in a continuous form in the analytical benchmark problem, but must be discretized in the simulator. While many of these challenges can be mitigated by increasing grid resolution, and decreasing the time step, one hits a limit in computational cost and practicality.

3.2.2.2 QA Testing Suite Development

The test suite consists of a hierarchical structure of tests, where each test, or benchmark problem, has a well-defined analytical solution. So far this FY, 52 tests have been developed and implemented, with several more anticipated next FY. A PFLOTRAN input deck is created for each test. An accompanying Python script analyzes the simulation output of each test, and compares it against the analytical solution, while also generating a plot figure. A test is considered passing if the maximum relative error is < 2%. The suite of tests is executed with a Bash script that is run using a terminal.

The hierarchical structure is shown in Figure 3-14. The highest structural level is defined by the physical process that is being tested. To date, the process types that have been tested so far are: heat conduction, single-phase liquid fluid flow, and single-phase gas fluid flow. Many of the benchmarks have been obtained from Kolditz et al. (2015). For each type of physical process, several problem formulations should be tested, which include steady and transient solutions, problems that test all three dimensions, the two types of boundary condition formulations (e.g., Neumann and Dirichlet types), initial conditions for primary dependent variables, and each applicable PFLOTRAN flow mode (e.g. governing equation).

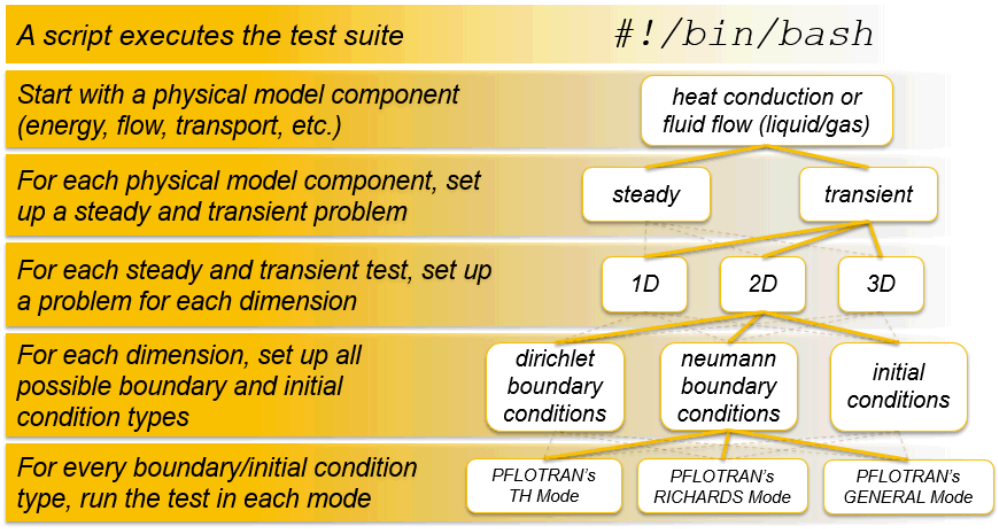

Figure 3-14. PFLOTRAN's QA test suite work flow.

At least 108 tests are required for the three physical processes, following the hierarchical structure shown in Figure 3-14. Adding more physical processes into the test suite will grow the number of tests proportionately. The large number of tests requires a non-trivial amount of effort to organize, maintain, and keep documentation current. To help streamline these efforts, version control for the set of scripts and input decks required to run the test suite, as well as the documentation, is achieved using Mercurial and is hosted on Bitbucket at https://bitbucket.org/pflotran/pflotran-doc-sandbox.

Each test is formally documented using the documentation program Sphinx (http://www.sphinx-doc.org). Documentation contains a mathematical description of the benchmark problem. Each time the test suite is executed, Sphinx automatically inserts the error comparison plot generated when executing the testing suite, the latest snapshot of the input deck required to run the problem, and the python script required to analyze the simulation results against the analytical solution. A more succinct form of test results can be viewed in the report card that is additionally generated each time the test suite is run. The report card gives the maximum relative error for each test, and an overall grade (see Figure 3-15). The current test suite documentation is available at http://www.documentation.pflotran.org/index.html#qa-test-suite. Figure 3-16 and Figure 3-17 show brief summaries of two of the tests, as an example.

```
....
/qa_tests/flow/transient/1D/BC_1st_2nd_kind/general_mode
maximum relative error: 0.04326830166l3%
Test PASS

/qa_tests/flow/transient/2D/BC_1st_2nd_kind/general_mode
maximum relative error: 1.84688258926%
Test PASS

/qa_tests/flow/transient/1D/BC_1st_kind/richards_mode
maximum relative error: 0.306751604017%
Test PASS

/qa_tests/flow/transient/1D/BC_2nd_kind/richards_mode
maximum relative error: 0.126000547719%
Test PASS

/qa_tests/flow/transient/1D/BC_1st_2nd_kind/richards_mode
maximum relative error: 0.04326830166l3%
Test PASS

/qa_tests/flow/transient/2D/BC_1st_2nd_kind/richards_mode
maximum relative error: 1.84683383281%
Test PASS

/qa_tests/gas/steady/1D/BC_1st_kind/general_mode
maximum relative error: 0.189771819005%
Test PASS

/qa_tests/gas/steady/1D/BC_1st_2nd_kind/general_mode
maximum relative error: 0.04270850300l3%
Test PASS

/qa_tests/gas/steady/2D/BC_1st_2nd_kind/general_mode
maximum relative error: 0.488813148902%
Test PASS

/qa_tests/gas/steady/3D/BC_2nd_kind/general_mode
maximum relative error: 9.43099918674%
Test FAIL

--------------------------
Total number of tests: 52
Passing tests: 49
Failing tests: 3
Grade: A
```

Figure 3-15. QA testing suite report card.

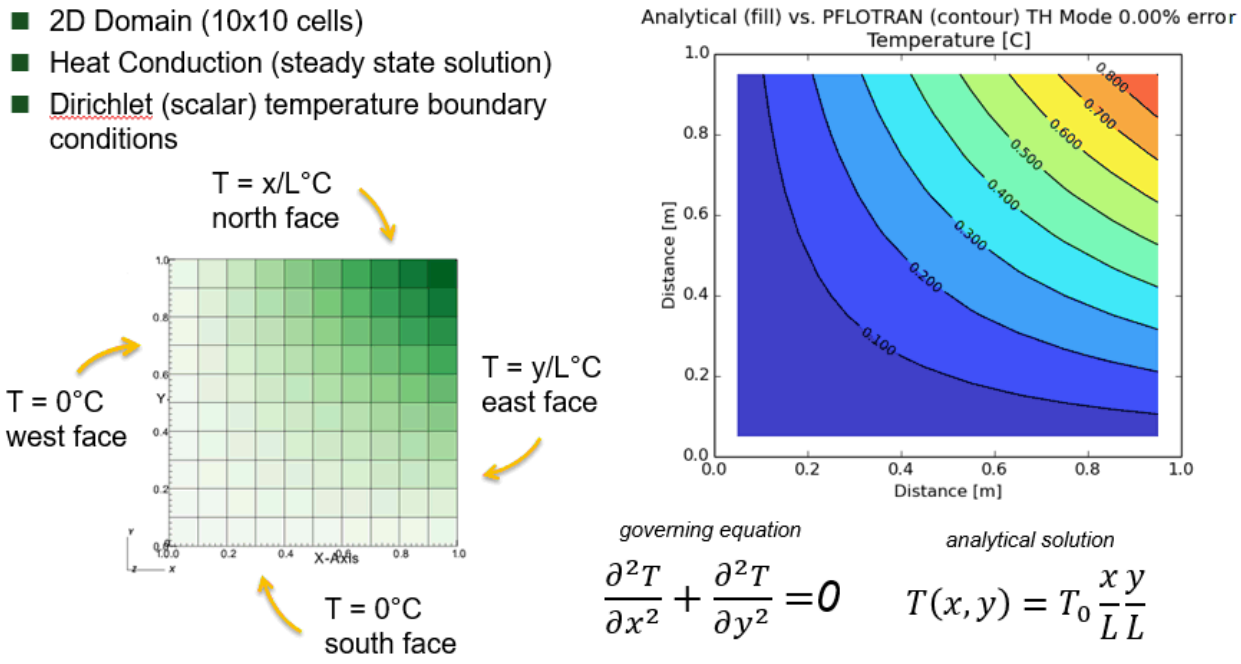

Figure 3-16. Two-dimensional steady state heat conduction benchmark with Dirichlet boundary conditions.

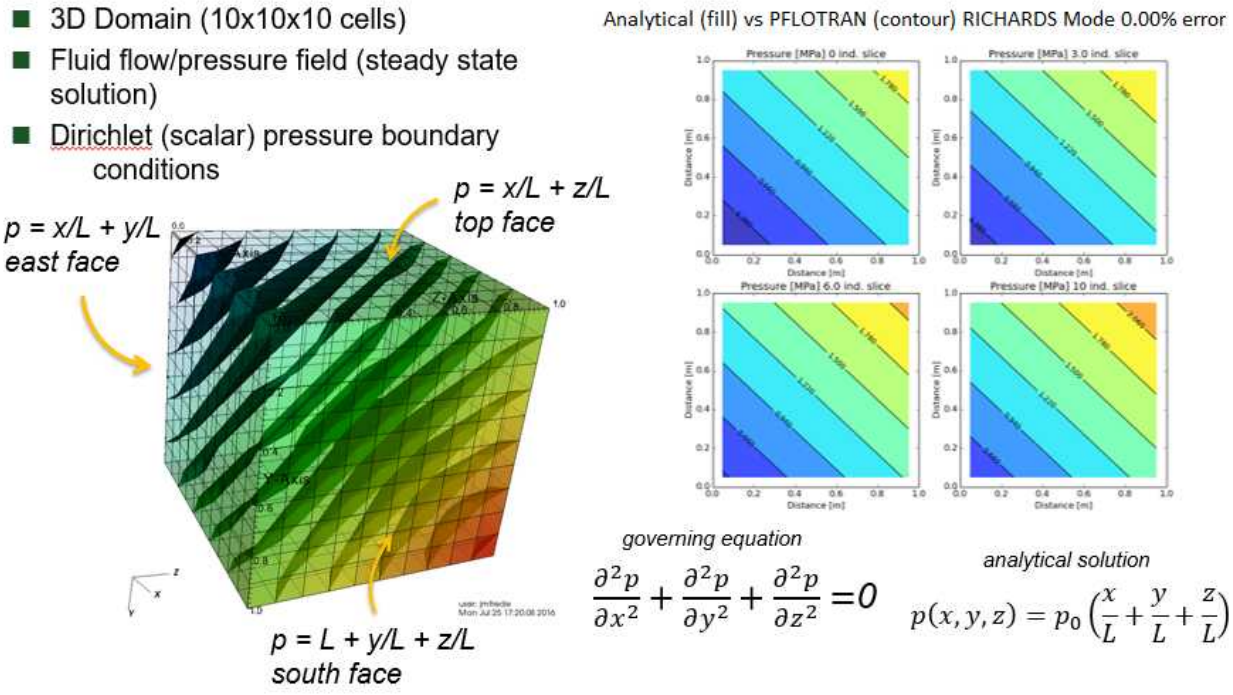

Figure 3-17. Three-dimensional steady state fluid flow (pressure field) benchmark with Dirichlet boundary conditions.

3.2.2.3 Ongoing Development

During the initial development of the testing suite, choices had to be made for the spatial and temporal discretization when defining the grid and time step size (for transient problems) in each test. These

choices were made using previous experience, but were also partly based on limiting the wall clock time for each simulation. It turned out that several tests (> 50%) were failing using this reasoning. After further investigation, it was found that the majority of failing tests had grids that were too coarse, or time steps that were too large. A systematic reduction in the grid spacing and time step size, by trial and error, was required for the tests to pass.

This experience exemplifies the importance of convergence studies, which are studies that show how numerical error decreases as the grid spacing and time step size go to zero. We are now in the process of re-organizing the python scripts which execute the current test suite, so that an automatic converge test can be run for each test within the test suite (optionally specified by a user keyword). Rather than running each test from a single input deck that contains a single "hard-coded" grid description and time stepping criterion, several input decks will be written automatically using a python script. The only difference in the input decks will be the grid and time stepping criterion. The first convergence test will begin with a coarse grid. If the test fails, then the grid spacing and time step size will be cut in half, and the test will be re-run. This process will be repeated until the test passes. Just like the plot that is automatically generated which compares the simulation solution against the analytical solution, a second plot will be generated which shows the error behavior as the grid resolution and time step size are decreased.

3.2.3 Reference Biosphere 1 – Well Water Ingestion Dose Model

An important metric in repository safety assessment is the annual dose rate to a human from radionuclides escaping the repository. In FY 2017, a well water ingestion dose model, called Reference Biosphere 1 (RB1), was built into the GDSA Framework PFLOTRAN code. RB1 calculates the ingestion dose rate for a person regularly consuming contaminated well water. RB1 does not include dose due to inhalation of volatile radionuclides degassing from the well water, which is an additional process that may be added at a later date.

As in the model of Olszewska-Wasiolek and Arnold (Olszewska-Wasiolek and Arnold 2011), the RB1 model includes dose due to "unsupported" radionuclides that are redistributed between aqueous and solid phases. Unsupported radionuclides are descendants in a decay chain that are not explicitly modelled in the transport calculations due to short half-lives. To include them in the dose calculation, the RB1 model must first calculate the aqueous concentrations of the unsupported radionuclides. While total concentrations of unsupported radionuclides in the aquifer are considered to be in secular equilibrium with supporting ancestors, aqueous concentrations further depend on emanation efficiency and relative adsorption. If these additional effects are not considered, dose rates can be extremely underestimated, as demonstrated below for ^{222}Rn.

3.2.3.1 Model Equations

The dose rate $H_{E,i}$ (Sv yr^{-1}) for a supported radionuclide i, such as ^{226}Ra, is calculated using the equation

$$H_{E,i} = \ddot{C}_{w,i} * I * dcf_i \qquad \text{Eq. 3.2.3.1}$$

where $\ddot{C}_{w,i}$ is the aqueous concentration (Bq m^{-3}), I is the consumption rate (e.g., 2 L day^{-1}), and dcf_i is the ingestion dose coefficient (Sv Bq^{-1}). This equation is identical to the dose equation in the IAEA Example Reference Biosphere (ERB) Model 1 (IAEA 2003). The equivalent equation for an unsupported radionuclide u is

$$H_{E,i,u} = \ddot{C}_{w,i}\epsilon_u\varphi_u * I * dcf_u \qquad \text{Eq. 3.2.3.2}$$

where ϵ_u is the adsorption enhancement factor and φ_u is the emanation factor. The sorption enhancement factor ϵ_u is the ratio of the retardation factors of the supported and unsupported radionuclides (Olszewska-Wasiolek and Arnold 2011). RB1 calculates ϵ_u from the user-provided adsorption

distribution coefficients of the unsupported and supported radionuclides in the aquifer cells hosting and supplying the well. The emanation factor φ_u is the fraction of the daughter radionuclide concentration unincorporated from immobile solid particles upon generation.

$\ddot{C}_{w,i}$ is calculated from

$$\ddot{C}_{w,i} = C_{w,i} A \lambda_i \quad \text{Eq. 3.2.3.3}$$

where $C_{w,i}$ is the aqueous molar concentration of radionuclide i in the extracted well water, A is Avagadro's number, and λ_i is the decay constant. If the well is not explicitly modeled in the simulation, $C_{w,i}$ is estimated from

$$C_{w,i} \cong \frac{C_{o,i}}{DF} \quad \text{Eq. 3.2.3.4}$$

where $C_{o,i}$ is the molar concentration of radionuclide i in the aquifer at the well location (mol per L water) and DF is the artificial dilution factor at the well. DF is 1 (i.e., no artificial dilution) for explicitly modeled extraction wells because the flow and transport code automatically accounts for dilution at the well. For a hypothetical well not explicitly modeled in the flow and transport calculations, the user may provide an estimated artificial dilution factor. DF may be estimated as a function of well discharge rate (Q_w), aquifer thickness, screened interval, plume geometry, plume characteristics, and regional aquifer Darcy flux (e.g., Mariner and Gardner 2015). Quantitatively, DF is the ratio of the overall well discharge rate to the plume water capture rate.

RB1 calculates the adsorption enhancement factor ϵ_u for each unsupported radionuclide as the ratio of retardation factors

$$\epsilon_u = \frac{Rf_i}{Rf_u} \quad \text{Eq. 3.2.3.5}$$

where Rf_i and Rf_u are the retardation factors of the supported parent and unsupported descendant, respectively. Retardation factors in RB1 are calculated from

$$Rf = 1 + K_d \frac{\rho_b^d}{\theta_w} \quad \text{Eq. 3.2.3.6}$$

where K_d is the adsorption distribution coefficient in the vicinity of the well, ρ_b^d is the dry bulk density of the aquifer media in the vicinity of the well, and θ_w is the water content in the vicinity of the well.

Selected outputs of RB1 are listed in Table 3-8. These outputs are calculated at each time step when the model is active.

Table 3-8. Selected Reference Biosphere 1 (RB1) outputs.

Output	Model Equation
Concentration of supported radionuclide in well water (mol m^{-3})	$C_{w,i} = C_{o,i}$ for extraction well $C_{w,i} = \frac{C_{o,i}}{DF}$ for hypothetical well
Radioactivity of supported radionuclide in well water (Bq m^{-3})	$\ddot{C}_{w,i} = C_{w,i} A \lambda_i$
Adsorption enhancement factor	$\epsilon_u = Rf_i / Rf_u$
Radioactivity of unsupported radionuclide in well water (Bq m^{-3})	$\ddot{C}_{w,i,u} = \ddot{C}_{w,i} \epsilon_u \varphi_u$
Dose rate from unsupported radionuclide (Sv yr^{-1})	$H_{E,i,u} = \ddot{C}_{w,i,u} * I * dcf_u$
Dose rate from supported radionuclide (Sv yr^{-1})	$H_{E,i} = \ddot{C}_{w,i} * I * dcf_i$
Dose rate from supported radionuclide and its unsupported descendants (Sv yr^{-1})	$Htot_{E,i} = H_{E,i} + \sum_u H_{E,i,u}$
Dose rate from all supported radionuclides and their unsupported descendants (Sv yr^{-1})	$Htot_E = \sum_i Htot_{E,i}$

3.2.3.2 Model Implementation

Details of the RB1 model implementation and how to use it are available online at http://documentation.pflotran.org/user_guide/cards/process_model_cards/ufd_biosphere_card.html.

3.2.3.3 Ingestion Dose Rate Coefficients

Ingestion dose rate coefficients for infants, adults, and children ages 1, 5, 10, and 15 years can be found in Table F.1 of ICRP (2012). This source includes coefficients for nearly all important isotopes with half-lives greater than approximately 30 minutes. A notable missing dose coefficient is for ^{222}Rn, which has a half-life of approximately 4 days.

Ingestion dose coefficients from ICRP (2012) and a ^{222}Rn dose coefficient from UNSCEAR (2000) are plotted in Figure 3-18 as a function of isotope decay constant. A sharp decrease in the coefficient is observed as the decay constant increases from 10^{-9} to 10^{-3} s^{-1} (i.e., as half-lives decrease from about one year to less than 15 minutes). Based on the trend in this figure, isotopes with very short half-lives (<15 minutes) likely have very low dose coefficients and contribute little to the overall dose rate. Hence, there is likely good justification for excluding them in performance assessments.

Interestingly, dose rate coefficients for ^{135}Cs, ^{36}Cl, and ^{99}Tc are quite low compared to the trend in Figure 3-18. ^{129}I is generally the dominant contributor to dose rate calculations in nuclear waste repository post-closure safety assessments because ^{129}I has a high ingestion dose rate coefficient to go along with its high mobility, long half-life, and significant instantaneous release fraction upon waste package breach.

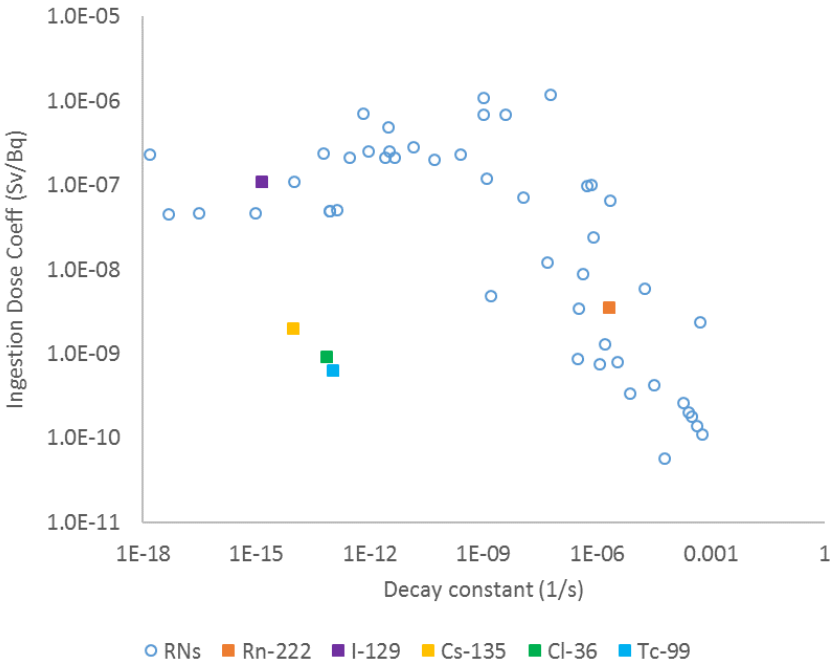

Figure 3-18. Ingestion dose coefficient plotted versus radionuclide decay constant.

3.2.3.4 Demonstration

The ^{226}Ra – ^{222}Rn pair is a good example of the potential importance of accounting for emanation efficiency and relative adsorption in unsupported radionuclides. ^{226}Ra has a high retardation factor while its daughter ^{222}Rn has no retardation. In this demonstration for well water from a sandy aquifer, radium has an aquifer retardation factor of approximately 5000 (Sheppard and Thibault 1990). If the mean emanation factor of ^{222}Rn is assumed to be 0.4 (Olszewska-Wasiolek and Arnold 2011), then the mean net aqueous enhancement of ^{222}Rn relative to ^{226}Ra is a factor of 2000. Thus, for an aqueous ^{226}Ra well water concentration of 1 Bq m^{-3}, the corresponding aqueous concentration of ^{222}Rn is 2000 Bq m^{-3}. Although ^{222}Rn has an ingestion dose coefficient that is about 1% of that for ^{226}Ra (Table 3-9), its enhanced aqueous concentration causes it to contribute much more to the total annual dose rate than ^{226}Ra.

Table 3-9 presents an example RB1 calculation of aqueous concentrations and annual dose rates for ^{226}Ra and its descendants. Figure 1 compares these calculations to those that exclude adsorption enhancement and emanation factors. These results show that the overall dose rate in this case would be underestimated by a factor of 26 if emanation efficiency and relative adsorption were ignored. As for ^{214}Pb and ^{214}Bi, their aqueous concentrations are somewhat higher than the ^{226}Ra aqueous concentration (Table 3-9), but their contributions to the overall dose rate are negligible due to their very low ingestion dose coefficients. Contribution due to ^{218}Po is not shown because the ingestion dose coefficient for ^{218}Po is not available and is likely negligible due to its short 3-minute half-life (Section 3.2.3.3).

Table 3-9. RB1 calculation of ingestion dose rates for ^{226}Ra and unsupported descendants.

Isotope	ϵ_u	φ_u	dcf (Sv Bq^{-1})	Aqueous Concentration (Bq m^{-3})	Ingestion Dose Rate (Sv yr^{-1})
^{226}Ra	NA[a]	NA[a]	2.8E-07[e]	1.00[d]	2.0E-07
^{222}Rn	5000[b]	0.40[c]	3.5E-09[f]	2000	5.1E-06
^{214}Pb	1.85[b]	1.0[d]	1.4E-10[e]	1.85	1.9E-10
^{214}Bi	5.0[b]	1.0[d]	1.1E-10[e]	5.0	4.0E-10

a = not applicable; b = Sheppard and Thibault (1990); c = Olszewska-Wasiolek and Arnold (2011); d = assumed for demonstration; e = ICRP (2012); f = UNSCEAR (2000)

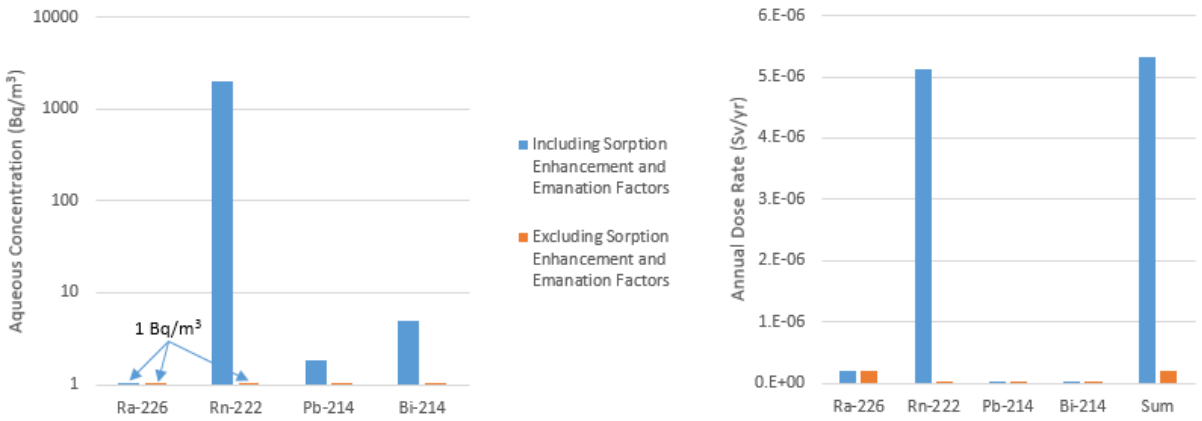

Figure 3-19. Demonstration of the potential importance of including adsorption enhancement and emanation factors for ^{226}Ra and unsupported descendants.

3.2.4 Waste Form Process Model Improvements

The Waste Form Process Model (WFPM) determines the radionuclide source term as a function of time due to degrading waste forms containing a radionuclide inventory. The WFPM has three main components, consisting of (i) a waste package degradation model, (ii) a waste form object, and (iii) a waste form dissolution mechanism. The waste package degradation model determines waste package breach. Once the waste package has breached, the waste form object begins dissolving according to its assigned dissolution mechanism, and the radionuclide source term is calculated. See Section 3.2.1 and Section 3.2.2 in Mariner et al. (2016) for an in depth description of the WFPM.

3.2.4.1 Waste Form Region

Previously, the radionuclide source term for each waste form object was released within the single grid cell which contained the waste form object's coordinate point location. An illustration of this concept is shown in Figure 3-20A, where the grid cell that contains the radionuclide source term due to the degrading waste form object is shaded in green. However, limiting the source term to a single grid cell can be problematic, especially when a waste form object is much larger than one grid cell (e.g. when the grid is refined at waste package regions). In this case, if the total mass rate is large, but released over a small, single grid cell, concentrations of the released radionuclides may reach solubility limits in the grid cell where the source term is located. While PFLOTRAN can handle phase partitioning of radionuclides, a better approach was desired.

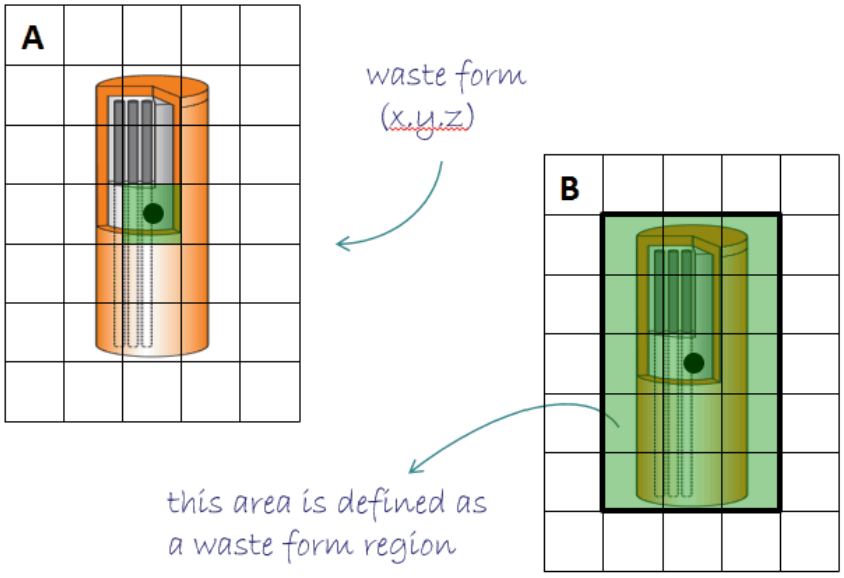

Figure 3-20. Differences between radionuclide source term release.

In the new approach, the location of a waste form object can now be specified with either a coordinate point, or a REGION object (a three-dimensional region in space in PFLOTRAN) which the waste form occupies. An illustration of the new concept is shown in Figure 3-20B, where the dark black box represents the waste form region, as defined by its REGION object. In this new concept, the same source term is now released over all of the grid cells that are contained within the waste form's region, rather than a single grid cell. The release is scaled by grid cell volume, according to

$$S_i = \frac{V_i}{V_r} S \qquad \text{Eq. 3.2.4.1}$$

where S_i is the source term [mol/sec] assigned to grid cell i, V_i/V_r is the ratio of the volume of grid cell i over the total volume of the waste form region (volume scaling factor), and S is the total waste form object source term [mol/sec]. When running on multiple processors, the waste form region may become split up among multiple processes. Because of this possibility, the scaling factor calculation requires calls to MPI (Message Passing Interface) routines, and the algorithm has been optimized for large parallel simulations running on a large number of processors.

3.2.4.2 Glass Dissolution Equation

This FY, the dissolution mechanism for GLASS type waste forms was also improved. Previously, the dissolution rate [kg m^{-2} day^{-1}] of high level waste contained within a glass waste form was described by Kienzler et al. (2012) as

$$R_g = 560e^{-7397/T(x,t)} \qquad \text{Eq. 3.2.4.2}$$

where R_g is the glass dissolution rate [kg m^{-2} day^{-1}], and $T(x,t)$ is the temperature [K] as a function of space and time (obtained from the simulation). The new glass dissolution equation is given by

$$R_g = K_0 10^{\eta pH} e^{-E_a/RT(x,t)} \left(1 - \frac{Q}{K}\right)^{1/V} + K_{long} \qquad \text{Eq. 3.2.4.3}$$

where K_0 is an intrinsic dissolution rate [kg m^{-2} sec^{-1}], $10^{\eta pH}$ is a unitless pH dependence term, E_a is an effective activation energy [J mol^{-1}], R is the universal gas constant [J mol^{-1} K^{-1}], $\left(1-\frac{Q}{K}\right)^{1/V}$ is an affinity term, where Q is an ion activity product of the glass dissolution (activity of H_4SiO_4), K is the equilibrium constant for the rate limited step (activity of H_4SiO_4 at saturation with the glass), V is an exponent term to the affinity term, and K_{long} is the long term dissolution rate when the pore fluid solution is at saturation with SiO_2 [kg m^{-2} day^{-1}]. This equation is derived from YMP-SAR DOE/RW-0573: Abraitis et al. (2000), Advocat et al. (1999), BSC 2004d, Section 7.2, Knauss et al. (1990), and McGrail et al. (1998).

The Kienzler et al. (2012) Eq. 3.2.4.2 can be obtained from the more general, new glass dissolution Eq. 3.2.4-3 by assigning the following values to the parameters: K_0 = 560/(24×3600) [kg m^{-2} s^{-1}], $K_{long} = 0$, $10^{\eta pH} = 1$ (or $\eta = 0$), E_a = 7397×8.314 [J mol^{-1}], $Q = 0$, $K = 1$, and $V = 1$. This is done automatically if the user specifies KIENZLER_DISSOLUTION within the GLASS mechanism block.

Moreover, the values for pH and Q in Eq. 3.2.4.3 can be specified by the user as static values, or they can be updated each time the glass dissolution routine is called from the evolving, calculated value from the simulation. If the latter option is chosen, the pH is calculated according to

$$pH(x,t) = -log_{10}[H^+]\gamma_{H^+} \qquad \text{Eq. 3.2.4.4}$$

where $[H^+]$ is the molality [mol kg-water^{-1}] of the hydrogen ion in space and time, and γ_{H^+} is the activity coefficient of the hydrogen ion in space and time. The value for Q is obtained similarly, according to

$$Q(x,t) = [SiO_2]\gamma_{SiO_2} \qquad \text{Eq. 3.2.4.5}$$

where $[SiO_2]$ is the aqueous molality [mol kg-water^{-1}] of silicon dioxide in space and time, and γ_{SiO_2} is the activity coefficient of silicon dioxide in space and time. To activate the update of pH and Q, the user must specify the keyword AS_CALCULATED rather than a static value in the input deck. Additionally, H^+ and SiO_2 must be included in the reactive transport process model as primary or secondary chemical species.

3.2.4.3 Waste Form Process Model Documentation

As part of PFLOTRAN's documentation overhaul, the WFPM was formally documented. The formal documentation is located at http://www.documentation.pflotran.org/theory_guide/pm_waste_form.html.

Additionally, development of the WFPM was presented at the 16th International High Level Radioactive Waste Management conference in Charlotte, North Carolina (Frederick et al. 2017a), and will also be presented at the 16th International Conference on the Chemistry and Migration Behavior of Actinides and Fission Products in the Geosphere (Migration 2017), in Barcelona, Spain (Frederick et al. 2017c).

3.2.5 Radionuclide Decay and Ingrowth Improvements

Radionuclide decay and ingrowth occurs both within the solid waste form bulk and after radionuclide release to the surrounding environment. Once released upon waste package breach, radionuclides dissolve into the aqueous phase, adsorb onto the host rock, and/or precipitate out of solution. The Waste Form Process Model is responsible for calculating radionuclide decay and ingrowth within the solid waste form. The UFD Decay Process Model is responsible for calculating radionuclide decay and ingrowth, as well as phase partitioning (e.g., aqueous, adsorbed, and/or precipitated phases) once the radionuclides are released into the surrounding host rock pore fluids.

This FY, the algorithm used to solve for radionuclide decay and ingrowth was improved. Previously, radionuclide decay and ingrowth was solved using a limited, 3-generation, analytical solution for isotope decay and ingrowth (Mariner et al. 2016, Section 3.2.3). The limitation of this analytical solution is that

there must be insignificant ingrowth of grandparent(s) during the time step. This is true in GDSA applications for many of the isotopes but not all. Therefore, an improved algorithm was developed that solves the Bateman equation exactly for any number of isotope generations using Newton's method of solution. The Bateman equation describes the abundance of a radionuclide in a decay chain as a function of time, based on decay rates and initial abundances

$$\frac{dC_i(t)}{dt} = -\lambda_i C_i(t) + \lambda_p C_p(t) \quad \text{Eq. 3.2.5.1}$$

where $C_i(t)$ is the radionuclide concentration [M] for isotope i with a decay rate [1/T] λ_i, and $C_p(t)$ is the radionuclide concentration [M] for isotope parent p with a decay rate [1/T] λ_p. Eq. 3.2.5.1 describes an isotope's change in concentration over time $\left(\frac{dC_i(t)}{dt}\right)$ due to its own decay $(\lambda_i C_i(t))$, plus ingrowth (if any) from the isotope's parents $\left(\lambda_p C_p(t)\right)$.

To solve using Newton's method, the equation is reformulated in terms of a residual equation and discretized as follows

$$0 = \frac{dC_i(t)}{dt} + \lambda_i C_i(t) - \lambda_p C_p(t) \quad \text{Eq. 3.2.5.2}$$

$$f\left(c^{k+1,p}\right) = \frac{c^{k+1,p} - c^k}{\Delta t} - R\left(c^{k+1,p}\right) \quad \text{Eq. 3.2.5.3}$$

where $f\left(c^{k+1,p}\right)$ is the residual, $\frac{c^{k+1,p} - c^k}{\Delta t}$ is the discretized rate of change in the isotope's concentration, and $R\left(c^{k+1,p}\right)$ is the source or sink term (e.g., the right hand side of Eq. 3.2.5.1). The integer k represents the time step, and the integer p represents the iteration number. A Jacobian matrix (J_{ij}) is formed according to

$$J_{ij} = \frac{\partial f_i\left(c^{k+1,p}\right)}{\partial c_j^{k+1,p}} \quad \text{Eq. 3.2.5.4}$$

which is a matrix of all partial derivatives of the solution $(c^{k+1,p})$ with respect to each unknown variable. Newton's method solves the following system for δc^p

$$J\delta c^p = -f\left(c^{k+1,p}\right) \quad \text{Eq. 3.2.5.5}$$

which can be used to update the concentration for the next iteration according to

$$c^{k+1,p+1} = c^{k+1,p} + \delta C c^p \quad \text{Eq. 3.2.5.6}$$

The linear system of equations described by Eq. 3.2.5.5 is solved in two steps. The first step is an LU decomposition (also known as LU factorization), while the second step is a direct solve using LU back substitution. Iteration proceeds until the 2-norm of the residual becomes less than the tolerance (which is set at 1e-12).

By default, the Waste Form and UFD Decay Process Models use the 3-generation analytical solution to solve for decay and ingrowth. However, the direct, implicit method of solution can be used instead by including the keyword IMPLICIT_SOLUTION in the PFLOTRAN input deck within the respective process model blocks.

3.2.6 Other Initiatives

3.2.6.1 EBS 1D-3D Refinement

PA requires simulation of flow and transport processes occurring at kilometer-scale distances in the natural barrier system of the host rock, and simulation of processes occurring at meter and centimeter scales (such as buffer/backfill saturation and waste package degradation) in the engineered barrier system of the repository. Though it is possible to discretize specific portions of the model domain at finer resolution, the disparity in scales of interest presents a challenge in maintaining a computationally manageable problem size. In FY 2017, we explored the possibility of using finely-discretized one-dimensional (1D) continua embedded in a three-dimensional (3D) model domain to achieve subgrid-scale refinement in and around each waste package in a simulation of a generic repository. This approach has the potential to save millions of grid cells (and a proportionately larger number of unknowns) in comparison to finely discretizing the 3D model domain in the region of the repository.

Each 1D continuum represents a cylindrical waste package and the surrounding cylindrical volume of engineered materials (such as steel waste package overpack, bentonite buffer, cement liner) between the waste package and the host rock wall of the disposal drift (Figure 3-21). The 1D continuum is discretized into concentric cylindrical shells, and the location of the outermost shell coincides with the location of the larger 3D grid cell in which the 1D continuum is embedded. Both the 3D grid and the 1D continua are defined using an explicit unstructured grid format which specifies the locations and volumes of cell centers and the locations and areas of connections between cells. In this way, the 1D continua are tightly coupled to the 3D domain, and the entire system of equations (whether for multiphase flow or reactive transport) is solved simultaneously using PFLOTRAN. Because the 1D continua connect to the larger 3D grid at the outermost shell only, their use is appropriate when radial transport (of gas, liquid, heat, and solutes) inward and outward from the waste package is expected to dominate within each volume represented by a 1D continuum, as is the case within a disposal drift filled with low permeability bentonite backfill.

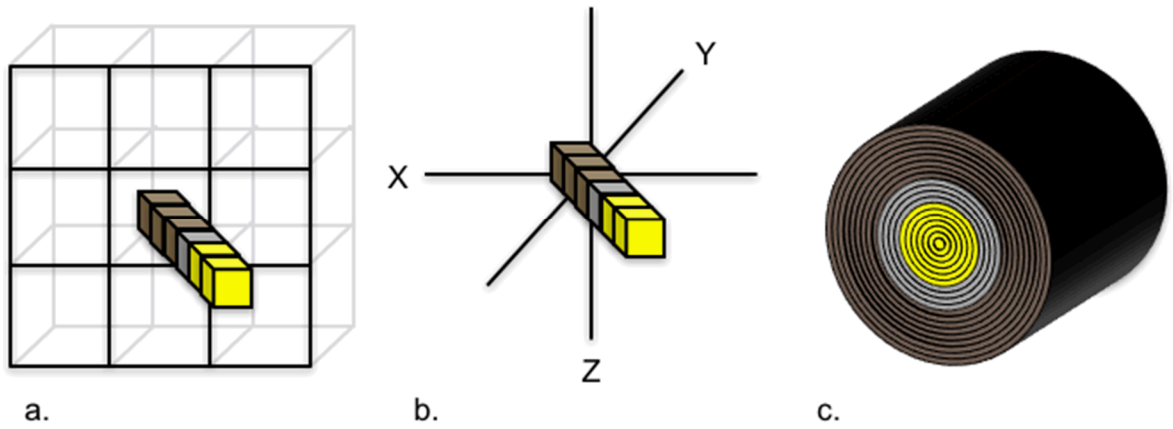

Figure 3-21. a) A 1D continuum is embedded in a 3D grid that occupies the X, Y, and Z dimensions. b) The 1D continuum occupies a virtual 4th dimension; one end of the 1D continuum coincides in space with a cell center in the 3D grid. c) Cell volumes and connection areas within the 1D continuum represent concentric shells of a cylindrical volume occupying the volume of the connected 3D cell.

A comparison of a 1D embedded continuum to various discretizations in 3D was made using a test problem involving single-phase coupled heat and fluid flow. Simulations were of a single 12-PWR waste package in a drift with a 5 x 5 m^2 cross section filled with bentonite buffer. Waste package volume (13.88 m^3) and heat source, and all material properties were identical to those used in PA simulations. Constant pressure and temperature were held at the top of the model domain; all other faces were no-flow boundaries. The model domain is shown in Figure 3-22. Five variations of the problem were run. One with all cells in the domain discretized to 5 m on a side (as drawn); one with a 16-cell 1D continuum representing a 5-m long, 13.88-m^3 waste package and surrounding buffer embedded in a 5 x 5 x 5 m^3 cell at the center of the drift; and three with increasingly finer 3D resolution of the same waste package and surrounding buffer (cell lengths of 5/3 m, 5/9 m, and 5/27 m).

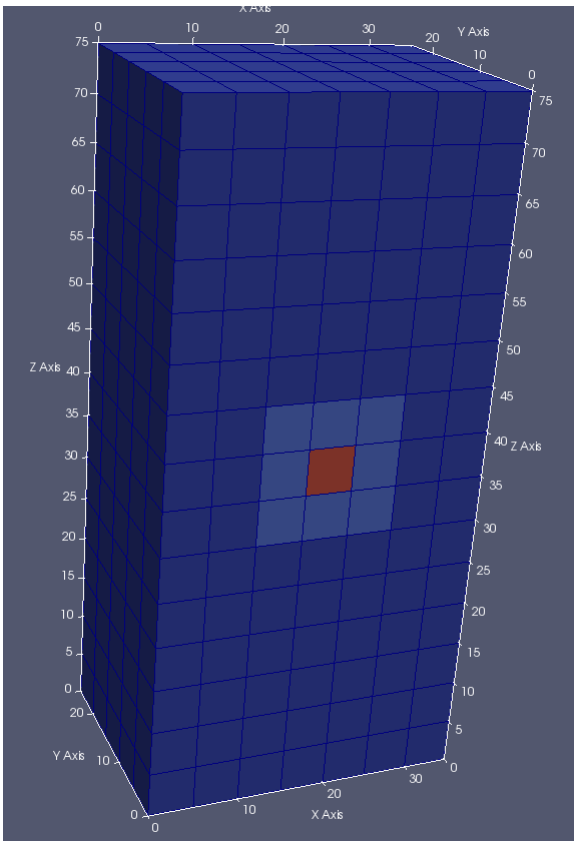

Figure 3-22. Model domain for 1D continuum test problem. Domain is discretized into cells 5 m on a side. The face of the drift, which extends through the model domain, is shown in orange.

Temperatures at the center of the waste package and in the buffer immediately adjacent to the waste package are shown in Figure 3-23. The case in which all cells are 5 m on a side can be considered the base case. In this case, a single 5 x 5 x 5 m^3 cell with material properties of bentonite buffer is the heat source, and its center is the point at which buffer temperature is monitored. The 1D continuum acts as a perfect heat source to the 3D cell. The temperature in the bulk 3D cell predicted by the 1D continuum simulation (solid red line) corresponds almost exactly to the temperature predicted in the 5-m discretization simulation (dashed teal line). However, the 1D continuum simulation predicts temperatures about 30 degrees warmer in both the waste package center and the buffer than predicted by the finely discretized 3D simulations. Excess heat within the 1D continuum (waste package) and the associated 3D (buffer/bulk) cell is due to the coarse grid resolution in the 3D domain. In the finest 3D discretization, the

temperature gradient (ΔT/ΔL) is numerically calculated using the cell length (ΔL) of 5/27 m. In the 1D continuum, the temperature gradient immediately outside the 1D continuum is numerically calculated using a cell length (ΔL) of 5 m. The larger ΔL results in a lower temperature gradient and slows heat flux away from the 1D continuum.

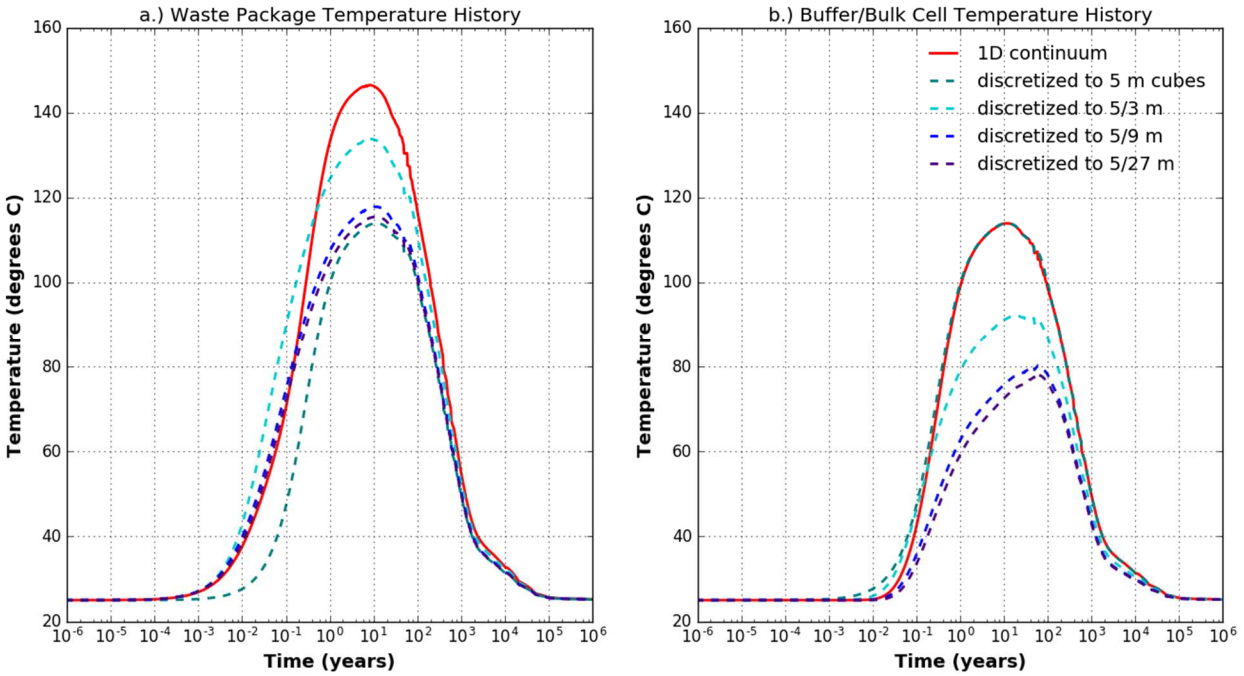

Figure 3-23. Temperature versus time at (a) the waste package center and (b) the buffer immediately adjacent to the waste package in various discretizations of the test problem.

The ability to finely discretize embedded 1D continua has the potential to improve resolution of waste package and buffer temperature, chemistry, and liquid saturation while minimizing problem size, but until the limitations of discretization immediately adjacent to the 1D continuum are overcome, this potential will not be reached.

3.2.6.2 Waste Package Degradation Improvements

Depending on the effectiveness of natural barriers, the rate at which waste package outer barriers degrade can have an important effect on repository performance. For example, in the case of a crystalline repository, if significant deep circulation of groundwater occurs due to melting ice or tectonic forces, the degradation rates of waste package barriers would likely significantly affect calculations of repository performance.

Currently, GDSA Framework simulates general corrosion of the waste package in one of two ways. It can use an Arrhenius equation to determine the rate of corrosion for each waste package as a function of the local temperature, or it can specify a waste package breach time for each waste package at the beginning of a realization. In either case, the waste package is currently assumed to disappear when breached and to provide zero barrier capability thereafter. No chemical corrosion reactions are simulated and no corrosion products accumulate. Rates or breach times are sampled from uncertainty distributions for each waste package so that there is spatial heterogeneity in failure times. When the rate model is used, the rate is calculated at each time step and is fully coupled to the local thermal conditions of the waste package.

The waste package degradation model of GDSA Framework can be improved in a number of ways. High priorities for improvement are:

- Adding additional corrosion mechanisms (e.g., localized corrosion, stress corrosion cracking),
- Simulating partial waste package performance after breach (e.g., diffusion of groundwater and radionuclides through pits or cracks; adsorption to corrosion products), and
- Directly simulating chemical and transport processes at the waste package surface (e.g., reactive transport).

Plans for FY 2018 include addressing all three of these potential enhancements, developing conceptual models for them, and performing standalone tests. Potential models could range from coupled reactive transport models to lower fidelity models. A major goal for FY 2018 will be to have a working localized corrosion model implemented in GDSA Framework to run alongside the general corrosion model for each waste package.

3.2.6.3 Colloid Modeling

The addition of non-equilibrium colloid facilitated transport to PFLOTRAN based on the design document developed by Reimus et al. (2016) was planned for FY 2017. However, due to limitations in time for dedicated code development, the implementation of the Reimus formulation for colloidal transport has been postponed to FY 2018 at the earliest.

3.3 Establishing GDSA Framework

A primary objective of the GDSA work package is to develop a disposal system modeling and analysis capability to evaluate repository performance for a range of disposal options. This capability, GDSA Framework, must be well-tested and accepted by peers. To this end, in addition to the verification testing discussed in Section 3.2.2, a significant effort this year has gone into publications, presentations, short course offerings, expanding the user base, and establishing a broader user group of collaborators.

The development of GDSA Framework benefits greatly from use in the broader scientific community. Users provide valuable feedback for developers and can contribute directly to code development by improving parts of the code or coupling new process models. Collaboration with outside users is made possible by online version control systems (e.g., Bitbucket.org) and open source access. By encouraging and facilitating use in the outside community, we expect to accelerate code development and acceptance.

This section discusses several outreach efforts put forth this year intended to facilitate the development of GDSA Framework and to establish GDSA Framework as a sound, powerful, and accessible repository safety assessment tool.

3.3.1 Collaborative Websites

The website pa.sandia.gov, officially launched in the fall of 2016, was developed to showcase GDSA Framework capability. At this website, viewers may peruse demonstrative examples of the GDSA capability found in presentations and reports generated over the past several years. The website provides links to software employed within GDSA (i.e. Cubit, Dakota and PFLOTRAN) and cites collaborating organizations and laboratories external to the Sandia lead organization (i.e. ANL, LANL, pflotran.org, PNNL) that have contributed to the development of GDSA Framework.

Figure 3-24 illustrates the hits by city on pa.sandia.gov from January through July 2017, measured by Google Analytics. Next to Albuquerque (Sandia) at 146 hits, Pitesti (Romania), Mexico City and Barcelona had 29, 19 and 14 hits, respectively.

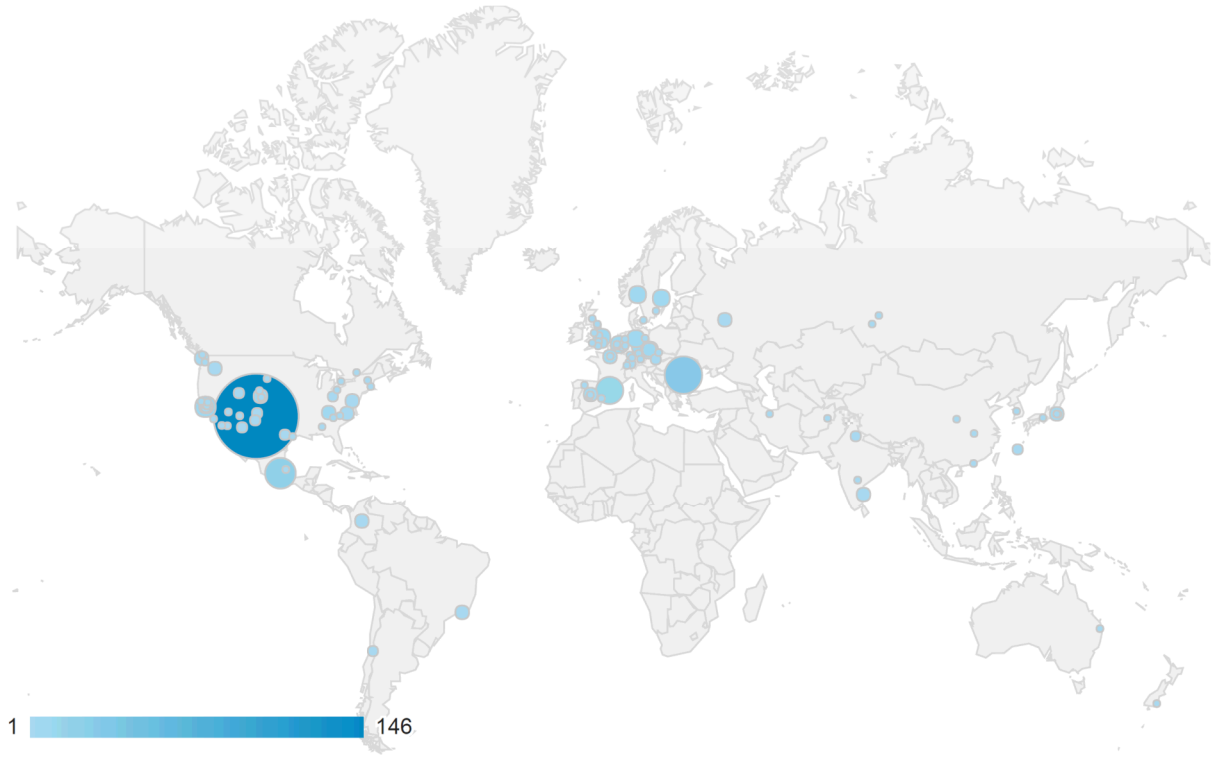

Figure 3-24. Hits on pa.sandia.gov from January through July 2017.

3.3.2 Publications

Table 3-10 lists presentations involving GDSA Framework delivered in FY 2017. They include presentations at public conferences spanning topics ranging from high level radioactive waste to computational science (SIAM).

Table 3-10. FY 2017 Publications Involving GDSA Framework.

Title	Source	Citation
Modeling Coupled Reactive Flow Processes in Fractured Crystalline Rock	IHLRWM 2017	Stein et al. (2017a)
Development of a Waste Form Process Model in PFLOTRAN	IHLRWM 2017	Frederick et al. (2017a)
Minimizing the Impact of Software Evolution on Radioactive Waste Management	IHLRWM 2017	Hammond and Frederick (2017)
Maintaining quality assurance within software evolution: Lessons learned with PFLOTRAN	SIAM Conference on Mathematical and Computational Issues in Geosciences 2017	Frederick and Hammond (2017)
Performance Assessment of a Generic Repository for Defense-Related HLW/SNF in Fractured Crystalline Host Rock	WM Symposia 2017	Sevougian et al. (2017b)
Probabilistic Performance Assessment for Deep Borehole Disposal of Cs/Sr Capsules	WM Symposia 2017	Freeze et al. (2017b)
Performance Assessment of a Generic Repository in Bedded Salt	AGU Fall Meeting 2016	Stein et al. (2016)
PFLOTRAN Verification: Development of a Testing Suite to Ensure Software Quality	AGU Fall Meeting 2016	Hammond and Frederick (2016)
Modeling Waste Package Degradation and Waste Form Dissolution for Geologic Repository Performance Assessment in PFLOTRAN	Migration 2017	Frederick et al. (2017b)
Estimating the Effect of Fracture Connectivity on Waste Isolation Using a High-Performance Reactive Transport Simulator, PFLOTRAN	Migration 2017	Sevougian et al. (2017c)
Multi-Scale Modeling in PFLOTRAN for Geologic Repository Performance Assessment: An Enhancement to GDSA Framework	Migration 2017	Stein et al. (2017b)
Isotope Partitioning, Decay, and Ingrowth across Multiple Phases in PFLOTRAN Code of GDSA Framework	Migration 2017	Mariner et al. (2017b)
Radon and the PFLOTRAN Ingestion Dose Model of GDSA Framework	Migration 2017	Mariner et al. (2017a)
PFLOTRAN Reaction Sandbox: A Flexible, Extensible Framework for Vetting Biogeochemical Reactions within an Open Source Subsurface Simulator	Migration 2017	Hammond (2017)

3.3.3 Short Courses

The GDSA group conducted two short courses in FY 2017 where GDSA capability was demonstrated within PFLOTRAN and attendees gained hands-on experienced running the simulator. The first short course was held in May 2017 at Sandia National Laboratories for two days. It had 26 attendees consisting of students, faculty and staff from Los Alamos National Laboratory, New Mexico Tech and Sandia National Laboratories.

The second short course was held in September 2017 for three days. It was conducted in Barcelona, Spain, the week prior to the Migration 2017 conference. Sandia teamed with Amphos21 Consulting Ltd., an environmental consulting firm based in Barcelona, to host the short course. Migration 2017 presented an excellent opportunity for the short course because Amphos21 has much experience with PFLOTRAN

and was a primary host of Migration 2017. Amphos21 advertised the short course on the Migration 2017 website and volunteered to secure a location for the short course, register students, and handle all associated costs, including registration fees (100 to 150 Euros, depending on timing and whether the attendee was a student). The short course was three days long and involved 27 attendees from 9 countries (Sweden, United Kingdom, Republic of Korea, Japan, Spain, Czech Republic, Germany, Norway, and Belgium). Most attendees planned to apply PFLOTRAN to nuclear waste disposal. One United Kingdom attendee with much experience using other THC codes intends to become a PFLOTRAN developer. In addition, Amphos21 demonstrated the iGP software it developed to serve as an interface between PFLOTRAN and GiD pre-/post-processing software. Amphos21 uses PFLOTRAN routinely and is expected to become further involved in PFLOTRAN development in the future.

At both short courses, attendees were taught the underlying theory behind PFLOTRAN through presentations from GDSA researchers. Numerous exercises or problem scenarios including,

- 1D variably saturated flow
- 1D Calcite precipitation-dissolution
- Copper leaching in a 5-spot flow regime
- Region groundwater flow with doublet (dipole) pumping wells
- Density dependent flow

were set up by interactively discussing keywords (cards) for each block of the input deck. The input decks were then executed by each attendee on their own laptop computers. Attendees were also instructed on

- Visualization of simulation results
- Python-based generation of simulation datasets (e.g. cell by cell porosity, permeability, etc.)
- Debugging erroneous input decks by deciphering PFLOTRAN error messaging
- Code testing.

At the short course in Barcelona, a morning session on GDSA Framework was also included. The interaction of Dakota, PFLOTRAN, Python, Paraview, and meshing programs was explained, and GDSA process model capabilities (e.g., decay and ingrowth, isotope partitioning, waste package degradation, waste form dissolution, radionuclide release, well water ingestion dose model) were introduced. In addition, deterministic and probabilistic applications to a generic repository in crystalline rock were demonstrated.

Feedback obtained through end-of-course questionnaires highlighted strengths and weaknesses of the short courses, so that improvements can be made in the future. Perhaps the largest issue was the diversity of the audience with regard to simulation and modeling capability. Experienced modelers would have preferred a faster pace of delivery, while novices expressed a desire for a slower introduction. Students generally thought the lengths of the courses were appropriate or too short.

3.3.4 Quality Assurance

Section 3.2.2 discusses in detail the PFLOTRAN verification testing initiated in FY 2017. This in-depth testing helps to establish the scientific integrity of GDSA Framework. Testing in FY 2017 focused on individual process models for heat conduction and separate liquid/gas phase fluid flow. It is expected that PFLOTRAN's verification testing coverage will be expanded to additional process models such as transport and biogeochemical reaction in the future. The test results for the flow and energy process models were compared individually where it was possible to obtain derived analytical solutions from the

literature. The derivation of analytical solutions for coupled process models is often not possible. Therefore, it is also anticipated that the code will be verified against established simulation capability for coupled processes such as an-isothermal multiphase flow or multicomponent reactive transport. Such verification efforts will further establish quality assurance for GDSA Framework.

4. SHALE REPOSITORY REFERENCE CASE

Clay-rich sedimentary strata have been considered a potential medium for disposal of radioactive waste in the United States since the forerunner to the DOE introduced a program to develop radioactive waste disposal technology in 1976 (Shurr 1977; Gonzales and Johnson 1985; Rechard et al. 2011). Clay-rich formations are an attractive disposal medium due to their low permeability, high sorption capacity, typically reducing porewaters (which limit radionuclide solubility), and ability to deform plastically, which promotes self-healing of fractures. Clay-rich formations suitable for isolation of radioactive waste span a range of rock types, varying in degree of foliation and degree of consolidation and induration, from unconsolidated mud (such as the Boom Clay) to argillite (such as the Callovo-Oxfordian argillite) (Hansen et al. 2010). For instance, the Glossary of Geology (Jackson 1997) defines mudstone ("an indurated mud having the texture and composition of shale, but lacking its fine lamination or fissility"), claystone ("an indurated rock with >67% clay-sized minerals"), shale ("a laminated, indurated rock with >67% clay-sized minerals"), and argillite ("a compact rock, derived from either mudstone or shale, that has undergone a somewhat higher degree of induration than mudstone or shale but is less clearly laminated than shale and without its fissility, and that lacks the cleavage distinctive of slate"), among others. In this report, we use the term "shale" imprecisely to represent all of the above.

The U.S. hosts several marine sedimentary sequences containing thick beds of clay-rich sediments potentially suitable for deep geologic disposal of radioactive waste (Gonzales and Johnson 1985; Perry et al. 2014; Perry and Kelley 2017). Of these, the Pierre Shale in the northern Great Plains was considered for radioactive waste isolation by Shurr (1977), who lists a number of criteria for assessing the suitability of a shale or similar clay-rich formation for geologic disposal of radioactive waste. The same or similar criteria are considered by later authors (Gonzales and Johnson 1985; Hansen et al. 2010; Perry et al. 2014; Jove Colon et al. 2014) and include:

- Depth – The isolation horizon should be from 300 to 900 m below surface.
- Shale thickness – Maximum thickness of the isolation medium is desired, and a minimum thickness of 150 m is preferred.
- Overburden thickness – Minimal thickness of overlying geologic units is preferred.
- Lithology and mineralogy – The repository interval should be a reasonably uniform shale or other clay-rich unit with few or no interbeds of more permeable lithology.
- Penetrations (boreholes) – Boreholes of any kind are undesirable, particularly if they penetrate to rocks below the disposal horizon. It is recognized that some holes are necessary to provide geologic information at depth.
- Structure – The disposal zone should have nearly horizontal bedding and the surrounding region should be structurally simple (e.g., no folding or faulting).
- Seismicity – Seismically inactive regions are preferred.
- Topography – Minimal topographic relief is desirable to limit the influence of topography on subsurface hydraulic gradients.
- Mineral and water resources – Regions with minimal exploitable mineral and water resources, at or below the surface, are preferred.

Locations of aerially extensive shale formations in the U.S. are shown in Figure 4-1.

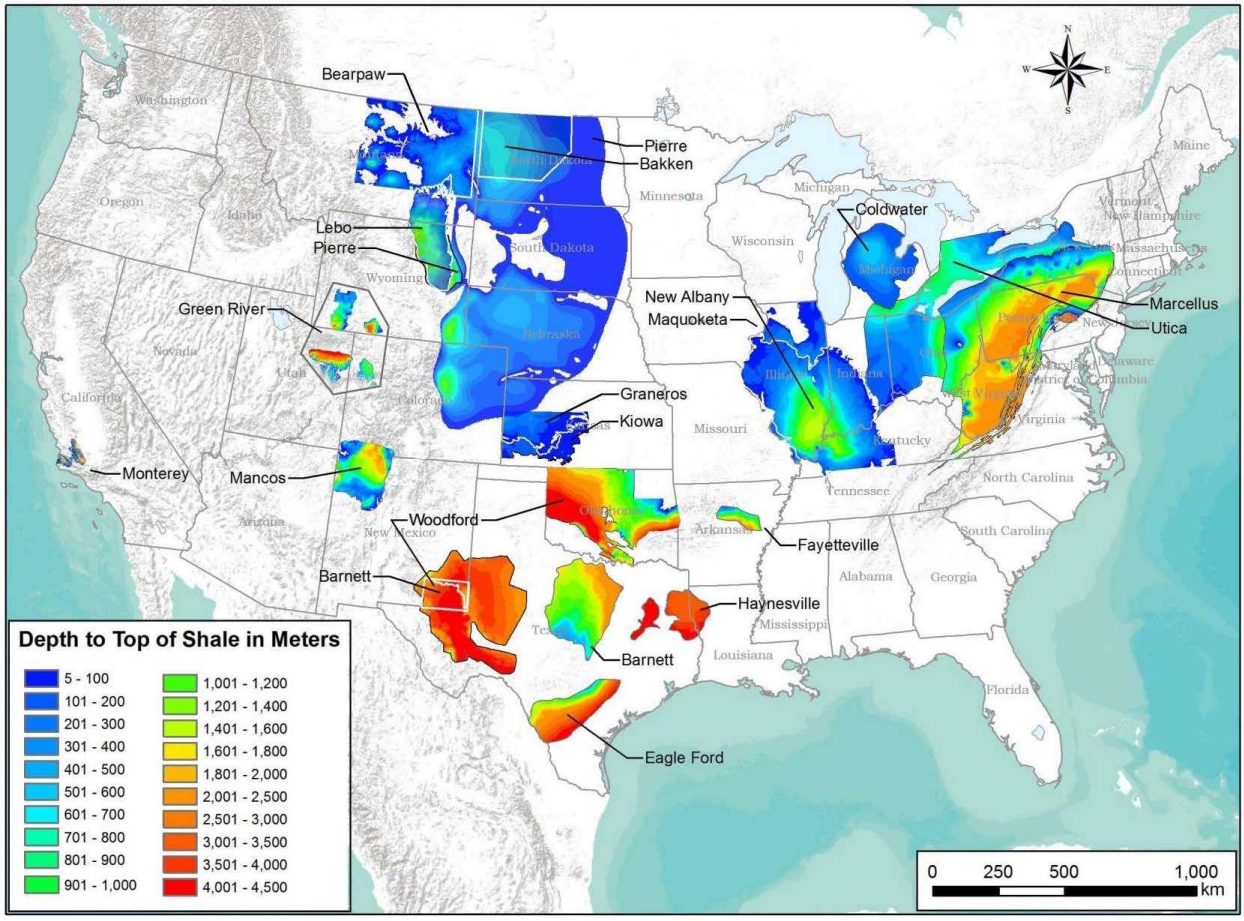

Figure 4-1. Locations of areally extensive shale formations in the U.S. Shale formations of an appropriate depth are the darker shades of blue. Figure from Perry and Kelley 2017.

This iteration of the shale reference case is an update to the clay reference case presented by Mariner et al. (2015) and builds upon the argillite reference case described by Jové Colón et al. (2014). Emplacement of pressurized water reactor (PWR) spent nuclear fuel (SNF) occurs in a mined repository located in a deep, homogeneous, thickly bedded, essentially flat-lying stratum in a geologically simple and stable environment. Two repository layouts are considered, one for 12-PWR waste packages emplaced in-drift and one for 4-PWR waste packages emplaced in horizontal boreholes.

The remainder of this section includes a description of the engineered barrier (Section 4.1), the natural barrier (Section 4.2), and the biosphere (Section 4.3), followed by a quantitative post-closure performance assessment (PA) (Sections 4.4 and 4.5). This is the first generic reference case completed with PFLOTRAN PA simulations to include a biosphere model. Many other updates to the reference case and associated PA simulations have been made since the previous shale reference case was completed (Mariner et al. 2015). These are summarized in Table 4-1.

Table 4-1. Comparison of current (2017) PA simulations to 2015 shale reference case PA simulations. Inventory count (MTHM and number of waste packages) includes *the virtual inventory beyond the reflection boundary condition*.

	2015 – 12-PWR	2017 – 12-PWR	2017 – 4-PWR
Waste Inventory	8,000 MTHM in 1600 WPs	21,000 MTHM in 4200 WPs	21,000 MTHM in 12,600 WPs
Waste Emplacement	In-drift axial emplacement 20 emplacement drifts 20-m drift spacing 10-m center-to-center WP spacing Bentonite buffer/backfill	In-drift axial emplacement 84 emplacement drifts 30-m drift spacing 20-m center-to-center WP spacing Bentonite buffer/backfill	Borehole emplacement 1400 emplacement boreholes 30-m borehole spacing 10-m center-to-center WP spacing Bentonite buffer/backfill
Grid	Structured 3.9 million cells	Unstructured 7 million cells	Unstructured 22 million cells
Boundary and Initial Conditions	Regional head gradient Regional geothermal heat flux Fully saturated	Regional head gradient Regional geothermal heat flux Fully saturated	Same as 12-PWR case
Natural Barrier	Shale (500 m thick) with high-k interbeds Aquifer above and below	Shale (585 m thick) with silty shale stratum Aquifer above and 2 below	Same as 12-PWR case
Shafts and Seals	2 vertical shafts without DRZ $D_e = 1.6 \times 10^{10}$	4 vertical shafts with hi-k DRZ $D_e = 8.1 \times 10^{11}$	Same as 12-PWR case
Radionuclides	5	18	Same as 12-PWR case
TH Modeling	Coupled heat and water transport	Coupled heat and water transport	Same as 12-PWR case
WP Degradation	Complete failure of all WPs assumed at start	WPs breach over time (sampled distribution)	Same as 12-PWR case
WF Degradation and	No decay in waste form	Decay in waste form is accounted for in instantaneous releases and	Same as 12-PWR case

Radionuclide Release		in releases due to WF dissolution	
Radionuclide Transport	Advection, diffusion, dispersion, isotope-based solubility, uniform sorption, no decay in precipitate phases	Advection, diffusion, element-based solubility, medium-specific sorption, decay in all phases	Same as 12-PWR case
Biosphere	No dose model	Well water ingestion dose model	Same as 12-PWR case

4.1 Engineered Barriers

Specific post-closure basis information related to the engineered barriers includes:

- Characteristics of the repository (Section 4.1.1),
- Inventory characterization (Section 0),
- Waste form characterization (Section 4.1.3),
- Waste package characterization (Section 4.1.4), and
- Characteristics of the buffer, drifts, and access halls (Section 4.1.5).

4.1.1 Engineered Barrier Characteristics

The shale reference case assumes a mined repository located approximately 500 m below land surface, accessed by vertical shafts, and containing 70,000 MTHM of commercial SNF, which is the maximum allowed by the Nuclear Waste Policy Act of 1983 and about half of the total commercial SNF inventory predicted by 2055 in the "no replacement scenario" (Carter et al. 2013).

This inventory could be accommodated in 13,398 12-PWR waste packages (Table 4-2) in 268 1035-m long emplacement drifts, each containing 50 waste packages emplaced lengthwise and spaced 20 m center-to-center. A 25-m long seal is placed at either end of each emplacement drift. Drifts are 4.5 m in diameter spaced 30 m center-to-center. These dimensions are similar to those described by Hardin and Kalinina (2016, Section 3) for a 12-PWR repository in shale, and would result in a total emplacement footprint of approximately 8.3 km^2.

The 70,000-MTHM inventory could be accommodated in 40,194 4-PWR waste packages (Table 4-3) in 4466 100-m long horizontal emplacement boreholes, each containing 9 waste packages spaced 10 m center-to-center. Thirty-five boreholes are spaced 30 m apart (center-to-center) along each side of 64 access drifts, 1035 m in length and 5.5 m in diameter. Access drifts are spaced 235-m center-to-center, leaving a 30 m distance between the ends of aligned boreholes. These dimensions are similar to those described by Hardin and Kalinina (2016, Section 2) for a 4-PWR repository in shale, and would result in a total emplacement footprint of approximately 15.6 km^2.

PA simulations use a half-symmetry model domain, in which approximately 15% (10,962 MTHM) of the 70,000 MTHM inventory is explicitly gridded. With the reflection boundary condition (see Section 4.2), 30% (21,924 MTHM) of the 70,000 MTHM inventory is included in PA simulations. Dimensions used in the simulations (Table 4-2 and Table 4-3) reflect the smaller inventory as well as adjustments needed to facilitate gridding.

Table 4-2. Dimensions and counts for the 12-PWR repository layout.

Parameters	Reference Case Value	Simulated Value
Waste Package (WP)		
WP length (m)	5.20 [a]	5.00
WP outer diameter (m)	1.37 [a]	1.67 (on a side)
WP center-to-center spacing (m)	20.0 [a]	20.0
Inventory per 12-PWR WP (MTHM)	5.225	5.225
Number of WPs	13,398	2100 / 4200 [b]
Emplacement Drift		
Drift diameter (m)	4.5 [a]	5.0 (on a side)
Drift center-to-center spacing (m)	30 [a]	30
Number of WPs per drift	50 [a]	50
Drift seal length (m)	25	25
Drift length, including seals (m)	1035	1035
Repository		
Repository Depth (m)	500	515
Number of drifts	268	42 / 84 [b]
Number of shafts	Not specified	2 / 4 [b]
Shaft access size (m^2)	Not specified	5 x 10
Emplacement footprint (km^2)	8.3	1.3 / 2.6 [b]

[a] Hardin and Kalinina (2016, Section 3)
[b] Value in half-symmetry domain / Value with reflection

Table 4-3. Dimensions and counts for the 4-PWR repository layout.

Parameters	Reference Case Value	Simulated Value
Waste Package (WP)		
WP length (m)	5.00 [a]	5.00
WP outer diameter (m)	0.82 [a]	0.56 (on a side)
WP center-to-center spacing (m)	10.0 [a]	10.0
Inventory per 4-PWR WP (MTHM)	1.742	1.742
Number of WPs	40,194	6300 / 12,600 [c]
Emplacement Borehole		
Borehole diameter (m)	1.82 [a]	1.67 (on a side)
Borehole center-to-center spacing (m)	30 [a]	30
Number of WPs per borehole	9 [a]	9
Borehole seal length (m)	10 [a]	10
Borehole length, including seals (m)	100 [a]	100
Access Drift		
Drift diameter (m)	5.5 [b]	5.0 (on a side)
Drift center-to-center spacing (m)	235	235
Number of borehole pairs per drift	35	35
Drift length (m)	1035	1035
Repository		
Repository Depth (m)	500	515
Number of access drifts	64	10 / 20 [c]
Number of boreholes	4466	700 / 1400 [c]
Number of shafts	Not specified	2 / 4 [c]
Shaft access size (m^2)	Not specified	5 x 10
Emplacement footprint (km^2)	15.6	2.4 / 4.9 [c]

[a] Hardin and Kalinina (2016, Section 2)
[b] Hardin et al. (2012, Section 4.3)
[c] Value in half-symmetry domain / Value with reflection

4.1.2 Inventory

For simplicity, PA simulations assume that the inventory consists entirely of PWR SNF assemblies, each containing 0.435 MTHM. Radionuclide inventories (Table 4-4) and decay heat versus time curves (Figure 4-2) are taken from Carter et al. (2013) and assume an initial enrichment of 4.73 wt% ^{235}U, 60 GWd/MTHM burn-up, and 100-year out of the reactor (OoR) storage prior to deep geologic disposal. This inventory is identical to that assumed for the crystalline reference case (Mariner et al. 2016) and for the previous iteration of the shale reference case (Mariner et al. 2015). Because the average burn-up of SNF under the "no replacement scenario" is predicted to be only 54 GWd/MTHM (Carter et al. 2013), the assumption of 60 GWd/MTHM results in a conservatively high heat load.

Table 4-4. PWR SNF inventory of selected radionuclides for the shale reference case.

Isotope	Inventory (g/MTIHM)[1]	Inventory (g/g waste)[2]	Atomic weight (g/mol)[3]	Approximate Decay Constant (1/s)
^{241}Am	1.46E+03	1.01E-03	241.06	5.08E-11
^{243}Am	2.69E+02	1.87E-04	243.06	2.98E-12
^{238}Pu	2.84E+02	1.97E-04	238.05	2.56E-10
^{239}Pu	7.40E+03	5.14E-03	239.05	9.01E-13
^{240}Pu	4.11E+03	2.85E-03	240.05	3.34E-12
^{242}Pu	8.17E+02	5.67E-04	242.06	5.80E-14
^{237}Np	1.40E+03	9.72E-04	237.05	1.03E-14
^{233}U	4.33E-02	3.01E-08	233.04	1.38E-13
^{234}U	5.11E+02	3.55E-04	234.04	8.90E-14
^{236}U	6.27E+03	4.35E-03	236.05	9.20E-16
^{238}U	9.10E+05	6.32E-01	238.05	4.87E-18
^{229}Th	1.48E-05	1.03E-11	229.03	2.78E-12
^{230}Th	1.04E-01	7.22E-08	230.03	2.75E-13
^{226}Ra	3.99E-05	2.77E-11	226.03	1.37E-11
^{36}Cl	5.01E-01	3.48E-07	35.97	7.30E-14
^{99}Tc	1.28E+03	8.89E-04	98.91	1.04E-13
^{129}I	3.13E+02	2.17E-04	128.9	1.29E-15
^{135}Cs	7.72E+02	5.36E-04	134.91	9.55E-15
All isotopes[4]	1.44E+06	1.00E+00	--	--

[1] from Carter et al. (2013, Table C-2)
[2](g isotope/g waste) = (g isotope/MTIHM)/(g waste/MTIHM), where g waste = g all isotopes
[3]Weast and Astle (1981)
[4]all isotopes are not listed here

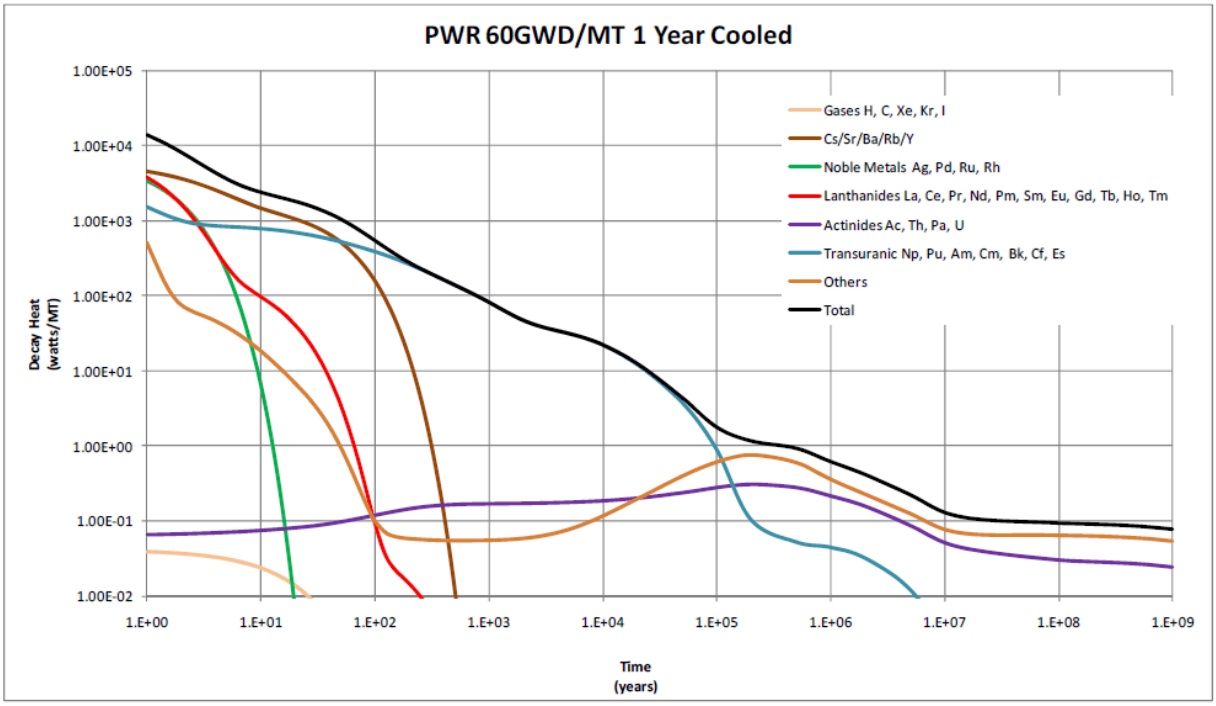

Figure 4-2. Heat of decay versus time for PWR SNF (60 GWd/MT burnup) from Carter et al. (2013). Shale reference case simulations assume 100-yr OoR storage and thus begin with the total wattage at 100 years.

4.1.3 Waste Form

Freeze et al. (2013c, Section 3.4.1.1) provides a description of commercial SNF, including the following characteristics. Spent uranium oxide (UO_2) fuel is a polycrystalline ceramic material with stable to high temperatures and the potential for slow degradation in the disposal environment. Cladding protects the fuel from degradation in the reactor, and can continue to protect the fuel from degradation in the repository. Cladding from commercial light-water reactors (i.e. boiling water reactors and pressurized water reactors) is generally made from Zircaloy, a zirconium alloy that is chemically stable and resistant to corrosion. In the reactor, fuel undergoes physical changes due to heating, radiation damage, and the build-up of fission products. Lighter elements (fission products) become concentrated in voids and the outer margins of the UO_2 matrix.

Concentration of fission products in voids of the waste form results in the waste form releasing radionuclides in two fractions: instant-release (upon waste package breach) and slow-release (according to the UO_2 matrix dissolution rate). See Mariner et al. (2016, Section 3.2.2) for a description of the UO_2 waste form degradation model implemented in PFLOTRAN and Section 4.4.2.5 for parameter values used in PA.

4.1.4 Waste Package

The shale reference case considers two waste package configurations: a 12-PWR waste package and a 4-PWR waste package. Both are assumed to consist of a stainless steel canister and a stainless steel overpack. The 12-PWR waste package is 5.2 meters in length and has a diameter of 1.37 m and contains 12 PWR SNF assemblies (5.22 MTHM), consistent with the 12-PWR waste package described by Hardin and Kalinina (2016, Section 3). The 4-PWR waste package is 5 meters in length and has a diameter of 0.84 m and contains 4 PWR SNF assemblies (1.74 MTHM), consistent with the 4-PWR emplacement described by Hardin and Kalinina (2016, Section 2).

Due to gridding limitations, the size of simulated 12-PWR waste packages is 1.67 x 1.67 x 5 m^3, and is larger in volume than 12-PWR waste packages are expected to be. The size of the simulated 4-PWR waste packages is 0.56 x 0.56 x 5 m^3, smaller than the expected volume of a 4-PWR waste package.

Waste package porosity is set equal to the fraction of void space within a 12-PWR waste package, which is 50% (Freeze et al. 2013b). Permeability is set several orders of magnitude higher than that of the surrounding materials, so that flow through waste packages is uninhibited. The waste package is given the thermal properties of stainless steel (Shelton 1934).

The shale reference uses a temperature-dependent waste-package degradation rate with a truncated log normal distribution on base degradation rate such that 50% of waste packages breach within a few tens of thousands of years. See Mariner et al. (2016, Section 4.3.2.5) for a description of the implementation in PFLOTRAN and Section 4.4.2.5 for parameter values used in PA.

4.1.5 Bentonite Buffer

The 12-PWR reference case assumes horizontal, in-drift emplacement with 12-PWR waste packages elevated on plinths of compacted bentonite and drifts buffered and filled with compacted bentonite pellets and/or bricks in one or two layers as shown in Figure 4-3 (Jove Colon et al. 2014). The 4-PWR reference case assumes emplacement of 4-PWR waste packages within rings of compacted bentonite buffer in horizontal emplacement boreholes (Figure 4-4). For simplicity, PA simulations assume that access drift and shafts are filled with compacted bentonite buffer; see the next section for a brief discussion of other materials likely to be used in these areas.

Compacted bentonite has low permeability, high sorption capacity (see Section 4.2.10.3), and may be engineered to achieve desirable thermal properties; for instance, quartz sand or graphite can be added to increase thermal conductivity (Choi and Choi 2008; Jobmann and Buntebarth 2009; Wang et al. 2015). The current set of simulations employs a single bentonite buffer with material properties appropriate for a compacted mixture of 70% bentonite and 30% quartz sand. The buffer is assigned a porosity of 0.35 (Liu et al. 2016), a permeability of 10^{-20} m^2 (Liu et al. 2016), and a water-saturated thermal conductivity of 1.5 W/m/K (Wang et al. 2014). Probabilistic simulations sample on permeability using a uniform uncertain distribution over the range 10^{-20} m^2 to 10^{-16} m^2.

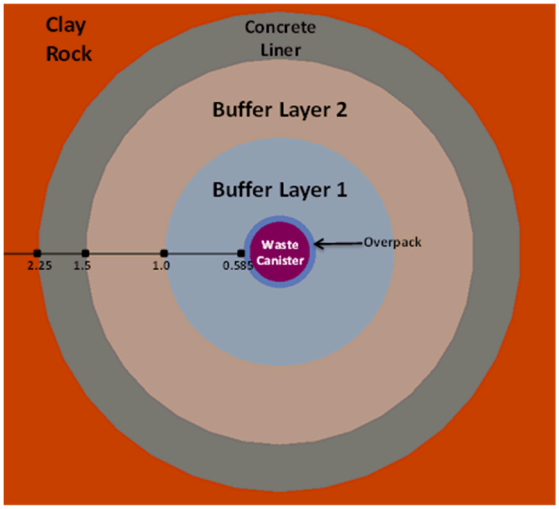

Figure 4-3. Schematic cross-section of a double-layer buffer in a 12-PWR disposal drift of a shale repository (Jove Colon et al. 2014).

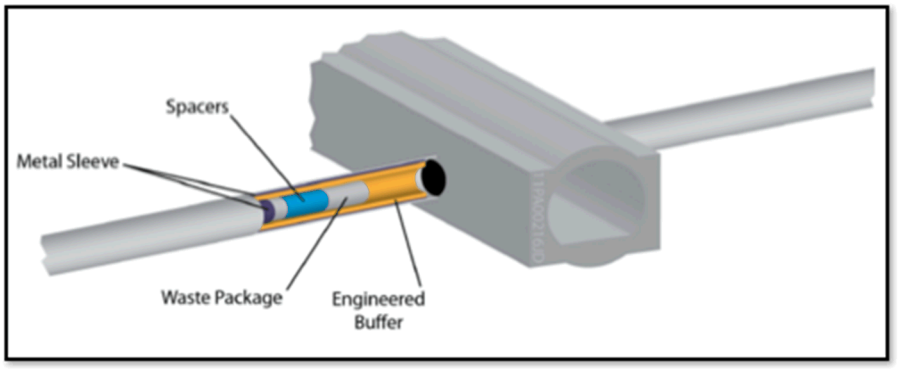

Figure 4-4. Schematic of a 4-PWR emplacement borehole. The shale reference case assumes that both the engineered buffer and the spacers are bentonite/sand buffer.

4.1.6 Other Materials

In a shale repository all access drifts and emplacement drifts would be supported with shotcrete (Jove Colon et al. 2014) or cement liners (Hardin and Kalinina 2016), and emplacement boreholes would be supported with steel liners (Hardin and Kalinina 2016). Seals of compacted bentonite supported by cement plugs would be placed at ends of disposal drifts, within shafts, and possibly at intervals within disposal and/or access drifts (ANDRA 2005). Access drifts and shafts except where sealed are likely to be filled with backfill rather than compacted bentonite, for instance crushed rock, or a mixture of crushed rock and swelling clay (e.g., ANDRA 2005).

Shotcrete, cement, steel liner and backfill materials are not simulated in the current PA.

4.2 Geosphere/Natural Barriers

Specific post-closure basis information related to the geosphere and natural barriers include:

- Characteristics of the natural barriers (e.g., location, geologic setting) (Section 4.2.1),
- Host rock characterization (Section 4.2.2),
- Disturbed rock zone (DRZ) characterization (Section 4.2.3), and
- Overburden characterization (Sections 4.2.4 through 4.2.9).

4.2.1 Natural Barrier Characteristics

The natural barrier system (NBS) comprises the shale formation hosting the repository, the disturbed rock zone (DRZ) adjacent to the repository, and geological formations above and below the host formation. On the basis of stratigraphic sequences observed in sedimentary basins throughout the U.S. (Gonzales and Johnson 1985; Perry et al. 2014), the NBS is conceptualized as a thick (on the order of thousands of meters) marine depositional sequence created by transgression and regression of inland seas, and consisting of thick layers of low permeability sediments such as shales and marls alternating with thinner layers of high permeability sediments such as limestones and sandstones.

The generic stratigraphic column for the shale reference case (Figure 4-5) has been updated this year for consistency with the regional geologic evaluation conducted by Los Alamos National Laboratory (Perry and Kelley, 2017). It consists of (from the bottom up): a 450 m thickness of indurated shale interrupted by a 30-m thick sandstone aquifer; a 75-m thick limestone aquifer; a 585 m thickness of sealing shale (the

host rock) including a 90 m thickness of a silty shale unit; a 60-m thick sandstone aquifer; and a 30 m thickness of unconsolidated overburden. Layer thicknesses and material properties are loosely based on the regional stratigraphy surrounding the Cretaceous Pierre Shale, which was chosen as an example for regional evaluation due to its large areal extent, accessible depth, stable tectonic history, and desirable mechanical and hydrological properties (Perry and Kelley 2017). The generic stratigraphic column and the rock properties described in the following sections are consistent with those used in previous models of generic clay repositories (Hansen et al. 2010; Bianchi et al. 2015) and within the range of those found in other marine depositional sequences in the U.S. (Gonzales and Johnson 1985; Perry et al. 2014).

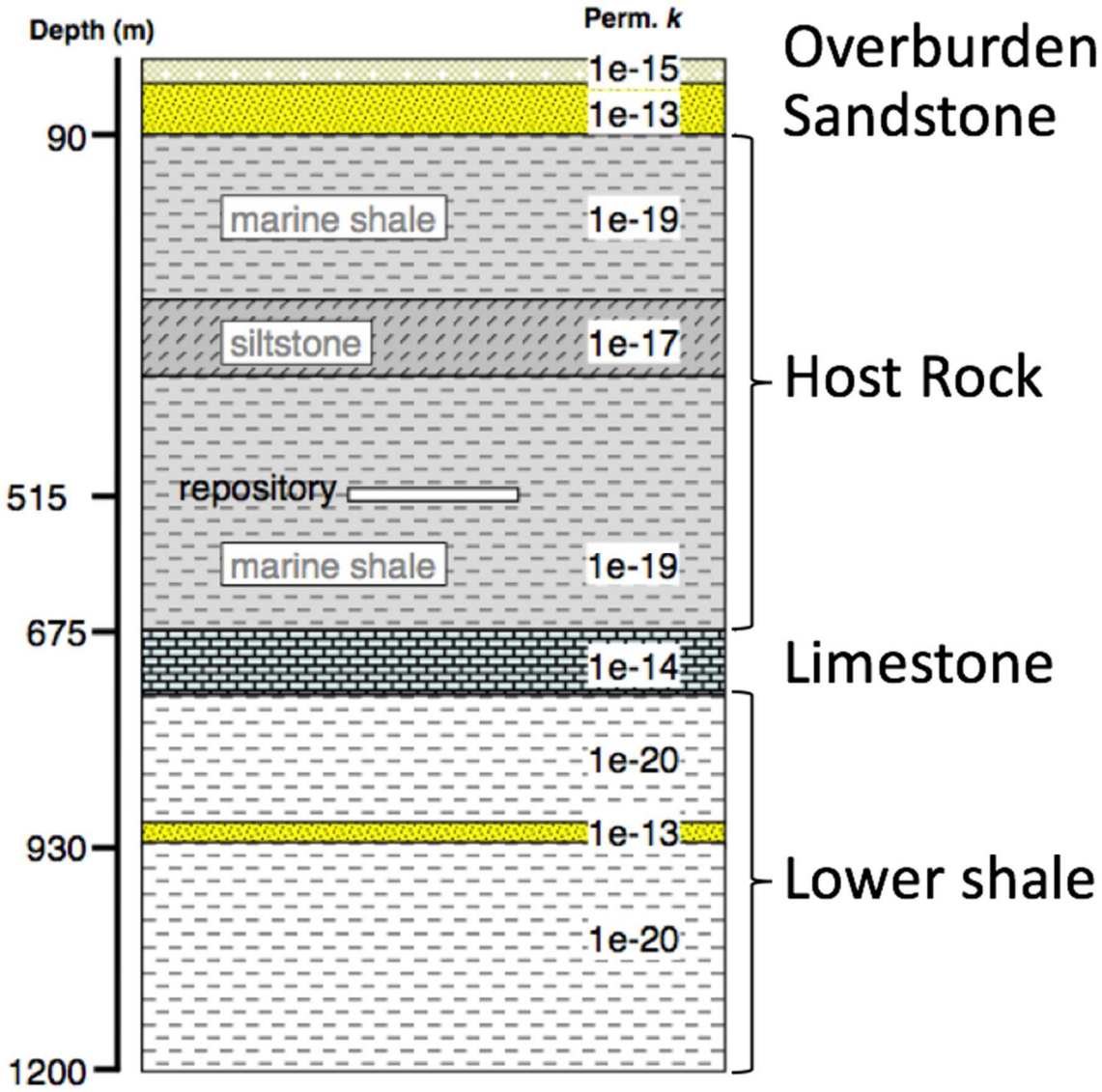

Figure 4-5. Generic stratigraphic column (Perry and Kelly 2017).

In the large sedimentary basins of the interior continental U.S., measured heat flow is generally less than 75 mW/m^2 (Blackwell et al. 2011). At repository depth, the host rock is saturated with pore fluids that are

reducing and likely saline (see Section 4.2.3). The driving force for regional flow at depth is on the order of 0.001 m/m (e.g., Downey and Dinwiddie 1988).

4.2.2 Shale Host Rock

The 585-m-thick generic shale host rock is conceptualized as a sealing shale, i.e. a shale with high clay content, low permeability, and low compressive strength (Bourg 2015). Shales under consideration for nuclear waste repositories and carbon capture and storage fall in the category of sealing shales, while shales that are hydraulically fractured for oil and gas extraction have distinctly different properties and can be categorized as brittle shales (Figure 4-6; Bourg 2015). Properties of the host rock shale are based on those of the Pierre Shale, a marine shale deposited during the Cretaceous when the Western Interior Seaway extended from the modern Gulf Coast across the Great Plains to the Arctic Ocean. The Pierre Shale locally contains thin interbeds of sandstone, limestone, and volcanic ash (bentonite) (Gonzalez and Johnson 1985). At its northwestern margin, thick massive sandstones divide the Pierre Shale into an upper shale and several lower shales (Schultz et al. 1980; Gonzales and Johnson 1985). At the western margin of the Pierre Shale other sandstone members occur within it; at the eastern margin calcareous, siliceous, and bentonitic members occur (Gonzalez and Johnson 1985; Schultz et al. 1980). The Red Bird Silty member is a silty shale that exists over much of the central Pierre Shale, dividing it into upper and lower shale members (Schultz et al. 1980).

Shales within the Pierre are typically comprised of 65 to 85% clay minerals (best estimate 70%) and have a porosity between 0.09 and 0.33 (best estimate 0.21) (Nopola 2013). Permeability calculated from laboratory measurements, borehole tests, and regional-scale flow models falls between 10^{-21} and 10^{-19} m^2 (Neuzil 1993; Neuzil 1994; Konikow and Neuzil 2007), although the permeability of individual samples (Neuzil 1986) and estimates of regional permeability based on the assumption of permeable faults can be higher (Bredehoeft et al. 1983). The compressive strength of the shale is ≤17 MPa (Gonzalez and Johnson 1985), and fractures induced by mining can be expected to self-heal within 20 years (Nopola 2013). Due to the high clay content, thermal conductivity is low – regional heat flow models assume a saturated thermal conductivity of 1.2 W/m/K (Forster and Merriam 1997).

Deterministic simulations assume that the generic shale host rock has a permeability of 10^{-19} m^2, a porosity of 0.2, and a thermal conductivity of 1.2 W/m/K. Probabilistic simulations sample on shale porosity using a uniform uncertain distribution between 0.1 and 0.25. Tortuosity (τ), a measure of the tortuous path length through a porous medium that contributes to calculation of the effective diffusion coefficient (see Sevougian et al. 2016, Appendix B), is calculated as a function of porosity using the relationship derived for the Opalinus Clay by Van Loon and Mibus (2015): $\tau = \phi^{1.4}$.

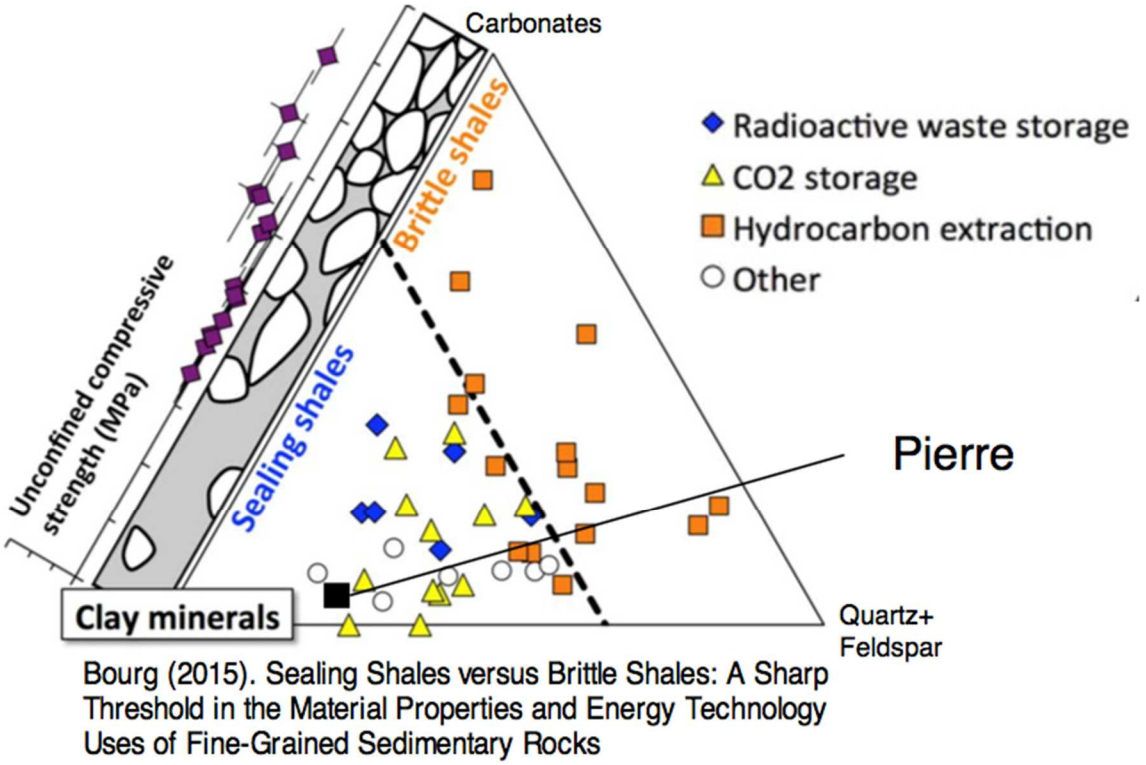

Figure 4-6. Sealing shales versus brittle shales (Bourg 2015) with the Pierre Shale plotted (Perry and Kelley 2017).

4.2.3 Disturbed Rock Zone (DRZ)

The DRZ is defined as the portion of the host rock adjacent to the engineered barrier system that experiences durable (but not necessarily permanent) changes due to the presence of the repository (Freeze et al. 2013b). The DRZ is expected to have elevated permeability with respect to the permeability of the host rock matrix for some period of time due to the changes in stress induced by mining. Although fractures in a sealing shale (see previous section) are likely to close within decades, PA simulations assume elevated permeability in the DRZ for the 1-million-year duration of the simulations. In deterministic simulations, the permeability of the DRZ (10^{-18} m^2) is 10 times that of the undisturbed host rock. In probabilistic simulations the permeability of the DRZ is sampled from a log uniform uncertain distribution between 10^{-18} m^2 and 10^{-16} m^2.

At 500 m below land surface, geomechanical modeling of a concrete-lined drift in the Pierre Shale predicts DRZ thickness slightly less than half the diameter of the excavated drift (Nopola 2013). Gridding constraints limit the options in PA simulations. As gridded in the 12-PWR model domain, the thickness of the DRZ surrounding the emplacement drifts is equal to one third the width of the drift, or 1.67 m. The thickness of the DRZ surrounding access drifts and shafts (which are gridded at a coarser resolution) is equal to the width of the access drift (5 m). As gridded in the 4-PWR model domain, the thickness of the DRZ surrounding emplacement boreholes is equal to one third the width of the borehole (0.55 m). The thickness of the DRZ surrounding access drifts and the shafts is 5 m.

4.2.4 Lower Shale

The lower shale represents a basal confining unit comprised of Mesozoic and older formations, whose stratigraphy could be considerably more complex than that represented here (see, for example, Downey and Dinwiddie 1988).

The reference case assumes the lower shale has experienced greater consolidation and induration than the host rock shale, assigning it a porosity of 0.1 and a permeability of 10^{-20} m^2. Thermal properties are identical to those of the host rock shale. Tortuosity is calculated as a function of porosity using the same relationship used for the host rock shale.

4.2.5 Lower Sandstone Aquifer

The lower sandstone aquifer (30-m thick) is modeled after the lower Cretaceous Dakota Sandstone, which consists of fluvial sandstone, siltstones, and shales, overlain by sandy deltaic deposits formed during the west to east transgression of the Cretaceous interior seaway (Bredehoeft et al. 1983; Downey 1986). Bredehoeft et al. 1983 estimate a homogeneous regional scale permeability of 2 x 10^{-12} m^2 for the Dakota Sandstone. Its porosity ranges from 0.19 to 0.22 at burial depths between 800 and 1800 m (Manger 1963).

In the reference case, the lower sandstone aquifer has a porosity of 0.2, a permeability of 10^{-13} m^2 and a saturated thermal conductivity of 3.1 W/m/K (the value reported for the Dakota by Forster and Merriam 1997). Tortuosity is calculated as a function of porosity using the relationship derived by Millington (1959) for spherical particles: $\tau = \phi^{1/3}$. Probabilistic simulations sample on aquifer permeability using a log uniform distribution between 10^{-14} and 10^{-12} m^2, a range of values toward the upper end of sandstone permeabilities (Freeze and Cherry 1979).

4.2.6 Limestone Aquifer

The limestone aquifer (75-m thick) is conceptualized as a fractured aquifer, similar in nature to the Niobrara Formation, which consists of chalks interbedded cyclically with marls (rocks containing high percentages of both carbonate and clay), and less frequently with shales and volcanic ash (Maldonado 2011). Porosity and permeability in the Niobrara depend on burial depth, decreasing from approximately 0.3 and 5 x 10^{-14} m^2 at shallow burial depths to approximately 0.05 and 5 x 10^{-17} m^2 at greater burial depths (Maldonado 2011).

In the reference case, the limestone aquifer has a porosity of 0.1, a permeability of 10^{-14} m^2 and a saturated thermal conductivity of 2.6 W/m/K (the value reported for limestone in the Niobrara by Forster and Merriam 1997). Tortuosity is calculated as a function of porosity using the same relationship used for the host rock shale. Probabilistic simulations sample on aquifer permeability using a log uniform distribution between 10^{-17} and 10^{-14} m^2.

4.2.7 Silty Shale

The silty shale unit (90 m-thick) within the host rock represents some of the vertical heterogeneity that could be encountered in a thick marine shale deposited in an interior sea. For instance, the Pierre Shale contains the approximately 90-m thick Red Bird Silty Member in addition to regional calcareous, siliceous, bentonitic, and sandstone members.

The reference case assumes properties for the silty shale between those of sandstone and shale, including a porosity of 0.2, a permeability of 10^{-17} m^2, and a saturated thermal conductivity of 1.4 W/m/K (Forster and Merriam 1997). Tortuosity is calculated as a function of porosity using the same relationship used for the host rock shale.

A 5-m thick DRZ surrounds each shaft in the silty shale. The permeability of the silty shale DRZ is 10^{-16} m^2.

4.2.8 Upper Sandstone Aquifer

The upper sandstone aquifer is the release pathway to the biosphere. The 60-m thickness could contain several distinct sandy members deposited in a nearshore environment as the interior sea receded. For instance, the Fox Hills sandstone shares a gradational contact with the Pierre Shale. Its basal unit is a sandy shale that grades to poorly consolidated sandstone. The overlying unit is a fine- to medium- grained sandstone, cross-bedded near the top. Above is a unit of thinly interbedded sandstone and siltstone/shale. The uppermost unit is a massive fine-grained sandstone. Lateral gradations, occasional erosional channels, concretions, lignite seams, an ash layer, and fossiliferous beds complete the picture (Cvankara 1976).

Ignoring the likely heterogeneous nature of the upper sandstone aquifer, the reference case assumes properties similar to those of the lower sandstone aquifer, including a porosity of 0.2, a horizontal permeability of 10^{-13} m^2 and a saturated thermal conductivity of 3.1 W/m/K. The presence of low permeability interbeds is approximated by assigning a vertical permeability that is 10 times less than horizontal permeability. Tortuosity is calculated as a function of porosity using the relationship derived by Millington (1959) for spherical particles: $\tau = \phi^{1/3}$. Probabilistic simulations sample on aquifer permeability using a log uniform distribution between 10^{-15} and 10^{-13} m^2 for horizontal permeability (a range of values toward the middle of sandstone permeabilities (Freeze and Cherry 1979)); vertical permeability is adjusted accordingly.

A 5-m thick DRZ surrounds each shaft in the upper sandstone aquifer. The permeability of the sandstone DRZ is 10^{-12} m^2.

4.2.9 Sedimentary Overburden

The unconsolidated sedimentary overburden (30-m thick) is given material properties including porosity (0.2) and permeability (10^{-15} m^2) appropriate for a silty glacial till (Freeze and Cherry 1979). It is assigned a thermal conductivity of 1.7 W/m/K and tortuosity is calculated as a function of porosity using the same relationship used for the host rock shale.

A 5-m thick DRZ surrounds each shaft in the sedimentary overburden. The permeability of the overburden DRZ is 10^{-14} m^2.

4.2.10 Chemical Environment

4.2.10.1 Pore Fluid Chemistry

Porewater of a deep, hydraulically isolated shale can be conceptualized as seawater (connate water) equilibrated (or partially so) with the surrounding mineral assemblage, isolated from the atmosphere, and in diffusive communication with porewaters of overlying and underlying geologic units, including aquifers in which water is flowing. Porewater composition within the shale will be transient on long time scales and dependent on distance to adjacent aquifers, porewater composition in adjacent aquifers, and time elapsed since the shale/aquifer system originated (Mazurek et al. 2011). Overall, porewater is likely to be of moderate ionic strength, reducing, and of neutral to slightly alkaline pH, similar to the porewaters of the Callovo-Oxfordian argillite (ANDRA 2005) or the Opalinus Clay (Turrero et al. 2006).

4.2.10.2 Solubility

ANDRA (2005b) report solubilities of radioelements in Callovo-Oxfordian porewater. Clayton et al. (2011) and Mariner et al. (2015) used these solubility values to model a generic shale repository, and we use them again here (Table 4-5). We ignore the complexity of the near field environment (elevated temperature and the presence of introduced materials including oxygen, waste form, waste package, and bentonite buffer) and likely far field variations of porewater chemistry with depth and assume homogeneous solubility limits throughout the model domain.

Table 4-5. Element solubility limits for clay reference case (Clayton et al. 2011, Table 3.3-23).

Element	Solubility Limit (mol/L)
Am	4×10^{-7}
Pu	2×10^{-7}
Np	4×10^{-9}
U	7×10^{-7}
Th	6×10^{-7}
Ra	1×10^{-7}
Cl	Infinitely Soluble
Tc	4×10^{-9}
I	Infinitely Soluble
Cs	Infinitely Soluble

4.2.10.3 Adsorption

Adsorption is modeled using a linear isotherm; distribution of a solute between the aqueous and adsorbed phase is characterized by the distribution coefficient K_d (Table 4-6), where the concentration in the adsorbed phase is proportional to the concentration in the aqueous phase. The use of K_d is a simplification of a complex system. K_d values depend on mineralogy, temperature, and pore water composition including ionic strength, pH, and eH (Miller and Wang 2012). It is expected that a site-specific PA would rely upon site-specific K_d values or other site-specific sorption parameters.

The clay reference case uses material-specific K_d values compiled in Clayton et al. (2011). Far field K_d values from the ANDRA (2005b) safety case for a repository in the Callovo-Oxfordian argillite are applied to the shale host rock, the siltstone unit within the host rock formation, the lower shale, and the unconsolidated overburden (Clayton et al. 2011, Table 3.3-23). Bentonite buffer K_d values from the same Andra safety case are applied to the bentonite buffer (Clayton et al. 2011, Table 3.3-19), except for Ra, which Clayton et al. 2011 assumed was non-adsorbing. Carbonate K_d values from the salt reference case presented in Clayton et al. (2011, Table 3.1-9) are applied to all three aquifers. Probabilistic simulations sample on Np K_d values in the buffer and in the host rock shale using log uniform uncertain distributions.

Table 4-6. Linear distribution coefficients (K_d) for clay reference case elements.

Element	Shale K_d[a] (mL/g)	Buffer K_d[b] (mL/g)	Aquifer K_d[c] (mL/g)
Am	50,000	12,000	89.4
Pu	900	1000	447
Np	900	1000	14.1
U	8000	100,000	0.775
Th	8000	3000	2646
Ra	1000	1000[e]	Non-adsorbing
Cl	Non- adsorbing	Non- adsorbing	Non- adsorbing
Tc	1150	114,000	50[d]
I	Non- adsorbing	Non- adsorbing	Non- adsorbing
Cs	400	380	500[d]

[a] Clayton et al. (2011) Table 3.3-23
[b] Clayton et al. (2011) Table 3.3-19
[c] Log-scale average of minimum and maximum values in Clayton et al. (2011) Table 3.1-9
[d] Mode of triangular distribution in Clayton et al. (2011) Table 3.1-9
[e] Same as shale.

4.3 Biosphere

Dose to the biosphere is simulated using the new RB1 dose model described in Section 3.2.3. RB1 is limited to dose from ingesting well water. As implemented in these simulations, a well, pumping at a rate of 500 gallons per day, supplies the drinking water for a rural family. The well is located in the shallow sandy aquifer at a distance of 5 km directly down-gradient from the repository. The well's screened interval spans the 60-m thickness of the aquifer. The well is explicitly simulated as a sink in the flow and transport model; therefore, no artificial dilution of the well water is imposed. The dose rate is calculated for an adult who consumes 2 liters per day on average.

The ingestion dose rate coefficients for the supported radionuclides in the shale repository simulations are shown in Table 4-7. Because ^{129}I and ^{36}Cl are the only radionuclides that reach the well in these simulations and both of these radionuclides have stable daughters, input parameters for unsupported radionuclides in the RB1 model are immaterial to these simulations and are not shown here.

Table 4-7. Adult ingestion dose coefficients (ICRP 2012, Table F.1).

Isotope	dcf (Sv Bq^{-1})
^{241}Am	2.0E-7
^{243}Am	2.0E-7
^{238}Pu	2.3E-7
^{239}Pu	2.5E-7
^{240}Pu	2.5E-7
^{242}Pu	2.4E-7
^{237}Np	1.1E-7
^{233}U	5.1E-7
^{234}U	4.9E-7
^{236}U	4.7E-7
^{238}U	4.5E-7
^{229}Th	4.9E-7
^{230}Th	2.1E-7
^{226}Ra	2.8E-7
^{36}Cl	9.3E-10
^{99}Tc	6.4E-10
^{129}I	1.1E-7
^{135}Cs	2.0E-9

4.4 Post-Closure Performance Assessment

4.4.1 Conceptual Model

The conceptual framework for this preliminary generic post-closure PA focuses on the components of the engineered barrier (Section 4.1), the natural barrier (Section 4.2), and the biosphere (Section 4.3) in the undisturbed scenario. Key characteristics of and processes occurring in key components of each system are summarized in Table 4-8. For ease of comparison to other reference case simulations (i.e., Mariner et al. 2015 (SNF repositories in salt and clay); Mariner et al. 2016 (SNF repository in crystalline rock); Sevougian et al. 2016 (defense waste repositories in crystalline rock and salt); and Sevougian et al. 2017 (defense waste repository in clay)), the primary performance metric is maximum radionuclide concentration rather than dose.

Table 4-8. Conceptual representation of key components in PA.

Region	Component	Key characteristics	Key processes included in PA
Engineered Barrier	Waste Form	Commercial SNF (UO_2)	Radionuclide decay, instant release fraction, waste form dissolution
	Waste Package	Stainless steel	Degradation and breach
	Bentonite Buffer	Low permeability, high sorption capacity	Radionuclide advection, diffusion, sorption, decay
Natural Barrier	Shale Host Rock	Low permeability, high sorption capacity	Radionuclide advection, diffusion, sorption, decay
	DRZ	Enhanced permeability	Radionuclide advection, diffusion, sorption, decay
	Upper Sandstone Aquifer	High permeability, potable water	Radionuclide advection, diffusion, sorption, decay
Biosphere	Pumping Well	500 gallons/day	Well water extraction, adsorption enhancement, dose by well water ingestion

Simulations assume (1) a mined repository at 515 m depth; (2) a head gradient of -0.0013 m/m from west to east (as in the salt and clay reference cases; Mariner et al. 2015); (3) a regional heat flux of 60 mW/m^2 and a mean annual surface temperature of 10 °C; and (4) a saturated model domain. Simulations that include the biosphere also assume a well located 5 km down gradient of the repository, screened in the 60-m thickness of the upper sandstone aquifer, and pumping 500 gallons/day. This pumping rate is on par with what a single rural family of six might use (Van der Leeden et al. 1990).

Processes accounted for in the conceptual model include waste package degradation, waste form (UO_2) dissolution, equilibrium-controlled radionuclide sorption and precipitation/dissolution, radioactive decay and ingrowth in all phases (aqueous, adsorbed, precipitate), coupled heat and fluid flow, and radionuclide transport via advection and diffusion. Mechanical dispersion is conservatively neglected in this iteration of the clay reference case. Including it would result in earlier arrival of radionuclides at observation points, but lower peak concentrations than reported here.

4.4.2 Numerical Implementation

PA simulations, comprising one deterministic simulation each of the 12-PWR and 4-PWR cases and a suite of 50 probabilistic simulations for the 12-PWR case, were completed using GDSA framework (Section 4.5): The unstructured mesh was gridded with Cubit (Blacker et al. 2016). Probabilistic inputs for the simulations were prepared using Dakota's Latin Hypercube Sampling (LHS) capability. Simulations of flow and transport were run with PFLOTRAN (Hammond et al. 2014).

4.4.2.1 Model Domain and Discretization

Two model domains were gridded, one for 12-PWR simulations (Figure 4-7) and one for the 4-PWR simulation. The half-symmetry model domains are 1575 m in width (*Y*) and 1200 m in height (*Z*). Each domain is long enough to place an observation point 5000 m down-gradient of the repository, making the 12-PWR domain 6855 m in length (*X*), and the 4-PWR domain (which has a longer repository footprint) 7935 m in length. Most of each domain is discretized into cells 15 m on a side. Emplacement drifts within the 12-PWR domain are discretized into cells 1.67 m (5/3 m) on a side. Emplacement boreholes within the 4-PWR domain are discretized into cells 0.56 m (5/9 m) on a side. Transitional zones of cells 5/3 m (in the 4-PWR domain) and 5 m (in both domains) on a side exist between the finely discretized emplacement zones and the remainder of the domain. The 12-PWR domain contains 6,925,936 cells, of

which approximately 3 million are the smaller cells in and around the repository. The 4-PWR domain contains 22,831,632 cells, of which approximately 18 million are the smaller cells in and around the repository. Figure 4-8 shows an *XY* slice through the 12-PWR repository at the *Z*-midpoint of the repository. Figure 4-9 shows an *XY* slice through the 4-PWR repository at the *Z*-midpoint of the repository. See Section 4.1.1 for details of repository layout.

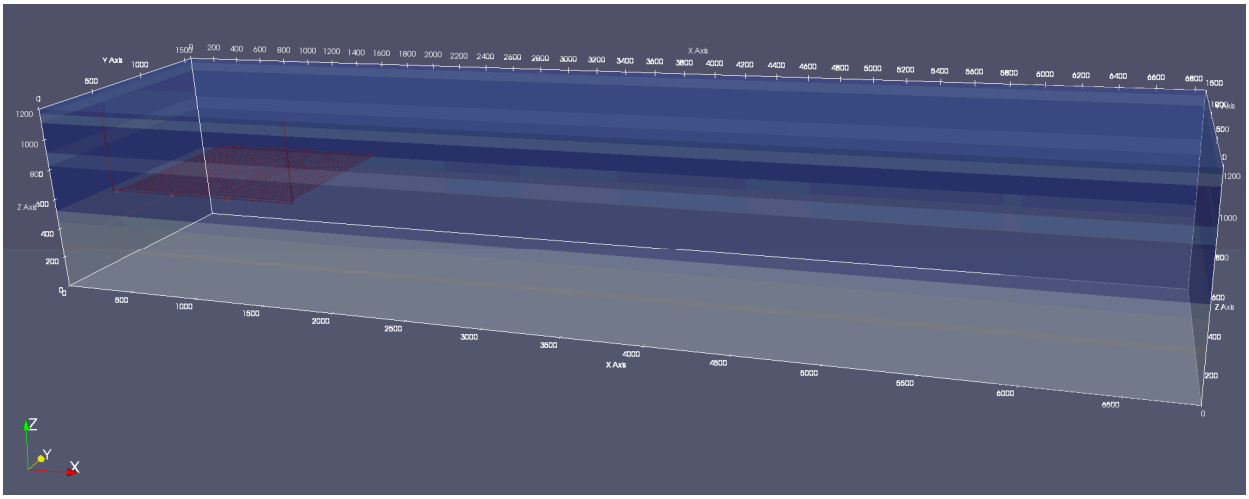

Figure 4-7. Transparent view of the 12-PWR model domain colored by material. The repository (red) is 500 m from the west (left) face of the domain and 515 m below the top face of the domain. 40-m long hallways connect the disposal panel to the south (front) face of the domain, which is a reflection boundary. Shades of blue represent the stratigraphic column described in Section 4.2.1.

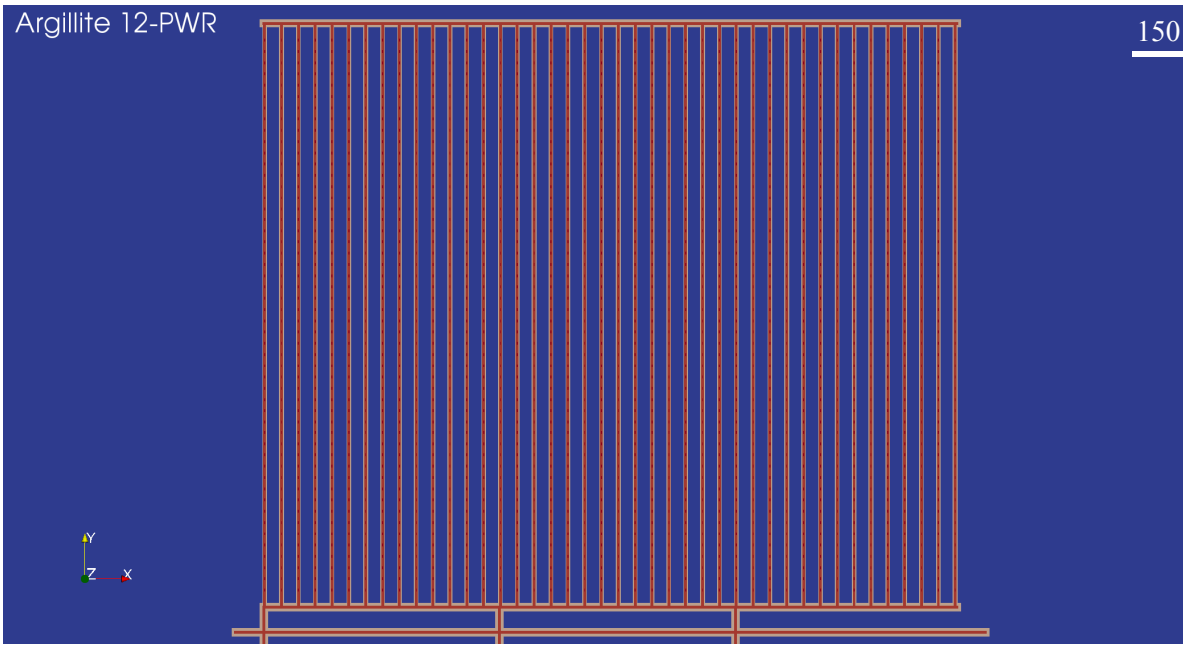

Figure 4-8. *XY* slice through the 12-PWR repository colored by material: blue, host rock; tan, DRZ; orange, buffer/backfill; red, waste packages. The base of the figure is the south face of the model domain, which is a reflection boundary. A vertical shaft is gridded at either end of the southern-most hall, which is approximately 1280 m long.

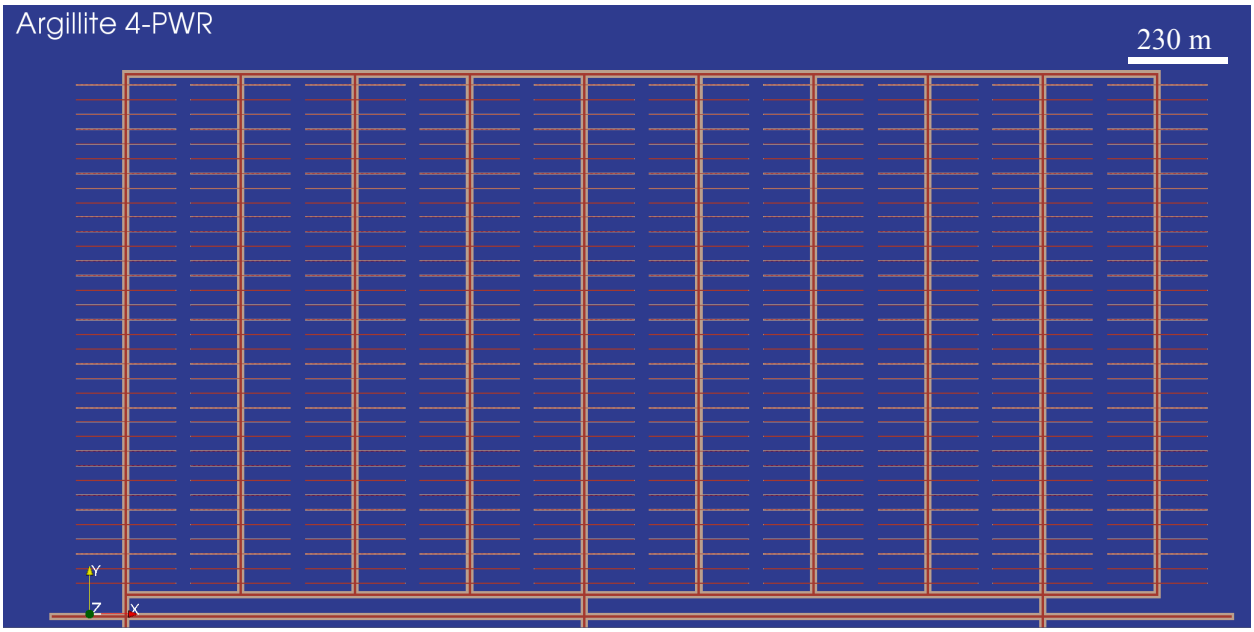

Figure 4-9. XY slice through the 4-PWR repository colored by material: blue, host rock; tan, DRZ, orange, buffer/backfill; red, waste packages. Image quality is insufficient to resolve all waste packages; each disposal borehole contains 9 waste packages. The base of the figure is the south face of the model domain, which is a reflection boundary. A vertical shaft is gridded at either end of the southern-most hall, which is approximately 2390 m long.

4.4.2.2 Initial Conditions

Initial conditions specified are pressure, temperature, and radionuclide concentrations. Initial pressures and temperatures throughout the model domain are calculated by applying a liquid flux of 0 m/s and an energy flux of 60 mW/m^2 to the base of the domain and holding temperature (10°C) and pressure (approximately atmospheric) constant at the top of the domain, and allowing the simulation to run to 10^6 years. Pressure at the top of the domain decreases from west (left) to east (right) with a head gradient of -0.0013 (m/m). This technique results in initial conditions that represent a geothermal temperature gradient and hydrostatic pressure gradient in the vertical direction, and a horizontal pressure gradient that drives flow from west to east. Simulations model include the 17 radionuclides listed in Table 4-4; initial concentrations of all radionuclides in all cells are 10^{-20} mol/L.

4.4.2.3 Boundary Conditions

Boundary conditions must be set for the six faces of the model domain. Fluxes of heat, fluid, and solute are set to zero at the south face of the model domain, creating a reflection boundary and virtually doubling the volume of the model domain. At all other faces, initial pressures and temperatures are held constant. Radionuclide concentrations are held such that any fluid entering the model domain contains 10^{-20} mol/L of each radionuclide, while fluid exiting the model domain is allowed to carry with it ambient concentrations. Diffusive flux across outflow boundaries is disallowed by specifying a zero concentration gradient.

4.4.2.4 Waste Package Heat Sources

Each waste package is modeled as a transient heat source. The energy (watts per waste package) entering the model domain is updated periodically according to values in a lookup table. The initial value is that for PWR SNF 100 yr OoR (calculated from the total decay heat at 100 years plotted in Figure 4-2). For

12-PWR waste packages (5.22 MTHM), the initial value is 3084 W; for 4-PWR waste packages (1.74 MTHM), the initial value is 1028 W. Between times specified in the lookup table, the energy input is linearly interpolated.

4.4.2.5 Waste Package Breach and Radionuclide Source Term

The waste package degradation model implemented in PFLOTRAN (Mariner et al. 2016, Section 4.3.2.5) calculates normalized remaining canister thickness at each time step as a function of a base canister degradation rate, a canister material constant, and temperature. Waste package breach occurs when this thickness reaches zero. Deterministic simulations assign a base canister degradation rate for each waste package by sampling on a truncated log normal distribution with a mean of $10^{-4.5}$/yr, a standard deviation of 0.5 (log units) and an upper truncation of -3.5 (log units). Probabilistic simulations sample on the mean degradation rate using a log uniform distribution from $10^{-5.5}$/yr to $10^{-4.5}$/yr. The mean and standard deviation parameter values used in these simulations are placeholders used to approximate the conceptual timeline for waste package failure as presented in Wang et al. (2014, Figure 2-19), where the waste package failure period extends from $10^{-4.3}$ to $10^{-6.5}$ yr, while also including heterogeneity across waste packages. Mechanistic models and appropriate data are needed for robust simulation of waste package degradation under predicted environmental conditions.

PFLOTRAN calculates the decayed radionuclide inventory in each waste package region at each time step. From the time of waste package breach, the waste form releases radionuclides in two fractions: instant-release and slow-release. The instant-release fraction is due to the accumulation of certain fission products in void spaces of the waste form and occurs at the time of waste package breach. The shale reference case assumes a non-zero instant-release fraction for ^{135}Cs, ^{129}I, ^{99}Tc, and ^{36}Cl (Table 4-9), and zero for all other radionuclides in the simulations. The slow-release fraction is due to fuel matrix (UO_2) dissolution, which is modeled using a fractional dissolution rate of 10^{-7}/yr starting from the time of waste package breach. This rate is the mode of a log triangular distribution (Table 4-10) appropriate for fuel 3,000-10,000 years OoR and strongly reducing conditions (SKB 2006; Ollila 2008); for a complete discussion refer to Sassani et al. (2016, Section 3.2.1). Probabilistic simulations sample on the waste form dissolution rate over the range 10^{-8}/yr to 10^{-6}/yr, but simplify the distribution to log uniform rather than log triangular. This distribution is identical to that used in the most recent generic crystalline repository PA (Mariner et al. 2016).

Table 4-9. Isotope instant release fractions recommended by Sassani et al. (2012) for PWR with 60 GWd/MTHM burn-up.

Isotope	Instant Release Fraction
^{135}Cs	0.1
^{129}I	0.1
^{99}Tc	0.07
^{36}Cl	0.05

Table 4-10. SNF dissolution rates; log triangular distribution from cited SKB (2006) in Sassani et al. (2016, Section 3.2.1)

Parameter	Rate (yr^{-1})	Time to 50% dissolution (yr)	Time to 99% dissolution (yr)
Min	10^{-8}	6.93×10^{7}	4.61×10^{8}
Mode	10^{-7}	6.93×10^{6}	4.61×10^{7}
Max	10^{-6}	6.93×10^{5}	4.61×10^{6}

4.4.2.6 Material Properties

Material properties are discussed in Sections 4.1 and 4.2; values used in PA simulations are summarized in Table 4-11 (deterministic parameter values) and Table 4-12 (sampled parameter ranges).

Table 4-11. Parameter values used in deterministic simulations.

Model Region	Permeability (m^2)	Porosity ϕ	τ	Effective Diffusion Coefficient[2] (m^2/s)	Saturated Thermal Conductivity (W/m/K)	Heat Capacity (J/kg/K)	Grain Density (kg/m^3)
Overburden	1×10^{15}	0.20	0.11	2.2×10^{11}	1.7	830	2700
Upper Sandstone	1×10^{-13}	0.20	0.58	1.2×10^{10}	3.1	830	2700
Host Rock Shale	1×10^{-19}	0.20	0.11	2.2×10^{11}	1.2	830	2700
Silty Shale	1×10^{-17}	0.20	0.11	2.2×10^{11}	1.4	830	2700
Limestone	1×10^{14}	0.10	0.04	4.0×10^{12}	2.6	830	2700
Lower Shale	1×10^{20}	0.10	0.04	4.0×10^{12}	1.2	830	2700
Lower Sandstone	1×10^{-13}	0.20	0.58	1.2×10^{10}	3.1	830	2700
Buffer	1×10^{20}	0.35	0.23	8.1×10^{11}	1.5	830	2700
Waste Package	1×10^{16}	0.50	1	5×10^{10}	16.7	466	5000

[1] Effective diffusion coefficient = $D_w \phi \tau s$, where the free water diffusion coefficient (D_w) = 1 x 10^{-9} m^2/s (Li and Gregory 1974) and saturation (s) = 1

[2] $\tau = \phi^{1.4}$ (Van Loon and Mibus 2015)

[3] $\tau = \phi^{1/3}$ (Millington 1959)

Table 4-12. Sampled parameters and their distributions.

Parameter	Range	Units	Distribution
SNF Dissolution Rate	10^{-8} – 10^{-6}	yr^{-1}	log uniform
Mean Waste Package Degradation Rate	$10^{-5.5}$ – $10^{-4.5}$	yr^{-1}	log uniform
Upper Sandstone k	10^{-15} – 10^{-13}	m^2	log uniform
Limestone k	10^{-17} – 10^{-14}	m^2	log uniform
Lower Sandstone k	10^{-14} – 10^{-12}	m^2	log uniform
Buffer k	10^{-20} – 10^{-16}	m^2	log uniform
DRZ k	10^{-18} – 10^{-16}	m^2	log uniform
Host Rock (Shale) Porosity	0.1 – 0.25	-	uniform
Np K_d Buffer	0.1 – 702	m^3kg^{-1}	log uniform
Np K_d Shale	0.047 – 20	m^3kg^{-1}	log uniform

4.5 Simulation Results

Deterministic and probabilistic results are discussed in terms of concentrations of the long-lived radionuclides ^{129}I ($t_{1/2} = 1.57\times10^7$ yr) and ^{237}Np ($t_{1/2} = 2.14\times10^6$ yr). ^{129}I is assumed to have unlimited solubility and to be non-adsorbing; it thus behaves nearly conservatively. ^{237}Np is solubility-limited and adsorbing. Temperature fields, flux vectors, and waste package breach times for a single deterministic simulation are also presented.

4.5.1 Deterministic Results

4.5.1.1 Temperature

The background geothermal gradient results in an initial repository temperature of 27.8 °C. In both simulations, waste package temperatures peak at approximately 20 years, reaching a high of 151 °C in the 12-PWR simulation and 104 °C in the 4-PWR simulation (Figure 4-10). These temperatures are the result of assuming a saturated repository and saturated thermal conductivities for buffer and host rock; they do not represent the temperatures that might be reached if an unsaturated repository were simulated.

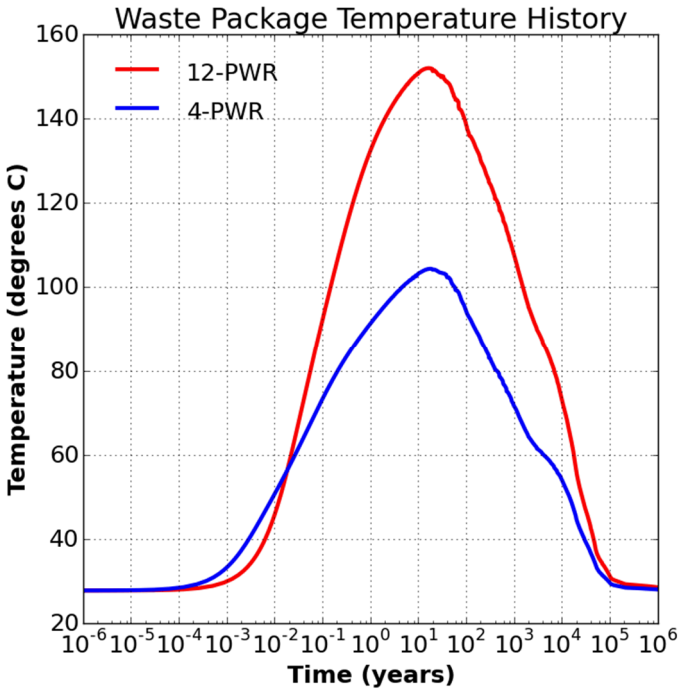

Figure 4-10. Waste package temperature versus time in the 12-PWR (red) and 4-PWR (blue) simulations.

4.5.1.2 Waste Package Breach

Ten percent of the waste packages have breached by 6000 y in the 12-PWR simulation, and by 8000 y in the cooler 4-PWR simulation (Figure 4-11). (Recall that waste package degradation rate is temperature dependent.) In both simulations nearly all the waste packages have breached by 1 My.

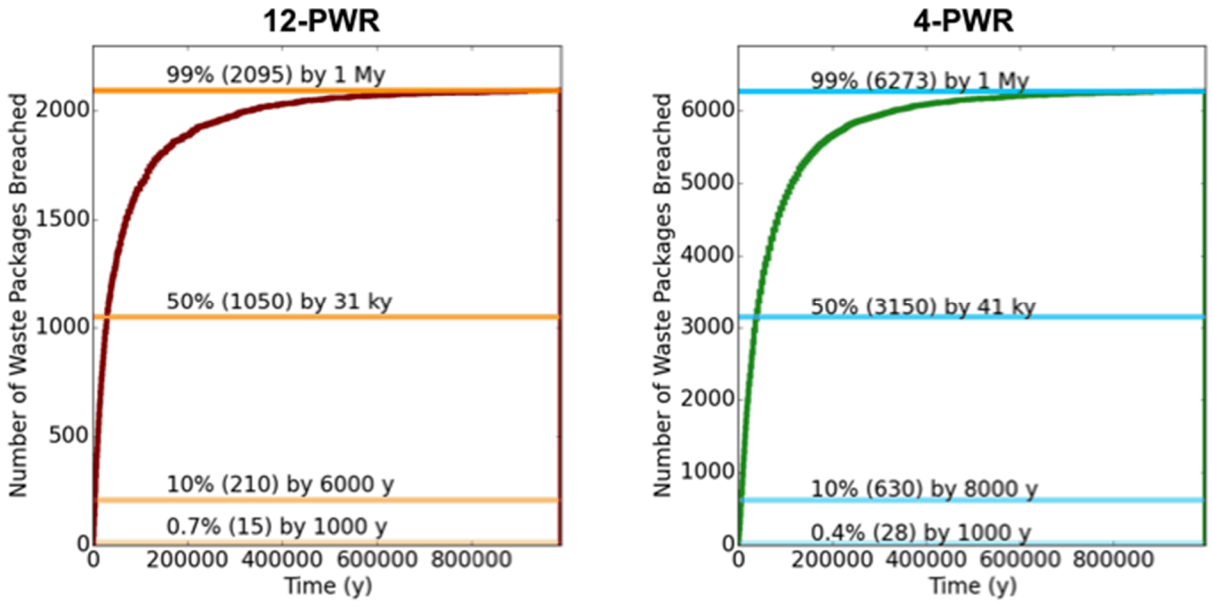

Figure 4-11. Cumulative number of waste packages breached versus time in 12-PWR (left) and 4-PWR (right) simulations.

4.5.1.3 I-129

The 12-PWR and 4-PWR simulations result in nearly identical concentrations at points within the upper sandstone aquifer (the conceptual path to the biosphere), with the greatest difference occurring near the repository (Figure 4-12). For this reason, only 12-PWR results are shown in more detail (Figure 4-13 through Figure 4-16).

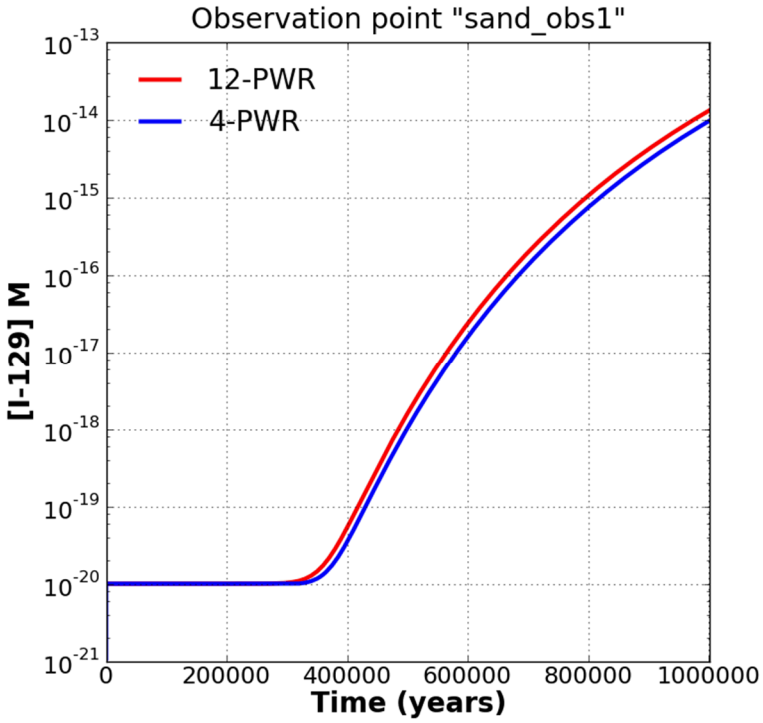

Figure 4-12. ^{129}I concentration in the upper sandstone aquifer ~30 m downgradient from the edge of the repository.

Transport away from the repository is diffusive within the host rock, and begins when the earliest waste packages breach. At 1000 y, a handful of waste packages have breached, and ^{129}I is confined to the immediate vicinity of the breached waste packages (Figure 4-13). At 10,000 y, fewer than 50% of the waste packages have breached, and ^{129}I remains confined to the near field (Figure 4-14). By 100,000 y, ^{129}I has reached the limestone aquifer, 160 m beneath the repository, at 10^{-15} M concentrations (Figure 4-15). By 1 My, ^{129}I has reached the upper sandstone aquifer, 425 m above the repository, at 10^{-15} M concentrations, and advected in both aquifers to the downstream end of the model domain, just over 5 km beyond the edge of the repository (Figure 4-16).

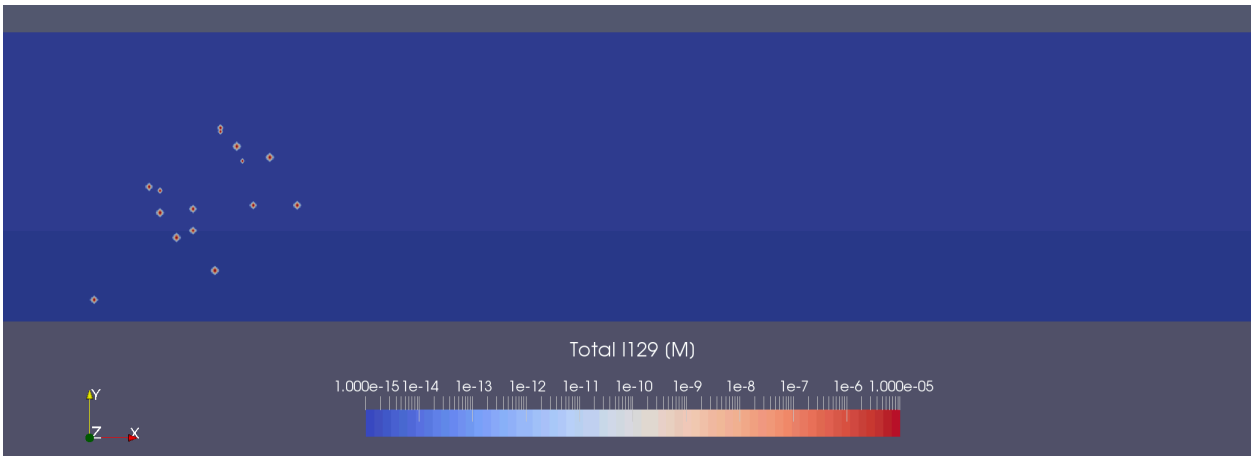

Figure 4-13. ^{129}I concentration at 1000 y in the 12-PWR simulation plotted in a horizontal slice through the model domain at the elevation of the repository.

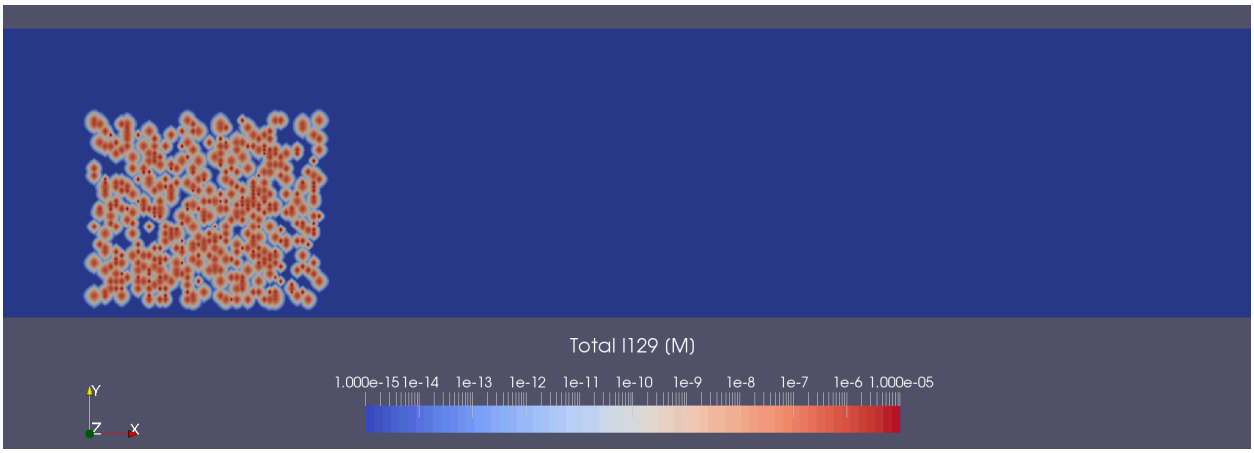

Figure 4-14. ^{129}I concentration at 10,000 y in the 12-PWR simulation plotted in a horizontal slice through the model domain at the elevation of the repository.

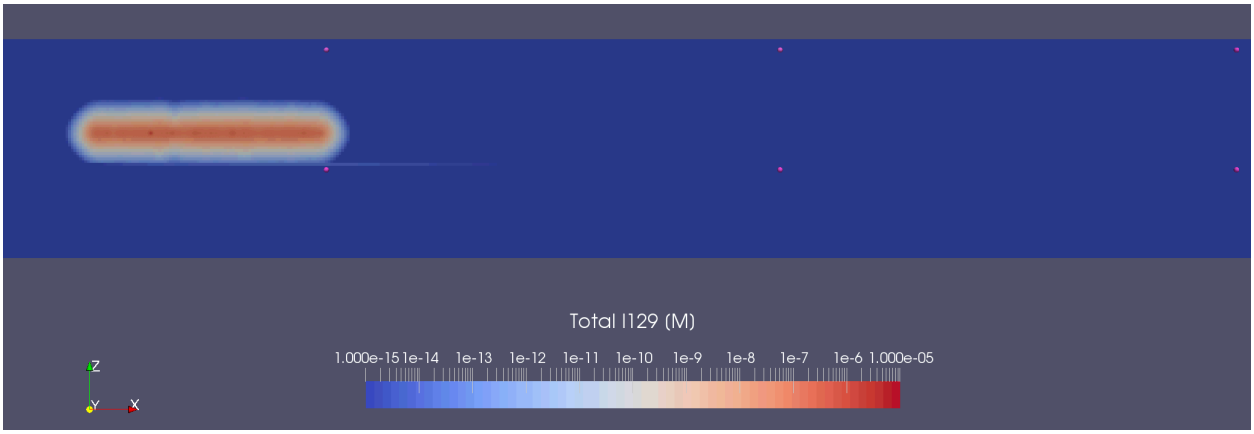

Figure 4-15. ^{129}I concentration at 100,000 y in the 12-PWR simulation plotted in a vertical slice through the model domain at the Y-midpoint of the repository.

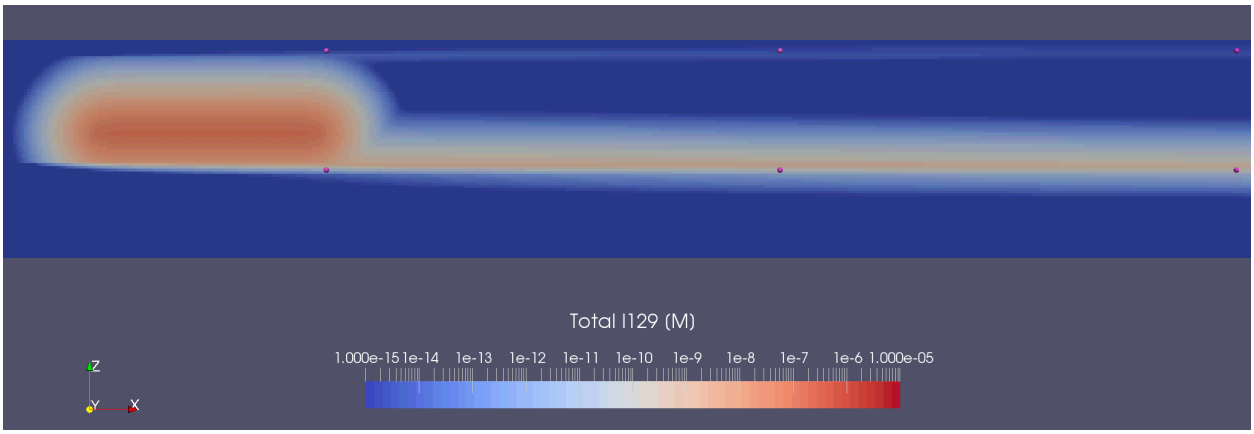

Figure 4-16. ^{129}I concentration at 1,000,000 y in the 12-PWR simulation plotted in a vertical slice through the model domain at the Y-midpoint of the repository.

4.5.1.4 Cl-36

^{36}Cl, which like ^{129}I, behaves conservatively (neither adsorbs nor precipitates) exists in the limestone aquifer at concentrations greater than 10^{-15} M by 1,000,000 y, but not in the upper sandstone aquifer (Figure 4-17). The plume of ^{36}Cl has much lower concentrations than that of ^{129}I because the ^{36}Cl release rate is much lower than that of ^{129}I. The lower release rate is due to a much lower inventory (Table 4-4), faster decay (Table 4-4), and a lower instant release fraction (Table 4-9).

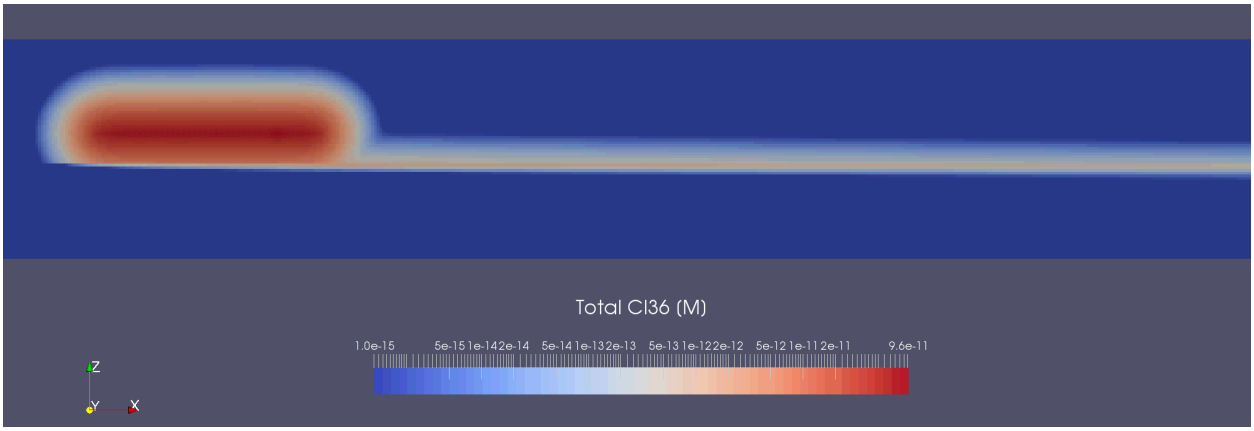

Figure 4-17. ^{36}Cl concentration at 1,000,000 y in the 12-PWR simulation plotted in a vertical slice through the model domain at the Y-midpoint of the repository.

4.5.1.5 Np-237

^{237}Np (and other radionuclide species that adsorb and/or precipitate) remain within the vicinity of the repository throughout the 1 My simulation (Figure 4-18).

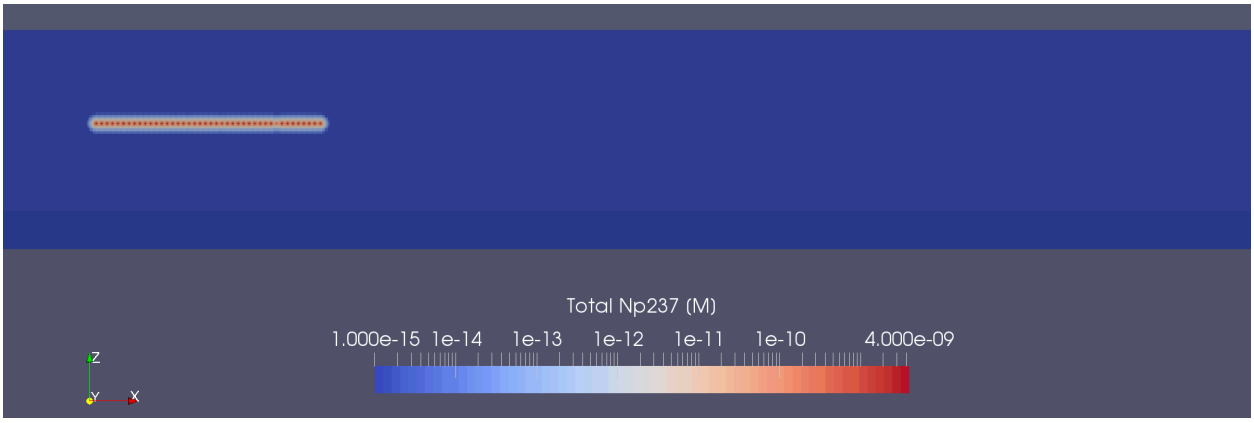

Figure 4-18. ^{237}Np concentration at 1,000,000 y in the 12-PWR simulation plotted in a vertical slice through the model domain at the Y-midpoint of the repository.

4.5.1.6 Dose Rate

Dose rate due to ingestion of well water is calculated for the pumping well in the sandy (upper) aquifer approximately 5 km downgradient of the repository. Simulations predict that ^{129}I and ^{36}Cl, which neither adsorb nor precipitate, contribute to dose rate at the well. A dose rate exceeding 10^{-14} Sv/yr is reached at about 0.5 My. The rate continues to increase for the remainder of the simulation, reaching a maximum of less than 2 x 10^{-10} Sv/yr at 1 My (Figure 4-19). For comparison, the international safety standard recommended by the IAEA for the public is 10^{-3} Sv/yr (IAEA 2014, p. 133). No other radionuclides occur at the pumping well in excess of the initial concentrations set for the background concentrations.

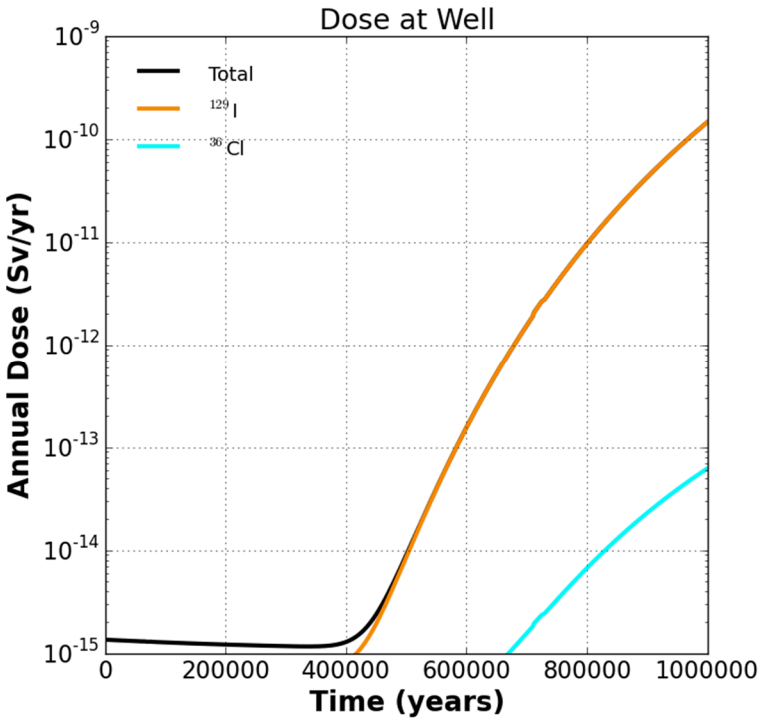

Figure 4-19. Annual dose at the pumping well as a function of time. Non-zero total annual dose (black) at early times is due to non-zero initial radionuclide concentrations.

4.5.2 Probabilistic Results

A suite of 50 probabilistic simulations was run using the 12-PWR model domain and the parameter distributions listed in Table 4-12. Concentrations of ^{129}I at three observation points in the upper sandstone aquifer and three observation points in the limestone aquifer were used to quantify uncertainty and sensitivity. In each aquifer, observation points are approximately 30, 2500, and 5000 m downgradient of the repository (Figure 4-20). Observation points are placed at the elevation in each aquifer that experiences the highest radionuclide concentration: in the lowest cell of the upper sandstone aquifer, and the highest cell of the limestone aquifer.

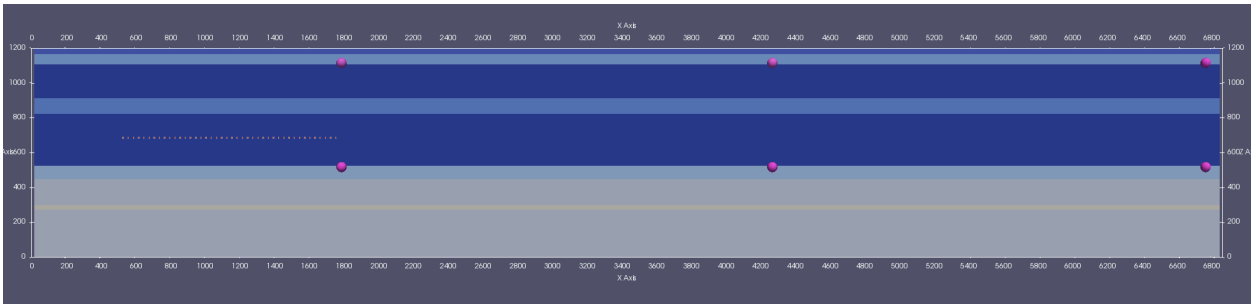

Figure 4-20. Locations of observation points in the 12-PWR model domain. From left in upper sandstone aquifer: "sand_obs1," "sand_obs2," and "sand_obs3." From left in limestone aquifer: "lime_obs1," "lime_obs2," and "lime_obs3."

4.5.2.1 Uncertainty

Breakthrough curves for ^{129}I are plotted in Figure 4-21 (sandstone aquifer) and Figure 4-22 (limestone aquifer). Total annual dose at the pumping well is plotted in Figure 4-23. In all simulations, ^{129}I concentration remains less than 10^{-12} M at "sand_obs1," less than 10^{-13} M at "sand_obs2," and less than 10^{-15} M at "sand_obs3," 5000 m downgradient of the repository. At all three locations, maximum predicted ^{129}I concentration varies by 6 to 7 orders of magnitude. Concentrations in the limestone aquifer are greater: less than 10^{-8} M at "lime_obs1" and less than 10^{-9} M at "lime_obs2" and "lime_obs3." At "lime_obs1," which is located approximately 160 m beneath the repository and 30 m east of the repository, the spread in maximum predicted ^{129}I concentration is slightly greater than 2 orders of magnitude. At the more distant observation points, maximum predicted ^{129}I concentration varies over more than 10 orders of magnitude, with approximately half the simulations predicting no increase in ^{129}I at "lime_obs2" and "lime_obs3." Dose rate at the pumping well does not exceed 10^{-9} Sv/yr, and in approximately 40% of the simulations does not exceed the dose rate due to initial radionuclide concentrations.

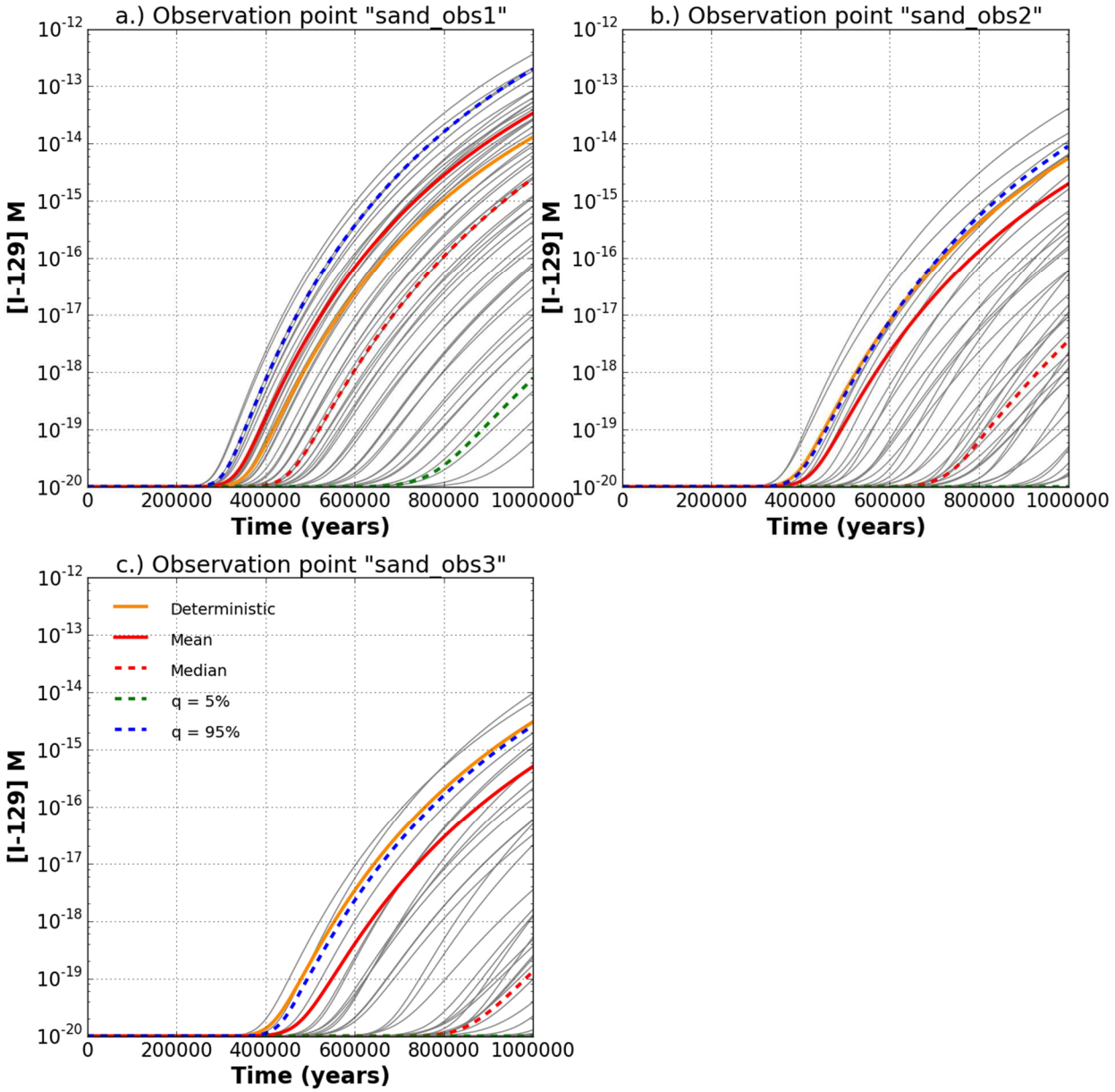

Figure 4-21. ^{129}I concentration versus time at three observation points in the upper sandstone aquifer: a) approximately 30 m downgradient of the repository; b) approximately 2500 m downgradient of the repository; c) approximately 5000 m downgradient of the repository.

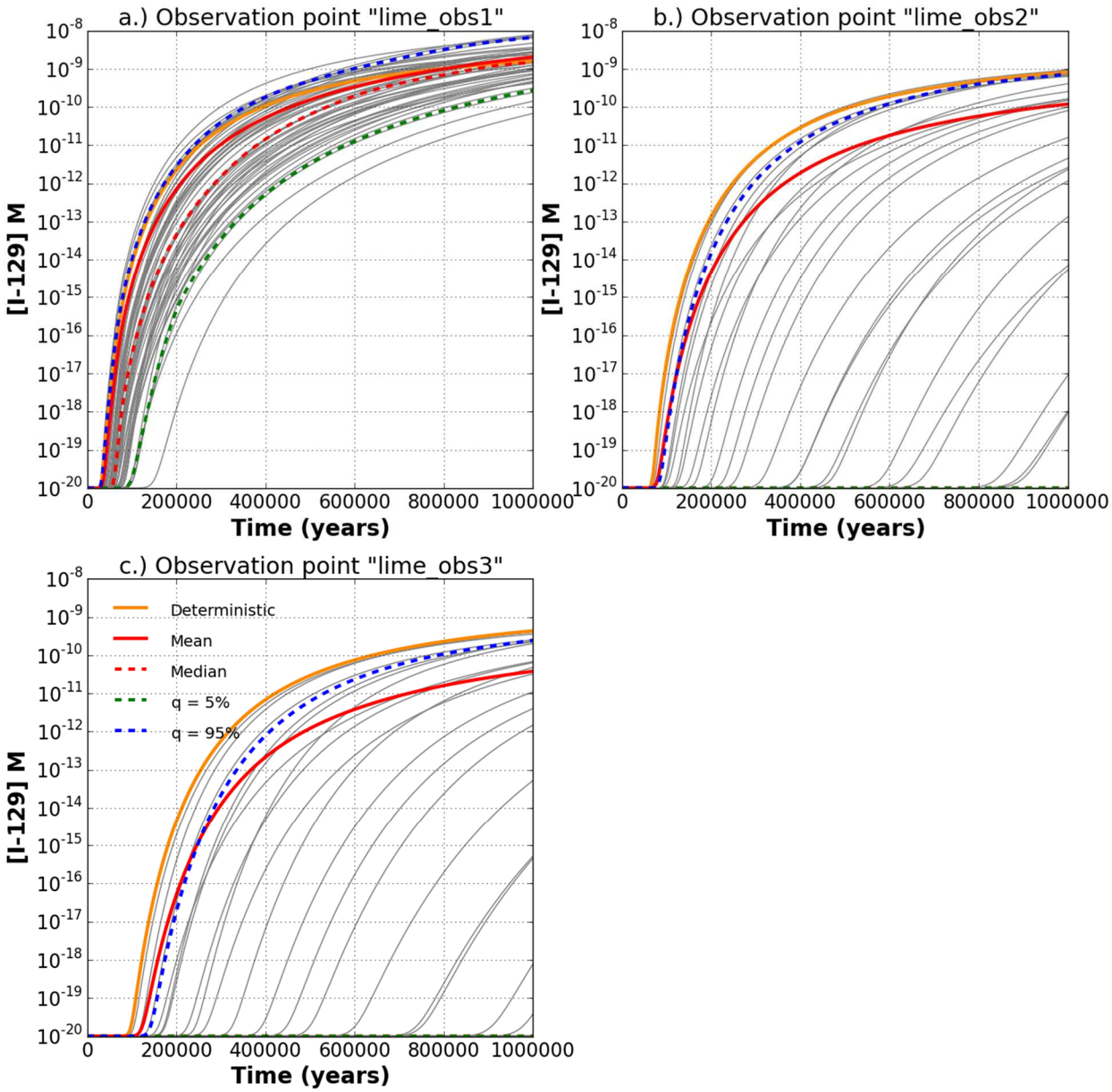

Figure 4-22. ^{129}I concentration versus time at three observation points in the limestone aquifer: a) approximately 30 m downgradient of the repository; b) approximately 2500 m downgradient of the repository; c) approximately 5000 m downgradient of the repository.

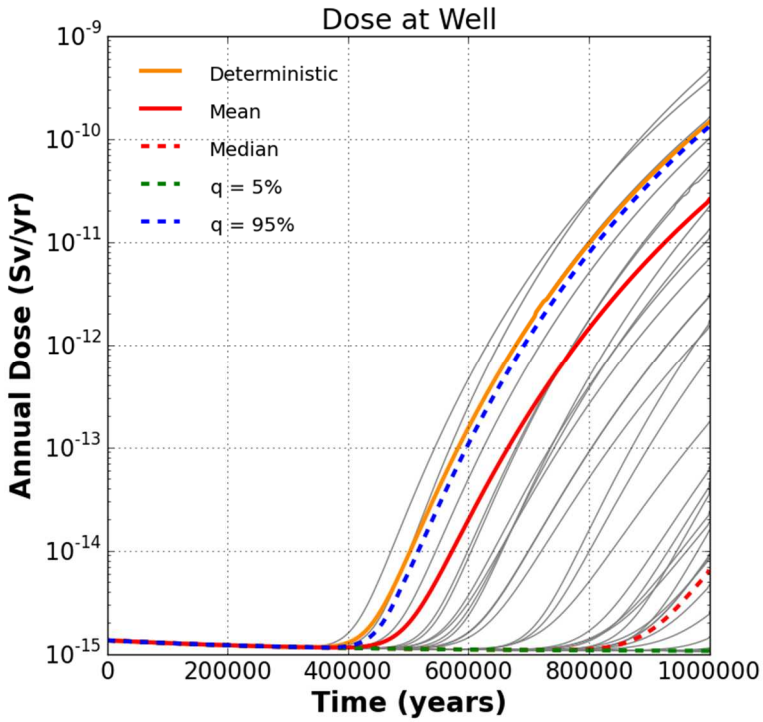

Figure 4-23. Annual dose at the pumping well approximately 5000 m downgradient of the repository. (Location coincides with the location of observation point "sand_obs3."

4.5.2.2 Sensitivity

Spearman rank correlation coefficients (SRCCs) (Helton et al. 2006) were calculated using Dakota to assess the sensitivity of maximum concentration of ^{129}I to sampled parameters (Figure 4-24). To calculate the SRCC for a given input parameter, variables in the input and output vectors for the 50 probabilistic simulations are ranked from smallest to largest and their ranks (1 through 50) are substituted for variable values. The SRCCs are then calculated as:

$$SRCC = \frac{cov(r_X, r_Y)}{\sigma_{r_X}\sigma_{r_Y}}$$

where $cov(r_X, r_Y)$ is the covariance of the ranked input (X) and output (Y) variables, σ_{r_X} is the standard deviation of the ranked input variable and σ_{r_Y} is the standard deviation of the ranked output variable, where output is the maximum ^{129}I concentration at an observation point regardless of time.

Maximum concentration of ^{129}I in the upper sandstone aquifer exhibits a strong positive correlation with shale porosity at "sand_obs1." Sensitivity to shale porosity decreases with distance from the repository, while the strength of the correlation with aquifer permeability increases (Figure 4-24).

Aquifer permeability increases in importance as distance from the repository increases because groundwater velocities in the aquifer are quite low when the aquifer permeability is sampled from the lower end of the permeability distribution. On the lower end of the distribution, permeability is on par with a typical sandstone or silt (Freeze and Cherry 1979). A low aquifer permeability combined with a low head gradient, as might occur for example for an aquifer in the Fox Hills Formation (Anna 2010), implies that as the observation point in the aquifer gets farther away, the aquifer itself can become a significant natural barrier. For this simulation, the head gradient is -0.0013 m/m and the porosity is 0.2, so

for the minimum aquifer permeability in the distribution (10^{-15} m^2) the mean travel time over a 5-km distance is around 2.4 My (and 240,000 y for 10^{-14} m^2).

Maximum concentration of ^{129}I in the limestone aquifer exhibits similar correlations including a strong positive correlation with shale porosity at "lime_obs1," and a strong positive correlation with aquifer permeability at greater distances from the repository (Figure 4-25). As with the upper sandstone aquifer, mean groundwater velocities can be very low in the limestone aquifer because the range of permeability is low and the head gradient is simulated to be the same across all units. This results in very long mean travel times for ^{129}I to reach the distant observation points and accounts for the strong correlation between ^{129}I concentration and aquifer permeability far from the repository.

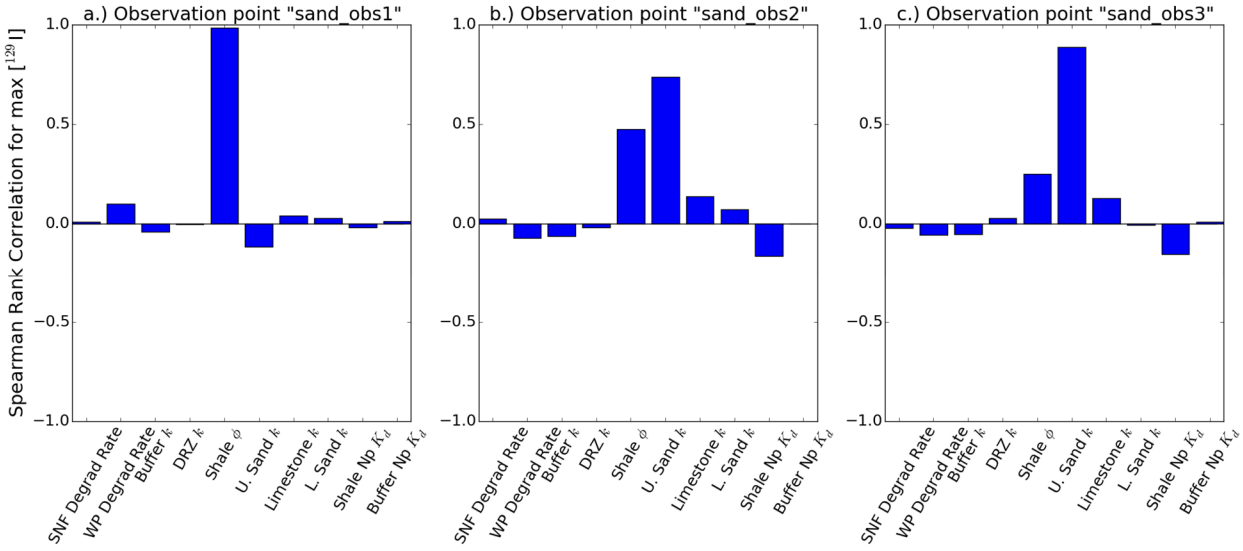

Figure 4-24. SRCCs in the upper sandstone aquifer.

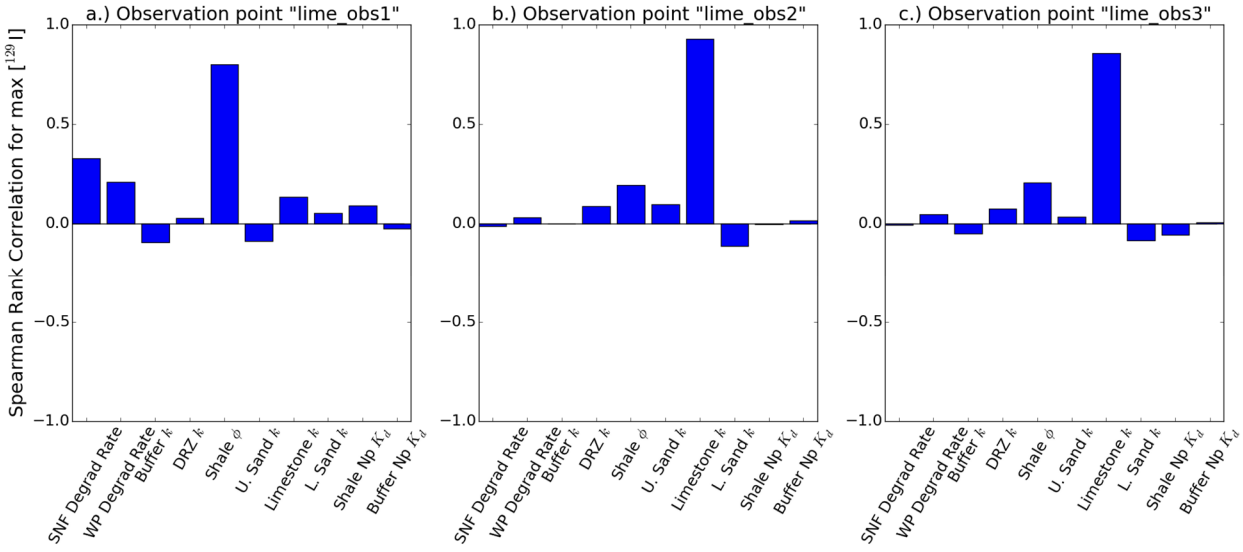

Figure 4-25. SRCCs in the limestone aquifer.

Scatter plots of ^{129}I concentration versus values of input variables offer additional insight into sensitivity for these simulations. In Figure 4-26, maximum ^{129}I concentration at the upper sandstone aquifer

observation points is plotted as a function of shale porosity and as a function of aquifer permeability. At the observation point closest to the repository ("sand_obs1") the dependence on shale porosity is obvious. At the furthest observation point ("sand_obs3"), ^{129}I concentrations remain at background levels when the aquifer permeability is sufficiently low (less than approximately 10^{-14} m^2) regardless of shale porosity.

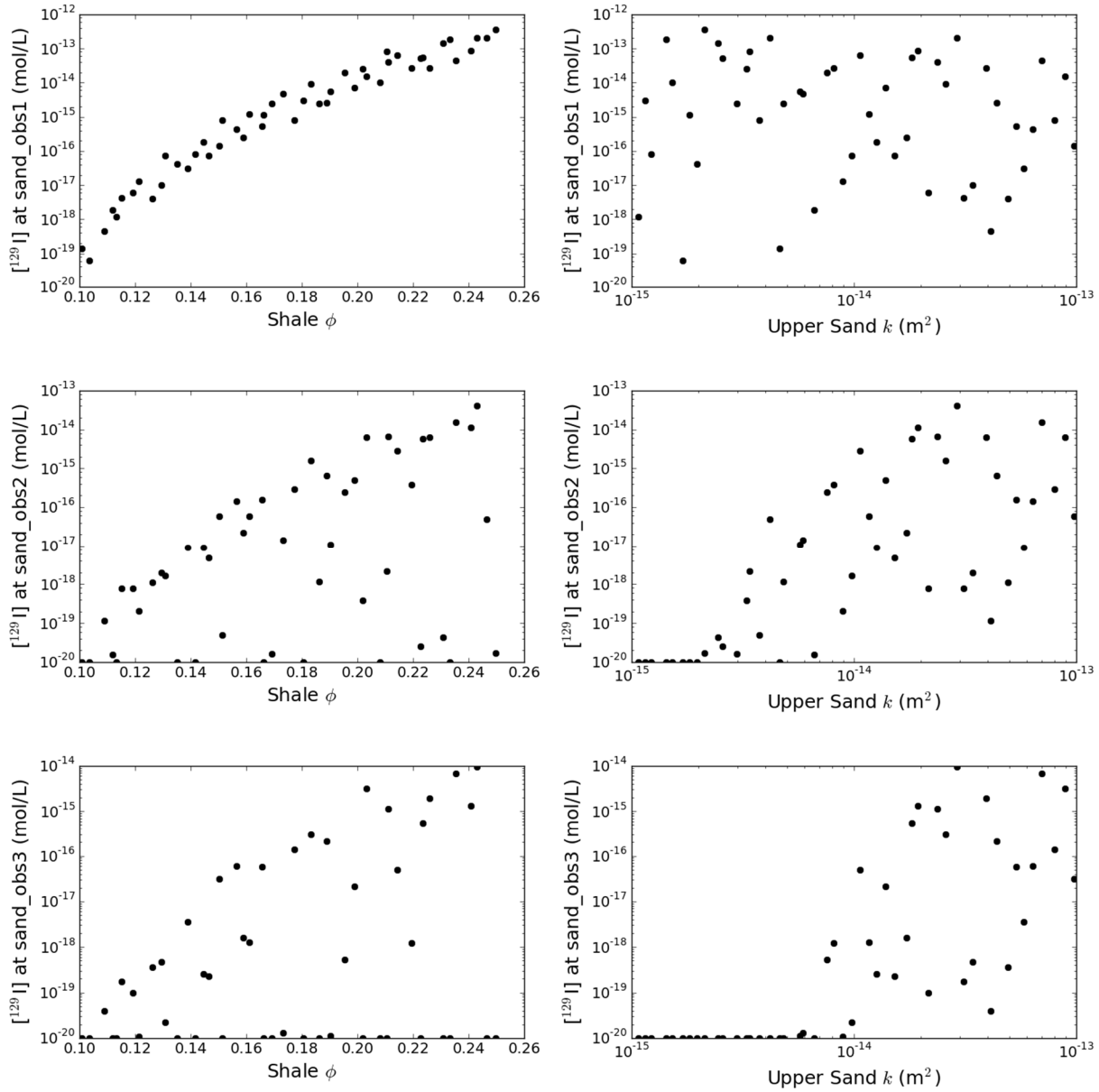

Figure 4-26. Scatter plots of maximum ^{129}I concentration versus shale porosity (left) and aquifer permeability (right) at the three observation points in the upper sandstone aquifer. From top to bottom: "sand_obs1," "sand_obs2," and "sand_obs3."

5. SUMMARY AND CONCLUSIONS

This report describes the FY 2017 activities of the Generic Disposal System Assessment (GDSA) group of the Spent Nuclear Fuel and Waste Science and Technology (SFWST) Campaign. The primary mission of the GDSA group is to develop a geologic disposal system modeling capability for nuclear waste that can be used to probabilistically assess the performance of disposal options and proposed sites. The GDSA capability is a framework called GDSA Framework that employs HPC-capable codes PFLOTRAN and Dakota. In FY 2017 the GDSA group added and improved process modeling capabilities, improved numerical convergence of flow and transport solutions through new analytical derivatives, expanded integration with other work packages for additional process models and data, developed two new generic reference simulations for the disposal of spent fuel in shale, and worked to expand its user base by presenting GDSA Framework results at multiple conferences and conducting two workshops on PFLOTRAN and GDSA Framework.

Code development this year focused on four major activities: analytical derivatives, waste form processes, dose rate calculations, and quality assurance. Analytical derivatives were developed and implemented to improve convergence of flow and transport calculations. This work resulted in significant improvements in run time (factor of three) as solver tolerances were tightened to 1.e-9. At a tighter tolerance of 5e-10, the solution using the new analytical derivatives converged in almost exactly the same run time while the numerical simulation failed. Waste form process models and decay and ingrowth processes were improved by adding spatial capabilities and implementing improved equations and solvers. A model was added for calculating dose rates due to ingestion of well water. The model implemented can account for enhanced dose rates due to highly mobile descendent radionuclides (e.g., ^{222}Rn) not explicitly simulated in the transport problem. Quality assurance activities this year involved testing flow and transport calculations and documenting the results. This year, 52 tests were developed and implemented. Documentation is available at pflotran.org.

As in the previous year, a significant effort was made to further integrate with work packages across the campaign. One of the key drivers for this year's integration work was to assure that the project R&D prioritization guidance, contained in the UFD R&D Roadmap (DOE 2012), is being used to develop a complete PA model (i.e., a complete GDSA Framework) by the year 2020. A key goal is to achieve a higher fidelity representation of the total system behavior by the use of fewer abstractions and by less decoupling of inherently coupled physical-chemical processes. Integration meetings in the fall and spring focused on the UFD R&D Roadmap, identifying gaps, prioritizing future work, and facilitating integration. The results of this work are summarized in three tables included in this report: 1) SFWST R&D activities considered for potential integration into GDSA Framework, 2) GDSA Tasks, and 3) GDSA Timeline. High priorities for integration in the next year include colloid transport modeling, clay alteration, THM model for buffer materials, salt coupled THM processes, and discrete fracture network modeling.

Generic repository system modeling this year centered on the development of two new shale repository reference cases, one for 12-PWR waste packages emplaced in-drift and one for 4-PWR waste packages emplaced in horizontal boreholes extending perpendicularly from central drifts. These models present major advances to the previous clay/shale repository reference case of FY 2015 in terms of extent, resolution, features, processes, and number of radionuclides. The generic shale host rock is 585-m thick and is conceptualized as a sealing shale, i.e. a shale with high clay content, low permeability, and low compressive strength. Moderately permeable aquifers overlie (sandstone) and underlie (limestone) the host rock. Waste packages fail largely between 6,000 and 200,000 years, and the spent nuclear fuel degrades at a mean fractional rate of 10^{-7} yr^{-1}. In both the 4-PWR and 12-PWR simulations, waste package temperatures peak at approximately 20 years, with the 12-PWR simulation peaking at 151 °C and the 4-PWR simulation peaking at 104 °C. Because of the temperature differences in these two reference cases, the mean waste package breach time is slightly lower for 12-PWR (31,000 y) than for 4-

PWR (41,000 y); however, concentrations of ^{129}I in the aquifers over time are very similar for the two reference cases. Simulations show that radionuclides move diffusively through the host rock and do not reach the aquifers in significantly elevated concentrations until about 100,000 years. Two radionuclides make it to the aquifers within the one-million-year modeling period, ^{129}I and ^{36}Cl. Sensitivity analyses indicate that uncertainty in shale porosity has a large effect on ^{129}I concentrations in the aquifers at locations above and below the repository. As observation points move down gradient in the aquifers, aquifer permeability overtakes shale porosity as the input parameter most highly correlated with ^{129}I concentrations. This happens because low permeability aquifers and low head gradients provide significant natural barriers to ^{129}I transport. The ingestion dose rate at an extraction well located five kilometers down gradient in the upper aquifer indicates a mean breakthrough of 10^{-15} Sv yr^{-1} after 400,000 years and an increase in the mean dose rate to nearly 3×10^{-11} Sv yr^{-1} by one million years. None of the 50 realizations result in dose rates exceeding 5×10^{-10} Sv yr^{-1} within the one-million-year modeling period.

A significant effort this year went into publications, presentations, short course offerings, expanding the user base, and establishing a broader user group of GDSA Framework collaborators. Results and developments of GDSA Framework were presented in several international venues. In addition, two PFLOTRAN workshops were held, one in Albuquerque and one in Barcelona. Outreach like this supports a primary objective of the GDSA work package by facilitating testing of, and feedback on, PFLOTRAN and GDSA Framework and by increasing the likelihood outside users will contribute directly to code development in the future. Collaboration with outside users is made possible by online version control systems (e.g., Bitbucket.org) and open source access. By encouraging and facilitating use in the outside community, we expect to accelerate development of GDSA Framework and to establish GDSA Framework as a leading geologic repository safety assessment tool.

Progress in the development of GDSA Framework continues to affirm that HPC-capable codes can be used to simulate important multi-physics couplings directly in a total system performance assessment of a geologic repository. The generic repository applications modeled to date indicate that the developing capability can simulate complex coupled processes in a multi-kilometer domain while simultaneously simulating the coupled behavior of sub-meter-scale features and processes within the repository.

While GDSA Framework has greatly advanced over the past several years, continued development is needed to ensure it is ready for application to potential sites that may be selected in the near future. The challenge is to address the remaining needs using available resources. Meeting this challenge will require close integration with technical teams across the SFWST Campaign.

6. REFERENCES

Adams, B. M., K. R. Dalbey, M. S. Eldred, L. P. Swiler, W. J. Bohnhoff, J. P. Eddy, D. M. Vigil, P. D. Hough and S. Lefantzi (2012). DAKOTA, A Multilevel Parallel Object-Oriented Framework for Design Optimization, Parameter Estimation, Uncertainty Quantification, and Sensitivity Analysis: Version 5.2+ User's Manual. SAND2010-2183. Sandia National Laboratories, Albuquerque, New Mexico.

Adams, B. M., M. S. Ebeida, M. S. Eldred, J. D. Jakeman, L. P. Swiler, W. J. Bohnhoff, K. R. Dalbey, J. P. Eddy, K. T. Hu, D. M. Vigil, L. E. Baumann and P. D. Hough (2013). Dakota, a Multilevel Parallel Object-Oriented Framework for Design Optimization, Parameter Estimation, Uncertainty Quantification, and Sensitivity Analysis, Version 5.3.1+ Theory Manual. SAND2011-9106, Updated May 22, 2013, http://dakota.sandia.gov/. Sandia National Laboratories, Albuquerque, New Mexico.

ANDRA (2005). Dossier 2005 Argile: Phenomological evolution of a geological repository. Agence Nationale pour la Gestion des Dechets Radioactifs. Paris, France**:** 527.

Anna, L. O. (2010). Effects of Groundwater Flow on the Distribution of Biogenic Gas in Parts of the Northern Great Plains of Canada and United States. Scientific Investigations Report 2010−5251. U.S. Geological Survey, Reston, Virginia.

Arnold, B. W., P. V. Brady, S. J. Bauer, C. Herrick, S. Pye and J. Finger (2011). Reference Design and Operations for Deep Borehole Disposal of High-Level Radioactive Waste. SAND2011-6749. Sandia National Laboratories, Albuquerque, New Mexico.

Balay, S., J. Brown, K. Buschelman, V. Eijkhout, W. D. Gropp, D. Kaushik, M. G. Knepley, L. Curfman McInnes, B. F. Smith and H. Zhang (2013). PETSc Users Manual. ANL-95/11 – Revision 3.4. Argonne National Laboratory, Argonne, Illinois.

Bianchi, M., H.-H. Liu and J. T. Birkholzer (2015). "Radionuclide transport behavior in a generic geological radioactive waste repository," *Ground Water*, **53**(3):440-451.

Blacker, T., S. J. Owen, M. L. Staten, R. W. Quador, B. Hanks, B. Clark, R. J. Meyers, C. Ernst, K. Merkley, R. Morris, C. McBride, C. Stimpson, M. Plooster and S. Showman (2016). CUBIT Geometry and Mesh Generation Toolkit 15.2 User Documentation. SAND2016-1649 R. Sandia National Laboratories, Albuquerque, New Mexico.

Blackwell, D. D., M. C. Richards, Z. S. Frone, J. F. Batir, M. A. Williams, A. A. Ruzo and R. K. Dingwall. (2011). "SMU Geothermal Laboratory Heat Flow Map of the Conterminous United States, 2011," Supported by Google.org. Available at http://www.smu.edu/geothermal. Retrieved August 21, 2015.

Bourg, I. C. (2015). "Sealing Shales versus Brittle Shales: A Sharp Threshold in the Material Properties and Energy Technology Uses of Fine-Grained Sedimentary Rocks," *Environmental Science & Technology Letters*, **2**(10):255-259.

Bredehoeft, J. D., C. E. Neuzil and P. C. D. Milly (1983). Regional Flow in the Dakota Aquifer: A Study of the Role of Confining Layers. Water-Supply Paper 2237. United States Geological Survey, Alexandria, Virginia.

Carter, J. T., A. J. Luptak, J. Gastelum, C. Stockman and A. Miller (2013). Fuel Cycle Potential Waste Inventory for Disposition. FCRD-USED-2010-000031 Rev 6. Savannah River National Laboratory, Aiken, South Carolina.

Chen, X., G. Hammond, C. Murray, M. Rockhold, V. Vermeul and J. Zachara (2013). "Applications of ensemble-based data assimilation techniques for aquifer characterization using tracer data at Hanford 300 area," *Water Resources Research*, **49**:7064-7076.

Chen, X., H. Murakami, M. Hahn, G. E. Hammond, M. L. Rockhold, J. M. Zachara and Y. Rubin (2012). "Three-Dimensional Bayesian Geostatistical Aquifer Characterization at the Hanford 300 Area using Tracer Test Data," *Water Resources Research*, **48**.

Choi, H. J. and J. Choi (2008). "Double-layered buffer to enhance the thermal performance in a high-level radioactive waste disposal system," *Nuclear Engineering and Design*, **238**(10):2815-2820.

Clayton, D., G. Freeze, T. Hadgu, E. Hardin, L. Lee, J. Prouty, R. Rogers, W. M. Nutt, J. Birkholzer, H. H. Liu, L. Zheng and S. Chu (2011). Generic Disposal System Modeling - Fiscal Year 2011 Progress Report. SAND 2011-5828P, FCRD-USED-2011-000184. Sandia National Laboratories, Albuquerque, New Mexico.

Cvankara, A. M. (1976). Geology of the Fox Hills Formation (Late Cretaceous) in the Williston Basin of North Dakota, with Reference to Uranium Potential. Report of Investigation. North Dakota Geological Survey. Grand Junction, CO.

DOE (2010). Program and Project Management for the Acquisition of Capital Assets. DOE O 413.3B, 11-29-2010. U.S. Department of Energy, Washington, D.C., available at https://www.directives.doe.gov/directives-documents/400-series/0413.3-BOrder-b.

DOE (2011). Used Fuel Disposition Campaign Disposal Research and Development Roadmap. FCRD-USED-2011-000065 REV 0. Fuel Cycle Technologies, Office of Nuclear Energy, US Department of Energy, Washington, DC.

DOE (2012). Used Fuel Disposition Campaign Disposal Research and Development Roadmap. FCR&D-USED-2011-000065, REV 1. U.S. DOE Office of Nuclear Energy, Used Fuel Disposition, Washington, D.C.

DOE (2015). Report on Separate Disposal of Defense High-Level Radioactive Waste. U.S. DOE Office of Nuclear Energy, Washington, D.C., available at http://www.yuccamountain.org/pdf/defense_repository_repor-2015t.pdf.

Downey, J. S. (1986). Geohydrology of Bedrock Aquifers in the Northern Great Plains in Parts of Montana, North Dakota, South Dakota, and Wyoming. U.S. Geological Survey Professional Paper. United States Geological Survey. Washington, DC**:** 87.

Downey, J. S. and G. A. Dinwiddie (1988). The Regional Aquifer System Underlying the Northern Great Plains in Parts of Montana, North Dakota, South Dakota, and Wyoming - Summary. Professional Paper 1402-A. United States Geological Survey, Washington, DC.

Forster, A. and D. Merriam (1997). "Heat Flow in the Cretaceous of Northwestern Kansas andImplications for Regional Hydrology," *Current Research in Earth Sciences*, **1997**(Bulletin 240, part 1.).

Frederick, J. M. and G. E. Hammond (2017). "Maintaining quality assurance within software evolution: Lessons learned with PFLOTRAN," 2017 SIAM Conference on Mathematical and Computational Issues in the Geosciences, Erlangen, Germany, Sep 11-12.

Frederick, J. M., G. E. Hammond, P. E. Mariner, E. R. Stein and S. D. Sevougian (2017a). "Development of a waste form process model in PFLOTRAN," Proceedings of the 16th International High-Level Radioactive Waste Management Conference, Charlotte, North Carolina, April 9-13, American Nuclear Society.

Frederick, J. M., G. E. Hammond, P. E. Mariner, E. R. Stein and S. D. Sevougian (2017b). "Modeling Waste Package Degradation and Waste Form Dissolution for Geologic Repository Performance

Assessment in PFLOTRAN," Migration 2017 - 16th International Conference on the Chemistry and Migration Behaviour of Actinides and Fission Products in the Geosphere, Barcelona, Spain, September 10-15, 2017.

Frederick, J. M., G. E. Hammond, P. E. Mariner, E. R. Stein and S. D. Sevougian (2017c). "Modeling waste package degradation and waste form dissolution for geologic repository performance assessment in PFLOTRAN," Proceedings of the 16th International Conference on the Chemistry and Migration Behavior of Actinides and Fission Products in the Geosphere, Barcelona, Spain, September 10-15.

Freeze, G., P. Gardner, P. Vaughn, S. D. Sevougian, P. E. Mariner and V. Mousseau (2013a). Evaluation of Advanced Performance Assessment Modeling Frameworks: Annotated Outline. FCRD-UFD-2013-000218, SAND2013-6913P. Sandia National Laboratories, Albuquerque, New Mexico.

Freeze, G., W. P. Gardner, P. Vaughn, S. D. Sevougian, P. Mariner, V. Mousseau and G. Hammond (2013b). Enhancements to the Generic Disposal System Modeling Capabilities. SAND2013-10532P, FCRD-UFD-2014-000062. Sandia National Laboratories, Albuquerque, New Mexico.

Freeze, G., P. E. Mariner, J. A. Blink, F. A. Caporuscio, J. E. Houseworth and J. C. Cunnane (2011). Disposal System Features, Events, and Processes (FEPs): FY11 Progress Report. FCRD-USED-2011-000254. SAND2011-6059P. Sandia National Laboratories, Albuquerque, New Mexico.

Freeze, G. and P. Vaughn (2012). Development of an Advanced Performance Assessment Modeling Capability for Geologic Disposal of Nuclear Waste: Methodology and Requirements. SAND2012-10208. Sandia National Laboratories, Albuquerque, New Mexico.

Freeze, G., M. Voegele, P. Vaughn, J. Prouty, W. M. Nutt, E. Hardin and S. D. Sevougian (2013c). Generic Deep Geologic Disposal Safety Case. FCRD-UFD-2012-000146 Rev. 1, SAND2013-0974P. Sandia National Laboratories, Albuquerque, New Mexico.

Freeze, G. A., E. R. Stein, P. V. Brady, C. Lopez, K. Travis and F. Gibb (2017a). Deep Borehole Disposal Safety Case. SFWD-SFWST-2017-000009; SAND2017-xxxxR (in progress). Sandia National Laboratories, Albuquerque, New Mexico.

Freeze, G. A., E. R. Stein, K. L. Kuhlman, G. E. Hammond and J. M. Frederick (2017b). "Probabilistic performance assessment for deep borehole disposal of Cs/Sr capsules, Paper 17143," Waste Management Symposia, Phoenix, Arizona, Mar 5-9.

Freeze, R. A. and J. A. Cherry (1979). Groundwater. Englewood Cliffs, New Jersey, Prentice-Hall, Inc.

Gonzales, S. and K. S. Johnson (1985). Shales and Other Argillaceous Strata in the United States. Oak Ridge National Laboratory. Oak Ridge, TN**:** 596.

Hammond, G., P. Lichtner and C. Lu (2007). "Subsurface multiphase flow and multicomponent reactive transport modeling using high performance computing," *Journal of Physics: Conference Series 78*:1-10.

Hammond, G. E. (2017). "PFLOTRAN Reaction Sandbox: A Flexible, Extensible Framework for Vetting Biogeochemical Reactions within an Open Source Subsurface Simulator," Migration 2017 - 16th International Conference on the Chemistry and Migration Behaviour of Actinides and Fission Products in the Geosphere, Barcelona, Spain, September 10-15, 2017.

Hammond, G. E. and J. M. Frederick (2016). PFLOTRAN verification: Development of a testing suite to ensure software quality, Abstract T23C-2944. 2016 AGU Fall Meeting. American Geophysical Union. San Francisco, California.

Hammond, G. E. and J. M. Frederick (2017). "Minimizing the Impact of Software Evolution on Radioactive Waste Management," 16th International High-Level Radioactive Waste Management Conference, Charlotte, North Carolina, April 9-13, American Nuclear Society.

Hammond, G. E. and P. Lichtner (2010). "Field-scale modeling for the natural attenuation of uranium at the Hanford 300 area using high performance computing," *Water Resources Research*, **46**.

Hammond, G. E., P. C. Lichtner, C. Lu and R. T. Mills (2011a). "PFLOTRAN: Reactive Flow and Transport Code for Use on Laptops to Leadership-Class Supercomputers." Groundwater Reactive Transport Models. F. Zhang, G. T. Yeh and J. Parker. Bentham Science Publishers.

Hammond, G. E., P. C. Lichtner and R. T. Mills (2014). "Evaluating the performance of parallel subsurface simulators: An illustrative example with PFLOTRAN," *Water Resources Research*, **50**(1):208-228.

Hammond, G. E., P. C. Lichtner, R. T. Mills and C. Lu (2008). "Toward petascale computing in geosciences: application to the Hanford 300 Area," *Journal of Physics Conference Series*, **125**:12051-12051.

Hammond, G. E., P. C. Lichtner and M. L. Rockhold (2011b). "Stochastic simulation of uranium migration at the Hanford 300 Area," *Journal of Contaminant Hydrology*, **120-121**:115-128.

Hansen, F. D., E. L. Hardin, R. P. Rechard, G. A. Freeze, D. C. Sassani, P. V. Brady, C. M. Stone, M. J. Martinez, J. F. Holland, T. Dewers, K. N. Gaither, S. R. Sobolik and R. T. Cygan (2010). Shale Disposal of U.S. High-Level Radioactive Waste. Sandia National Laboratories, Albuquerque, New Mexico.

Hardin, E., T. Hadgu, D. Clayton, R. Howard, H. Greenberg, J. Blink, M. Sharma, M. Sutton, J. Carter, M. Dupont and P. Rodwell (2012). Repository Reference Disposal Concepts and Thermal Load Management Analysis. FCRD-UFD-2012-000219 Rev. 2. US Department of Energy, Washington, DC.

Hardin, E. and E. Kalinina (2016). Cost Estimation Inputs for Spent Nuclear Fuel Geologic Disposal Concepts. Sandia National Laboratories. Albuquerque, NM**:** 57.

Helton, J. C., J. D. Johnson, C. J. Sallaberry and C. B. Storlie (2006). Survey of Sampling-Based Methods for Uncertainty and Sensitivity Analysis. Sandia National Laboratories, Albuquerque, New Mexico.

IAEA (2003). "Reference Biospheres" for Solid Radioactive Waste Disposal. International Atomic Energy Agency, Vienna, Austria.

IAEA (2012). The Safety Case and Safety Assessment for the Disposal of Radioactive Waste. Specific Safety Guide SSG-23. International Atomic Energy Agency, Vienna, Austria.

IAEA (2014). Radiation protection and safety of radiation sources: international basic safety standards. GSR Part 3. International Atomic Energy Agency, Vienna, Austria.

ICRP (2012). Compendium of Dose Coefficients based on ICRP Publication 60. ICRP Publication 119. Ann. ICRP 41(Suppl.). Elsevier Ltd. for the International Commission on Radiological Protection (ICRP),

Jackson, J. A. (1997). Glossary of Geology. Alexandria, VA, American Geological Institute.

Jobmann, M. and G. Buntebarth (2009). "Influence of graphite and quartz addition on the thermo-physical properties of bentonite for sealing heat-generating radioactive waste," *Applied Clay Science*, **44**(3-4):206-210.

Jové Colón, C. F., P. F. Weck, D. C. Sassani, L. Zheng, J. Rutqvist, C. I. Steefel, K. Kim, S. Nakagawa, J. Houseworth, J. Birkholzer, F. A. Caporuscio, M. Cheshire, M. S. Rearick, M. K. McCarney, M. Zavarin, A. Benedicto-Cordoba, A. B. Kersting, M. Sutton, J. L. Jerden, K. E. Frey, J. M. Copple and W. L. Ebert (2014). Evaluation of Used Fuel Disposition in Clay-Bearing Rock. FCRD-UFD-2014-000056 , SAND2014-18303 R. Sandia National Laboratories, Albuquerque, New Mexico.

Kienzler, B., M. Altmaier, C. Bube and V. Metz (2012). Radionuclide Source Term for HLW Glass, Spent Nuclear Fuel, and Compacted Hulls and End Pieces (CSD-C Waste). KIT Scientific Reports 7624. Karlsruhe Institute of Technology, Baden-Württemberg, Germany.

Kolditz, O., W. Wang and S. Bauer (2015). Thermo-Hydro-Mechanical-Chemical Processes in Fractured Porous Media: Modelling and Benchmarking, Closed Form Solutions. Switzerland, Springer International Publishing.

Konikow, L. F. and C. E. Neuzil (2007). "A method to estimate groundwater depletion from confining layers," *Water Resources Research*, **43**(7).

Li, Y. H. and S. Gregory (1974). "Diffusion of ions in sea-water and in deep-sea sediments," *Geochimica et Cosmochimica Acta*, **38**(5):703-714.

Lichtner, P. C. and G. E. Hammond (2012). Quick Reference Guide: PFLOTRAN 2.0 (LA-CC-09-047) Multiphase-Multicomponent-Multiscale Massively Parallel Reactive Transport Code. LA-UR-06-7048. December 8, 2012. Los Alamos National Laboratory, Los Alamos, New Mexico.

Liu, J. F., Y. Song, F. Skoczylas and J. Liu (2016). "Gas migration through water-saturated bentonite-sand mixtures, COx argillite, and their interfaces," *Canadian Geotechnical Journal*, **53**(1):60-71.

Lu, C. and P. C. Lichtner (2007). "High resolution numerical investigation on the effect of convective instability on long term CO_2 storage in saline aquifers," *Journal of Physics Conference Series*, **78**:U320-U325.

Maldonado, A. C. (2011). Elastic and Mechanical Properties of the Niobrara Formation with Application to Hydraulic Fracture Design. Master of Science, Colorado School of Mines.

Manger, G. E. (1963). Porosity and Bulk Density of Sedimentary Rocks. United States Geological Survey Bulletin. United States Geological Survey. Washington, DC**:** 60.

Mariner, P. E., J. M. Frederick and G. E. Hammond (2017a). "Radon and the PFLOTRAN Ingestion Dose Model of GDSA Framework " Migration 2017 - 16th International Conference on the Chemistry and Migration Behaviour of Actinides and Fission Products in the Geosphere, Barcelona, Spain, September 10-15, 2017.

Mariner, P. E. and W. P. Gardner (2015). "Estimation of Dilution, Capture, and Dose for IAEA Reference Biospheres," International High-Level Radioactive Waste Management Conference, Charleston, South Carolina.

Mariner, P. E., W. P. Gardner, G. E. Hammond, S. D. Sevougian and E. R. Stein (2015). Application of Generic Disposal System Models. FCRD-UFD-2015-000126, SAND2015- 10037 R. Sandia National Laboratories, Albuquerque, New Mexico.

Mariner, P. E., G. E. Hammond and J. M. Frederick (2017b). "Isotope Partitioning, Decay, and Ingrowth across Multiple Phases in PFLOTRAN Code of GDSA Framework," Migration 2017 - 16th International Conference on the Chemistry and Migration Behaviour of Actinides and Fission Products in the Geosphere, Barcelona, Spain, September 10-15, 2017.

Mariner, P. E., E. R. Stein, J. M. Frederick, S. D. Sevougian and G. E. Hammond (2016). Advances in Geologic Disposal System Modeling and Application to Crystalline Rock. FCRD-UFD-2016-000440, SAND2016-9610 R. Sandia National Laboratories, Albuquerque, New Mexico.

Mazurek, M., P. Alt-Epping, A. Bath, T. Gimmi, H. N. Waber, S. Buschaert, P. De Canniere, M. De Craen, A. Gautschi, S. Savoye, A. Vinsot, I. Wemaere and L. Wouters (2011). "Natural tracer profiles across argillaceous formations," *Applied Geochemistry*, **26**(7):1035-1064.

Meacham, P. G., D. R. Anderson, E. J. Bonano and M. G. Marietta (2011). Sandia National Laboratories Performance Assessment Methodology for Long-Term Environmental Programs: The History of

Nuclear Waste Management. SAND2011-8270. Sandia National Laboratories, Albuquerque, New Mexico.

Miller, A. W. and Y. Wang (2012). "Radionuclide Interaction with Clays in Dilute and Heavily Compacted Systems: A Critical Review," *Environmental Science & Technology*, **46**(4):1981-1994.

Millington, R. J. (1959). "Gas Diffusion in Porous Media," *Science*, **130**(3367):100-102.

Mills, R., C. Lu, P. C. Lichtner and G. Hammond (2007). "Simulating subsurface flow and transport on ultrascale computers using PFLOTRAN," 3rd Annual Scientific Discovery through Advanced Computing Conference (SciDAC 2007), BostonJournal of Physics Conference Series, U387-U393.

Navarre-Sitchler, A., R. M. Maxwell, E. R. Siirila, G. E. Hammond and P. C. Lichtner (2013). "Elucidating geochemical response of shallow heterogeneous aquifers to CO_2 leakage using high-performance computing: implications for monitoring CO_2 sequestration," *Advances in Water Resources*, **53**:44-55.

Neuzil, C. E. (1986). "Groundwater-Flow in Low-Permeability Environments," *Water Resources Research*, **22**(8):1163-1195.

Neuzil, C. E. (1993). "Low Fluid Pressure within the Pierre Shale - A Transient-Response to Erosion," *Water Resources Research*, **29**(7):2007-2020.

Neuzil, C. E. (1994). "How Permeable Are Clays and Shales," *Water Resources Research*, **30**(2):145-150.

Nopola, J. R. (2013). Preliminary Evaluation of the Pierre Shale as a Nuclear Waste Repository. Master of Science, South Dakota School of Mines and Technology.

NWTRB (2015). Designing a Process for Selecting a Site for a Deep-Mined, Geologic Repository for High-Level Radioactive Waste and Spent Nuclear Fuel: Overview and Summary. Report to the United States Congress and the Secretary of Energy, November 2015. U.S. Nuclear Waste Technical Review Board, Washington, D.C.

Oberkampf, W. L. and T. G. Trucano (2007). Verification and Validation Benchmarks. SAND2007-0853. Sandia National Laboratories, Albuquerque, New Mexico.

Ollila, K. (2008). Dissolution of unirradiated UO_2 and UO_2 doped with ^{233}U in low- and high-ionic strength NaCl under anoxic and reducing conditions. Working Report 2008-50. Posiva Oy, Eurajoki, Finland.

Olszewska-Wasiolek, M. A. and B. W. Arnold (2011). "Radioactive Disequilibria in the Saturated Zone Transport Model and the Biosphere Model for the Yucca Mountain Repository — The Case of Radon-222," International High-Level Radioactive Waste Management Conference, Albuquerque, New Mexico, 767-772.

Perry, F. V. and R. E. Kelley (2017). Regional Geologic Evaluations for Disposal of HLW and SNF: The Pierre Shale of the Northern Great Plains. Los Alamos National Laboratory. Los Alamos, NM.

Perry, F. V., R. E. Kelley, P. F. Dobson and J. E. Houseworth (2014). Regional Geology: A GIS Database for Alternative Host Rocks and Potential Siting Guidelines. FCRD-UFD-2014-000068, Unlimited Release Report LA-UR-14-20368. Los Alamos National Laboratory, Los Alamos, New Mexico.

Rechard, R. P. (1995). Performance Assessment of the Direct Disposal in Unsaturated Tuff of Spent Nuclear Fuel And High-Level Waste Owned by US Department of Energy. SAND94-2563/1,2,3. Sandia National Laboratories, Albuquerque, New Mexico.

Rechard, R. P. (2002). "General approach used in the performance assessment for the Waste Isolation Pilot Plant," Scientific Basis for Nuclear Waste Management XXV, Boston, Massachussetts, November 26-29, 2001, Materials Research Society.

Rechard, R. P., B. Goldstein, L.H. Brush, J.A. Blink, M. Sutton, and F.V. Perry (2011). Basis for Identification of Disposal Option for Research and Development for Spent Nuclear Fuel and High-Level Waste. FCRD-USED-2011-000071. SAND2011-3781P, Sandia National Laboratories, Albuquerque, New Mexico.

Rechard, R. P. and C. T. Stockman (2014). "Waste degradation and mobilization in performance assessments of the Yucca Mountain disposal system for spent nuclear fuel and high-level radioactive waste," *Reliability Engineering and System Safety*, **122**(2):165-188.

Rechard, R. P. and M. S. Tierney (2005). "Assignment of probability distributions for parameters in the 1996 performance assessment for the Waste Isolation Pilot Plant, Part 1: Description of process," *Reliability Engineering and System Safety*, **88**(1):1-32.

Reimus, P. W., M. Zavarin and Y. Wang (2016). Colloid-Facilitated Radionuclide Transport: Current State of Knowledge from a Nuclear Waste Repository Risk Assessment Perspective. FCRD-UFD-2016-000446. Los Alamos National Laboratory, Los Alamos, New Mexico.

Roache, P. J. (2002). "Code verification by the method of manufactured solutions," *Journal of Fluids Engineering-Transactions of the Asme*, **124**(1):4-10.

Sassani, D., J. Jang, P. Mariner, L. Price, R. Rechard, M. Rigali, R. Rogers, E. Stein, W. Walkow and P. Weck (2016). The On-line Waste Library (OWL): Usage and Inventory Status Report. FCRD-UFD-2016-000080. Sandia National Laboratories, Albuquerque, New Mexico.

Sassani, D. C., C. F. Jové Colón, P. Weck, J. L. Jerden, K. E. Frey, T. Cruse, W. L. Ebert, E. C. Buck, R. S. Wittman, F. N. Skomurski, K. J. Cantrell, B. K. McNamara and Z. Soderquist (2012). Integration of EBS Models with Generic Disposal System Models. FCRD-UFD-2012-000277, SAND2012-7762P. Sandia National Laboratories, Albuquerque, New Mexico.

Schultz, L. G., H. A. Tourtelot, J. R. Gill and J. G. Boerngen (1980). Geochemistry of the Pierre Shale and Equivalent Rocks of Late Cretaceous Age. Geological Survey Professional Paper. United States Geological Survey. Washington, DC**:** 123.

Sevougian, S. D., G. A. Freeze, W. P. Gardner, G. E. Hammond and P. E. Mariner (2014). Performance Assessment Modeling and Sensitivity Analyses of Generic Disposal System Concepts. SAND2014-17658. Sandia National Laboratories, Albuquerque, New Mexico.

Sevougian, S. D., G. A. Freeze, P. Vaughn, P. Mariner and W. P. Gardner (2013). Update to the Salt R&D Reference Case. FCRD-UFD-2013-000368, SAND2013-8255P. Sandia National Laboratories, Albuquerque, New Mexico.

Sevougian, S. D., E. R. Stein, M. B. Gross, T. F. Corbet, M. J. Rigali, L. L. Price, J. M. Frederick and G. E. Hammond (2017a). Defense Waste Repository Safety Analysis and Host Geology Evaluation Status Report. Sandia National Laboratories. Albuquerque, NM.

Sevougian, S. D., E. R. Stein, M. B. Gross, G. E. Hammond, J. M. Frederick and P. E. Mariner (2016). Status of Progress Made Toward Safety Analysis and Technical Site Evaluations for DOE Managed HLW and SNF. Sandia National Laboratories. Albuquerque, NM**:** 188.

Sevougian, S. D., E. R. Stein, M. B. Gross, G. E. Hammond, J. M. Frederick and P. E. Mariner (2017b). Performance assessment of a generic repository for defense-related HLW/SNF in fractured crystalline host rock, Paper 17059. Waste Management Symposia. Phoenix, Arizona.

Sevougian, S. D., E. R. Stein, G. E. Hammond, P. E. Mariner and J. M. Frederick (2017c). "Estimating the Effect of Fracture Connectivity on Waste Isolation Using a High-Performance Reactive Transport Simulator, PFLOTRAN," Migration 2017 - 16th International Conference on the Chemistry and

Migration Behaviour of Actinides and Fission Products in the Geosphere, Barcelona, Spain, September 10-15, 2017.

Shelton, S. M. (1934). "Thermal conductivity of some irons and steels over the temperature range 100 to 500 C," *Bureau of Standards Journal of Research*, **12**(4/6):441-450.

Sheppard, M. I. and D. H. Thibault (1990). "Default soil solid/liquid partition coefficients, Kds, for four major soil types: a compendium," *Health Physics*, **59**(4):471-482.

Shurr, G. W. (1977). The Pierre Shale, Northern Great Plains: A Potential Isolation Medium for Radioactive Waste. Open-File Report. United States Geological Survey. Reston, VA**:** 27.

SKB (2006). Data report for the safety assessment SR-Can. SKB TR-06-25. Svensk Kärnbränslehantering AB, Stockholm, Sweden.

Stein, E. R., J. M. Frederick, G. E. Hammond, K. L. Kuhlman, P. E. Mariner and S. D. Sevougian (2017a). "Modeling Coupled Reactive Flow Processes in Fractured Crystalline Rock," 16th International High-Level Radioactive Waste Management Conference, Charlotte, North Carolina, April 9-13, American Nuclear Society.

Stein, E. R., G. E. Hammond and C. F. Jové Colón (2017b). "Multi-Scale Modeling in PFLOTRAN for Geologic Repository Performance Assessment: An Enhancement to GDSA Framework," Migration 2017 - 16th International Conference on the Chemistry and Migration Behaviour of Actinides and Fission Products in the Geosphere, Barcelona, Spain, September 10-15, 2017.

Stein, E. R., S. D. Sevougian, G. E. Hammond, J. M. Frederick and P. E. Mariner (2016). Performance assessment of a generic repository in bedded salt for DOE-managed nuclear waste, Abstract MR41C-2711. 2016 Fall Meeting. American Geophysical Union. San Francisco, California.

Turrero, M., A. Fernández, J. Peña, M. Sánchez, P. Wersin, P. Bossart, M. Sánchez, A. Melón, A. Garralón and A. Yllera (2006). "Pore water chemistry of a Paleogene continental mudrock in Spain and a Jurassic marine mudrock in Switzerland: Sampling methods and geochemical interpretation," *Journal of Iberian Geology*, **32**(2):233-258.

UNSCEAR (2000). Sources and Effects of Ionizing Radiation, United Nations Scientific Committee on the Effects of Atomic Radiation, UNSCEAR 2000 Report to the General Assembly, with Scientific Annexes. United Nations, New York, New York.

Van der Leeden, F., F. L. Troise and D. K. Todd (1990). The Water Encyclopedia. Chelsea, Michigan, Lewis Publishers.

Van Loon, L. R. and J. Mibus (2015). "A modified version of Archie's law to estimate effective diffusion coefficients of radionuclides in argillaceous rocks and its application in safety analysis studies," *Applied Geochemistry*, **59**:85-94.

Vaughn, P., G. Freeze, J. Lee, S. Chu, K. D. Huff, W. M. Nutt, T. Hadgu, R. Rogers, J. Prouty, E. Hardin, B. Arnold, E. Kalinina, W. P. Gardner, M. Bianchi, H. H. Liu and J. Birkholzer (2013). Generic Disposal System Model: Architecture, Implementation, and Demonstration. FCRD-UFD-2012-000430 Rev. 1, SAND2013-1539P. Sandia National Laboratories, Albuquerque, New Mexico.

Wang, Y., T. Hadgu, E. Matteo, J. N. Kruichak, M. M. Mills, R. Tinnacher, J. Davis, H. S. Viswanathan, S. Chu, T. Dittrich, F. Hyman, S. Karra, N. Makedonska, P. Reimus, M. Zavarin, P. Zhao, C. Joseph, J. B. Begg, Z. Dai, A. B. Kersting, J. Jerden, J. M. Copple, T. Cruse and W. Ebert (2015). Used Fuel Disposal in Crystalline Rocks: FY15 Progress Report. FCRD-UFD-2015-000125. Sandia National Laboratories, Albuquerque, New Mexico.

Wang, Y., E. Matteo, J. Rutqvist, J. Davis, L. Zheng, J. Houseworth, J. Birkholzer, T. Dittrich, C. W. Gable, S. Karra, N. Makedonska, S. Chu, D. Harp, S. L. Painter, P. Reimus, F. V. Perry, P. Zhao, J. B.

Begg, M. Zavarin, S. J. Tumey, Z. R. Dai, A. B. Kersting, J. Jerden, K. E. Frey, J. M. Copple and W. Ebert (2014). Used Fuel Disposal in Crystalline Rocks: Status and FY14 Progress. FCRD-UFD-2014-000060, SAND2014-17992 R. Sandia National Laboratories, Albuquerque, New Mexico.

Weast, R. C. and M. J. Astle, Eds. (1981). CRC Handbook of Chemistry and Physics. Boca Raton, Florida, CRC Press, Inc.